Neuronal wiring diagram of an adult brain

Sven Dorkenwald[1,2], Arie Matsliah[1], Amy R Sterling[1,3], Philipp Schlegel[4,5], Szi-chieh Yu[1], Claire E. McKellar[1], Albert Lin[1,6], Marta Costa[5], Katharina Eichler[5], Yijie Yin[5], Will Silversmith[1], Casey Schneider-Mizell[7], Chris S. Jordan[1], Derrick Brittain[7], Akhilesh Halageri[1], Kai Kuehner[1], Oluwaseun Ogedengbe[1], Ryan Morey[1], Jay Gager[1], Krzysztof Kruk[3], Eric Perlman[8], Runzhe Yang[1,2], David Deutsch[1,9], Doug Bland[1], Marissa Sorek[1,3], Ran Lu[1], Thomas Macrina[1,2], Kisuk Lee[1,10], J. Alexander Bae[1,11], Shang Mu[1], Barak Nehoran[1,2], Eric Mitchell[1], Sergiy Popovych[1,2], Jingpeng Wu[1], Zhen Jia[1], Manuel Castro[1], Nico Kemnitz[1], Dodam Ih[1], Alexander Shakeel Bates[4,5,12,13], Nils Eckstein[14], Jan Funke[14], Forrest Collman[7], Davi D. Bock[15], Gregory S.X.E. Jefferis[4,5], H. Sebastian Seung[1,2]*, Mala Murthy[1]*, the FlyWire Consortium

[1]Princeton Neuroscience Institute, Princeton University, Princeton, USA
[2]Computer Science Department, Princeton University, Princeton, USA
[3]Eyewire, Boston, USA
[4]Neurobiology Division, MRC Laboratory of Molecular Biology, Cambridge, UK
[5]Drosophila Connectomics Group, Department of Zoology, University of Cambridge, Cambridge, UK
[6]Center for the Physics of Biological Function, Princeton University, Princeton, USA
[7]Allen Institute for Brain Science, Seattle, USA
[8]Yikes LLC, Baltimore, USA
[9]Department of Neurobiology, University of Haifa, Haifa, Israel
[10]Brain & Cognitive Sciences Department, Massachusetts Institute of Technology, Cambridge, USA
[11]Electrical and Computer Engineering Department, Princeton University, Princeton, USA
[12]Harvard Medical School, Boston, USA
[13]Centre for Neural Circuits and Behaviour, The University of Oxford, Oxford, UK
[14]Janelia Research Campus, Howard Hughes Medical Institute, Ashburn, USA
[15]Department of Neurological Sciences, University of Vermont, Burlington, USA

*Correspondence to sseung@princeton.edu and mmurthy@princeton.edu

Abstract

Connections between neurons can be mapped by acquiring and analyzing electron microscopic (EM) brain images. In recent years, this approach has been applied to chunks of brains to reconstruct local connectivity maps that are highly informative, yet inadequate for understanding brain function more globally. Here, we present the first neuronal wiring diagram of a whole adult brain, containing 5×10^7 chemical synapses between ~130,000 neurons reconstructed from a female *Drosophila melanogaster*. The resource also incorporates annotations of cell classes and types, nerves, hemilineages, and predictions of neurotransmitter identities. Data products are available by download, programmatic access, and interactive browsing and made interoperable with other fly data resources. We show how to derive a projectome, a map of projections between regions, from the connectome. We demonstrate the tracing of synaptic pathways and the analysis of information flow from inputs (sensory and ascending neurons) to outputs (motor, endocrine, and descending neurons), across both hemispheres, and between the central brain and the optic lobes. Tracing from a subset of photoreceptors all the way to descending motor pathways illustrates how structure can uncover putative circuit mechanisms underlying sensorimotor behaviors. The technologies and open ecosystem of the FlyWire Consortium set the stage for future large-scale connectome projects in other species.

Nomenclature

segmentation	product of automated pipeline
proofreading	the process of correcting errors in the automated segmentation
reconstruction	segmented + proofread → the final product
synapse	one synaptic link between a pre and a postsynaptic site; a presynaptic site is usually part of multiple synapses
connection	the combination of all synapses between two neurons

Introduction

While rudimentary nervous systems existed in more ancient animals (Arendt, Tosches, and Marlow 2016), brains evolved perhaps half a billion years ago (Ma et al. 2012), and are essential for the generation of sophisticated behaviors. It is widely accepted that dividing a brain into regions is helpful for understanding brain function (Mesulam 1998). Wiring diagrams at the level of neurons and synapses have been controversial (Sporns, Tononi, and Kötter 2005; Costandi 2012; Jabr 2012). Skepticism flourished (Sporns, Tononi, and Kötter 2005; Costandi 2012; Jabr 2012) largely due to a lack of technologies that could reconstruct such wiring diagrams (Lichtman and Denk 2011; Denk, Briggman, and Helmstaedter 2012). The situation began to change in the 2000s (Denk and Horstmann 2004; Lichtman and Sanes 2008), due to the efforts of a small community of researchers. Here we report a significant milestone attained by these efforts, the first neuronal wiring diagram of a whole adult brain.

The brain of *Drosophila melanogaster* may seem tiny, but its 10^5 neurons and 10^8 synapses enable a fly to see, smell, hear, walk, and, of course, fly. Flies engage in dynamic social interactions (Coen et al. 2014), navigate over distances (Fisher 2022), and form long-term memories (Cognigni, Felsenberg, and Waddell 2018). Portions of fly brains have been reconstructed from electron microscopic (EM) images, which are sharp enough to reveal the fine branches of neurons and the synapses that connect them. The resulting wiring diagrams of neural circuits have provided crucial insights into how the brain generates social (Schretter et al. 2020; Deutsch et al. 2020), memory-related (C.-H. Li and Yang 2020) or navigation (Hulse et al. 2020) behaviors. Wiring diagrams of other fly brain regions have been mapped and related to visual (S.-Y. Takemura et al. 2013; S. Takemura et al. 2017), auditory (Baker et al. 2022), and olfactory (F. Li et al. 2020; Alexander S. Bates et al. 2020; P. Schlegel et al. 2021) functions. Similarities with mammalian wiring diagrams (Borst and Helmstaedter 2015) are striking.

The above wiring diagrams and many others from mammals (MICrONS Consortium et al. 2021; Shapson-Coe et al. 2021; Loomba et al. 2022; Turner et al. 2022; Nguyen et al. 2023) have come from pieces of brain. But recordings of *Drosophila* neural activity have revealed nearly brain-wide encoding of sensory (Pacheco et al. 2021) and motor (Brezovec et al. 2022; Schaffer et al. 2021; Aimon et al. 2022) variables. These studies and others in vertebrates highlight that understanding how the brain processes sensory information or

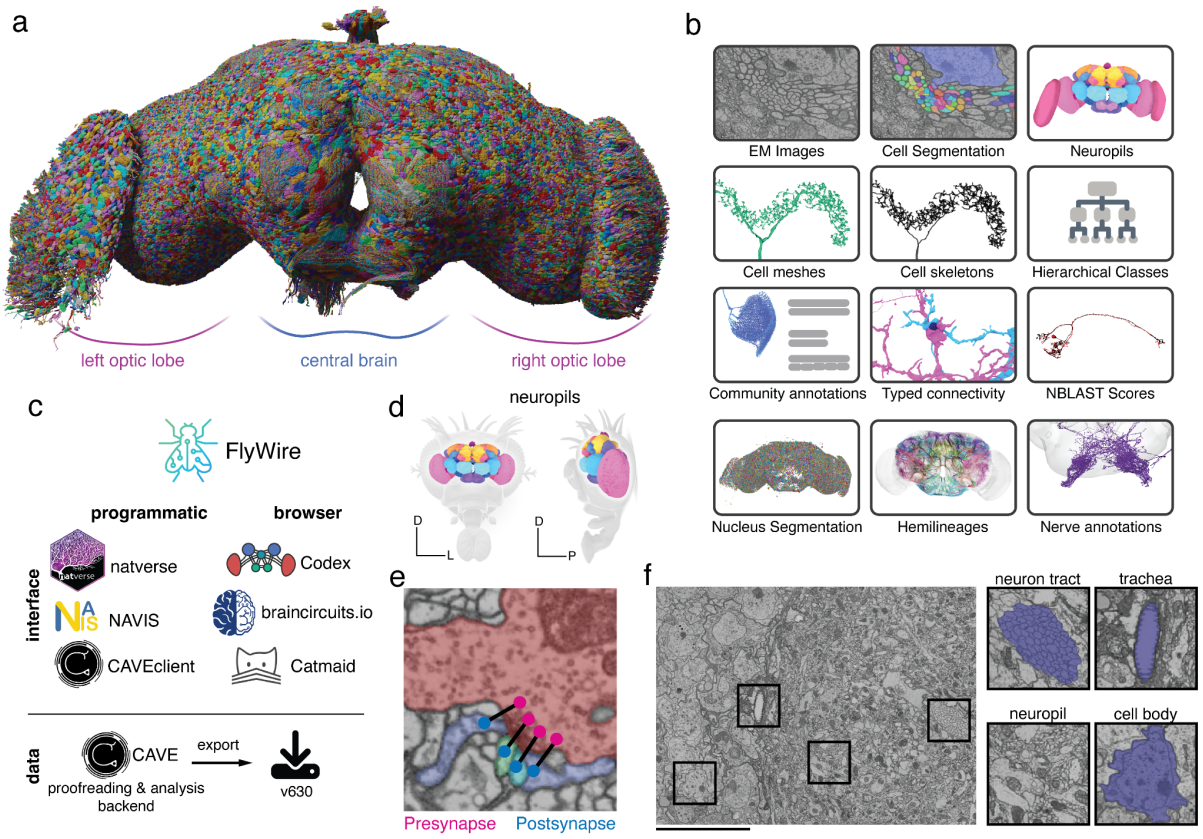

Figure 1. A connectomic reconstruction of a whole fly brain. (a) All neuron morphologies reconstructed with FlyWire. All neurons in the central brain and both optic lobes were segmented and proofread. Note: image and dataset are mirror inverted relative to the native fly brain. (b) An overview of many of the FlyWire resources which are being made available. FlyWire leverages existing resources for EM imagery by Zheng et al. (Zheng et al. 2018), synapse predictions by Buhmann et al. (Buhmann et al. 2021; Heinrich et al. 2018) and neurotransmitter predictions by Eckstein et al. (Eckstein et al. 2023). Annotations of the FlyWire dataset such as hemilineages, nerves, and hierarchical classes are established in our companion paper by Schlegel et al. (c) FlyWire uses CAVE (*in prep*) for proofreading, data management, and analysis backend. The data can be accessed programmatically through the CAVEclient, navis and natverse (Alexander Shakeel Bates et al. 2020), and through the browser in Codex, Catmaid Spaces (*in prep*) and braincircuits.io (Gerhard et al., *in prep*). Static exports of the data are also available. (d) The *Drosophila* brain can be divided into spatially defined regions based on neuropils (Ito et al. 2014) (Ext. Data Fig. 1-1). Neuropils for the lamina are not shown. (e) Synaptic boutons in the fly brain are often polyadic such that there are multiple postsynaptic partners per presynaptic bouton. Each link between a pre- and a postsynaptic location is a synapse. (f) Neuron tracts, trachea, neuropil, cell bodies can be readily identified from the EM data which was acquired by Zheng et al. (Zheng et al. 2018). Scale bar: 10 µm

drives behavior will require understanding global information flow at the scale of the entire brain.

The closest antecedent to our whole brain is the reconstruction of a fly “hemibrain” (Scheffer et al. 2020), a resource that has already become indispensable to *Drosophila* researchers (F. Li et al. 2020; P. Schlegel et al. 2021; Klapoetke et al. 2022; Wang et al. 2021). It is estimated to contain about 20,000 neurons that are “uncropped,” i.e., minimally truncated by the borders of the imaged volume, and 14 million synapses between them. Our reconstruction of an entire adult brain contains 127,978 neurons (Fig. 1a), and 53 million

synapses between them. These and many other data products (Fig. 1b) are available for download, programmatic access, and interactive browsing and made interoperable with other fly data resources through a growing ecosystem of software tools (Fig. 1c). The primary portal to the data is FlyWire Codex (codex.flywire.ai, manuscript *in prep*), which makes the information visualizable and queryable.

The wiring diagram from our whole brain reconstruction is complete enough to deserve the name "connectome." It is a clear leap beyond *C. elegans* (300 neurons, $<10^4$ synapses) (White et al. 1986; Varshney et al. 2011; Cook et al. 2019) and the 1st instar larva of *Drosophila* (3,000 neurons, 5×10^5 synapses) (Winding et al. 2023). Our connectome advances beyond the hemibrain in ways that are not simply numerical. It encompasses the subesophageal zone (SEZ) of the central brain, important for diverse functions such as gustation and mechanosensation (see companion paper Shiu et al. (Shiu et al. 2023) as well as Eichler et al.(Eichler et al. 2023)), and containing many of the processes of neurons that descend from the brain to the ventral nerve cord to drive motor behaviors. It includes annotations for nearly all sexually-dimorphic neurons, analyzed in a companion paper (Deutsch et al. *in prep*). Our reconstruction of both optic lobes goes far beyond existing maps of columnar visual circuitry (S. Takemura et al. 2017; Shinomiya et al. 2019, 2022). Connections between the optic lobes and central brain are included, as explored by a companion paper (Kind et al., *in prep*). Also included are neurons that extend into the brain through the nerves and neck connective, which are essential for tracing sensorimotor pathways, as illustrated by the present paper and companion papers (*list in prep*).

Schlegel et al. have compared our wiring diagram with the hemibrain where they overlap and showed that cell type counts and large strong connections were largely in agreement. This means that the combined effects of natural variability across individuals and "noise" due to imperfect reconstruction tend to be modest, so our wiring diagram of a single brain should be useful for studying any normal *Drosophila* individual. That being said, there are known male-female differences (Cachero et al. 2010). In addition, Schlegel et al. report high variability for principal neurons of the mushroom body, a brain structure required for olfactory learning and memory. Some mushroom body connectivity patterns have even been found to be near random (Caron et al. 2013; Murthy, Fiete, and Laurent 2008), though deviations from randomness have since been identified (Zheng et al. 2022). In short, *Drosophila* wiring diagrams are useful because of their stereotypy, yet also open the door to studies of connectome variation.

Our reconstruction utilized image acquisition and analysis techniques that are distinct from those used for the hemibrain (Methods and Discussion). However, we have built directly on the hemibrain in an important way. The companion paper by Schlegel et al. annotated cell types of central brain neurons, principally by matching them with hemibrain neurons. This approach was enabled by a growing ecosystem of software tools serving interoperability between different fly data sources (Fig. 1c). Because annotations of cell types are essential for scientific discovery, Schlegel et al. (Philipp Schlegel et al. 2023) should be cited along with the present manuscript by those who use the FlyWire resource. Annotations in the SEZ and optic lobes, largely absent from the hemibrain, were contributed by *Drosophila* labs in the FlyWire Consortium, as well as by citizen scientists. Synapse predictions (Buhmann et al. 2021; Heinrich et al. 2018) and estimates of neurotransmitter identities (Eckstein et al. 2023) were also contributed by the community.

In addition to describing the FlyWire resource, this manuscript also presents analyses that illustrate how the data products can be used. Additional whole-brain network analyses are provided in a companion paper (Lin et al., *in prep*). From the connectome with its huge numbers of neurons and synapses, we derive a projectome, a reduced map of projections between 78 fly brain regions known as neuropils (Fig. 1d, Ext. Data Fig. 1-1). We trace synaptic pathways and analyze information flow from the inputs to the outputs of the brain, across both hemispheres, and between the central brain and the optic lobes. In particular, the organization of excitation and inhibition in pathways from photoreceptors in the ocelli to descending motor neurons immediately suggests hypotheses about circuit mechanisms of behavior.

Results

Reconstruction of a whole fly brain at electron microscopic resolution

Images of an entire adult female fly brain (Fig. 1e, f) were previously acquired by serial section transmission EM, and released into the public domain by Zheng et al. (Zheng et al. 2018). We previously realigned the EM images (Popovych et al. 2022), automatically segmented all neurons in the images (Macrina et al. 2021), created a computational system that allows interactive proofreading of the segmentation, and assembled an online community known as FlyWire (Dorkenwald, McKellar, et al. 2022). During the initial phase, much proofreading was done by a distributed community of *Drosophila* labs in the FlyWire Consortium, and focused on neurons of interest to these labs. During the later phase, the remaining neurons were mainly proofread by two centralized teams at Princeton and Cambridge, with significant contributions from citizen scientists worldwide. The recruitment and training of proofreaders and their workflows are described in the Methods.

Chemical synapses were automatically detected in the images as pairs of presynapse-postsynapse locations (Buhmann et al. 2021; Heinrich et al. 2018). The whole brain contains 0.0188 mm^3 of neuropil volume and ~130 million synapses. This works out to 6.9 synapses/μm^3, much denser than the <1 synapse/μm^3 reported for mammalian cortex (Schüz and Palm 1989; Dorkenwald et al. 2017). The central brain and left and right optic lobes contain 0.0103, 0.0042, and 0.0043 mm^3 of neuropil volume, respectively, with synapse counts in approximately the same proportion. Synapses were combined with proofread neurons to yield the connectome, using the Connectome Annotation Versioning Engine (CAVE*,* manuscript *in prep*).

We already showed that FlyWire proofreading can yield accurate results (Dorkenwald, McKellar, et al. 2022) through comparison with light microscopic reconstructions of neurons that are known to be highly stereotyped across individual flies. A second method is to subject neurons to an additional round of proofreading (J. S. Kim et al. 2014; Scheffer et al. 2020), which was previously shown to yield few changes (Dorkenwald, McKellar, et al. 2022). Because proofreading workflows and personnel have changed over time, and accuracy can vary across brain regions, we repeated this evaluation by subjecting 826 neurons from the central brain to a second round of proofreading. Relative to the second

round, our first round of proofreading achieved an average F1-Score of 99.2% by volume (Ext. Data Fig. 1-2 a,b).

A third validation method is to quantify how many of the automatically detected synapses are attached to proofread segments, as opposed to being isolated in tiny “orphan” segments (Buhmann et al. 2021; Heinrich et al. 2018). We found high attachment rates of presynapses (92.3% or ~120,100,000 presynapses attached) while attachment rates of postsynapses were lower (43.9% or ~57,200,000 postsynapses attached) due to less proofreading and reattachment of twigs which contain most of the postsynapses (Dorkenwald, McKellar, et al. 2022) (Ext. Data Fig. 1-2 c,d). Attachment rates were generally in agreement between the two hemispheres of FlyWire and with the hemibrain (Ext. Data Fig. 1-2 e,f,g) and varied by neuropil (Ext. Data Fig. 1-3). The bottom line is that accuracy of our connectome is state of the art. As with the hemibrain (Scheffer et al. 2020), false negative synapses are the dominant kind of error but false positives exist as well - for this reason all analyses we present below (and connections indicated in Codex) use a threshold of 5 synapses to determine a connection between two neurons). Assuming that such errors are statistically independent, accuracy is expected to be high for detection of connections involving multiple synapses (Scheffer et al. 2020; Schneider-Mizell et al. 2016; Meinertzhagen 2018).

FlyWire’s reconstruction remains open for proofreading and annotations and new versions of the resource will be released in future. This allows for the correction of remaining errors as they are discovered and further rounds of validation to be performed. Additionally, as explained below, proofreading of photoreceptor axons in the compound eyes is still ongoing. The first public release (called version 630) has been extensively validated for neurons in the central brain. All neurons in the optic lobe were proofread but additional validation will likely identify and correct minor reconstruction errors.

Intrinsic neurons of the brain

Of the 127,978 proofread neurons in FlyWire, 114,423 are fully contained within the brain (including both central brain and optic lobes, but excluding afferent and efferent neurons, with projections into and out of the brain, respectively; Fig. 2a,b). These intrinsic neurons (Fig. 2c left) belong to the brain only, in contrast to other neurons that are shared by the brain with other structures. Intrinsic neurons of the brain make up three quarters of the adult fly nervous system (Methods), indicating a high degree of centralization in the brain. The large fraction is related to the fact that the brain is substantially larger than the ventral nerve cord (VNC) (Phelps et al. 2021; S.-Y. Takemura et al. 2023; Marin et al. 2023). Intrinsic neurons amount to 84% of brain neurons. Their predominance means that the brain primarily communicates with itself, and only secondarily with the outside world.

The nervous system of the larval fly is less centralized; intrinsic neurons of the brain make up one quarter to one third of its nervous system (Winding et al. 2023). The closest structure to a brain in *C. elegans* is the nerve ring (Brittin et al. 2021), which is co-located with multiple sensory organs in the worm’s head. The nerve ring contains no intrinsic neurons, as all neurons in the nerve ring also extend neurites into the rest of the nervous system. The absence of intrinsic neurons is consistent with the convention that the nerve ring is not commonly called a brain.

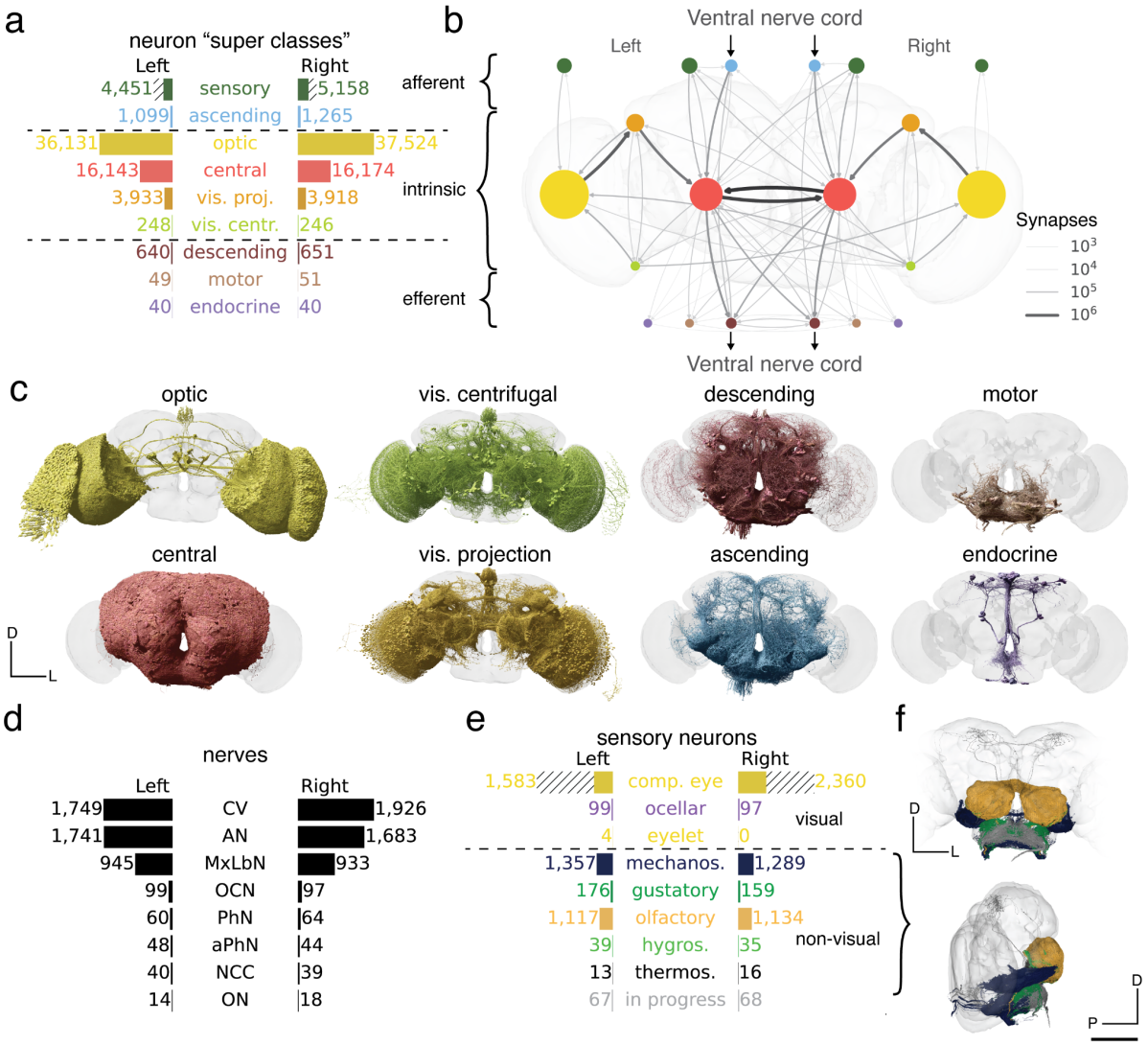

Figure 2. Neuron categories. (a) We grouped neurons in the fly brain by “flow”: intrinsic, afferent, efferent. Each flow class is further divided into “super classes" based on location and function. Neuron annotations are described in more detail in our companion paper by (Philipp Schlegel et al. 2023). The first public release is missing ~8,000 retinula cells in the compound eyes and four eyelets in one hemisphere which are indicated by hatched bars. (b) Using these neuron annotations, we created an aggregated synapse graph between the super classes in the fly brain. (c) Renderings of all neurons in each super class. (d) There are eight nerves into each hemisphere in addition to the ocellar nerve and the cervical connective (CV). All neurons traversing the nerves have been reconstructed and accounted for. (e) Sensory neurons can be subdivided by the sensory modality they respond to. In FlyWire, almost all sensory neurons have been typed by modality. The counts for the medial ocelli were omitted and are shown in Fig. 7b. (f) Renderings of all non-visual sensory neurons. Scale bar: 100 µm

While the above statistics are based on neuron numbers, they are conceptually related to volume-based measures of encephalization used in studies of brain evolution (Jerison 1955). For comparison, the rat brain occupies 65% of its central nervous system by volume (Swanson 1995). Our neuron-based measure of encephalization cannot yet be computed for rodents, but this will become possible as connectomics continues to scale.

Afferent and efferent neurons

Brain neurons that are not intrinsic can be divided into two categories, depending on the locations of their cell bodies. For afferent (sensory, ascending) neurons, the cell body is outside the brain, while for efferent (descending, motor, endocrine) neurons, the cell body is contained in the brain. Overall, it is generally accurate to think of an afferent neuron as a brain input, and an efferent neuron as a brain output. The relation to information flow is actually more subtle, however, as many fly neurites carry some mixture of presynapses and postsynapses on both dendrites and axons (Eckstein et al. 2023; Winding et al. 2023; Schneider-Mizell et al. 2016).

Schlegel et al. exhaustively identified all afferent and efferent neurons contained in cross sections of nerves and the neck connective running between the brain and VNC (Fig. 2d). Almost 95% of these neurons were in the neck connective, antennal nerve, and maxillary-labial nerve. Although afferents are truncated in our reconstruction, Schlegel et al. (Philipp Schlegel et al. 2023) along with other community members (Eichler et al. 2023; H. Kim et al. 2020) were able to determine the sensory organs corresponding to 5,362 of the 5,495 non-visual sensory neurons (Fig. 2e,f). Non-visual sensory neurons enter the brain through nerves (Fig. 2d) that mostly terminate in the antennal lobe or the SEZ (we define the SEZ as containing the following neuropils: SAD, GNG, AMMC, and PRW (Sterne et al. 2021); see Ext. Data Fig. 1-1 for neuropil definitions). The antennal lobe (AL) is the first relay center for processing of olfactory information, and many of the olfactory receptor neuron (ORN) inputs to the AL were reconstructed in the hemibrain as well. The SEZ receives more diverse inputs, including the projections of both mechanoreceptor and gustatory receptor neurons - these projections were not contained in the hemibrain. The nerves contained few efferent neurons, among which were head motor neurons (N=100) or endocrine neurons (N=80) (Fig. 2a,b,c). A large fraction of efferent neurons have branches in the SEZ, including most of the 100 motor neurons.

Visual afferents are by far the most numerous kind of sensory input, and enter the brain directly rather than through nerves. This is the last class of neuron that remains to be fully proofread. There are photoreceptor axons coming from the compound eyes (~12,800 of which N=3,943 have already been proofread in both eyes), ocelli (N=270), and eyelets (8 of which N=4 have been proofread).

The neurons traversing the neck connective were grouped into 1,303 efferent (descending) and 2,364 afferent (ascending) neurons (Fig. 2a,b,c). In a companion paper, Eichler et al. (*in prep*) typed these neurons and matched them to reconstructions from two separate EM datasets of a VNC (Phelps et al. 2021; Azevedo et al. 2022; Cheong et al. 2023).

Optic lobes and central brain

Of the 114,423 intrinsic neurons, 32,422 are fully contained in the central brain, and 73,655 are fully contained in the optic lobes and ocellar ganglia (this number excludes the photoreceptors, which are sensory afferent neurons, see above). Given that the visual areas dominate the count, it seems safe to say that *Drosophila* is a highly visual animal. The optic lobes, which are largely absent from the first larval instar, are a major reason that the adult fly brain so dominates its nervous system.

The optic lobes and ocellar ganglia also contain 7,851 neurons that project into the central brain, so called visual projection neurons (VPNs). We provide a more detailed analysis of connections in the ocellar ganglion in Fig. 7. Many VPNs are columnar types that tile the visual field. VPNs target specific neuropils (e.g., AOTU, PLP, and PVLP) or optic glomeruli (Wu et al. 2016; Otsuna and Ito 2006) in the central brain. The influence of VPNs can be very strong; 879 central neurons receive more than half their synapses from VPNs.

The hemibrain already characterized many VPN types along with their outputs in the central brain (Scheffer et al. 2020). Our whole brain reconstruction reveals many other aspects of VPN connectivity, such as their inputs in the medulla, lobula, or lobula plate - Schlegel et al. have typed these neurons based on their axonal projections in the brain and comparing to reconstructions in the hemibrain (Scheffer et al. 2020). In addition to feedforward targeting of central neurons, VPNs make 20% of their synapses onto other VPNs, and 21% onto optic lobe neurons. Companion papers investigate the visual projections to the central complex (Kim et al, *in prep*) and the mushroom body (Heckman and Clowney, *in prep*).

There are 494 neurons that project from the central brain to the optic lobes (Otsuna and Ito 2006). We call these visual centrifugal neurons (VCNs), and they are distinct from previously defined types of visual centrifugal neurons that are fully contained in the optic lobe, and their functions are mostly unknown. VCNs are 15× less numerous than VPNs. Nevertheless, half of all optic lobe neurons receive 5 or more synapses from VCNs, showing that much early visual processing incorporates feedback from the central brain. Centrifugal inputs to the retina are found in many vertebrate species, including humans (Repérant et al. 2006).

Many VCNs arborize broadly in the optic lobe, appearing to cover the entire visual field. Some VCNs, however, cover only a subset of columns within a portion of the visual field. A few optic lobe neurons receive as many as 50% of their synapses from VCNs. These belong to the class of peptidergic neurons involved in circadian rhythmicity, which are detailed in a companion paper (Zandawala et al., *in prep*). Tm5c is a columnar type (necessary for *Drosophila*'s preference for UV over visible light (Karuppudurai et al. 2014)) with more than 10% of its input from VCNs.

A lamina wide-field neuron (Lawf2) can receive more than 10% of its input from VCNs, and a major input source is octopaminergic (OA-AL2b2). It was previously shown that gain modulation of Lawf2 neurons increases during flight (Tuthill et al. 2014), and this effect is mimicked by bath application of octopamine. Transcriptomic studies showed that Lawf2 neurons express octopamine receptors at high levels (Davis et al. 2020).

Neuron super-classes

The neuron classes introduced above are organized into a hierarchy, as explained in our companion paper (Philipp Schlegel et al. 2023). The three "flow" classes (afferent, intrinsic, efferent) are divided into nine "super-classes" mentioned above (Fig. 2a). A simplified representation of the connectome as a graph in which nodes are super-classes is shown in Fig. 2b. Node sizes reflect neuron number, and link widths indicate connection number. This is the first of several simplified representations that we will introduce to tame the complexity of the connectome. Before continuing in this vein, we pause to discuss the properties of individual neurons and synapses.

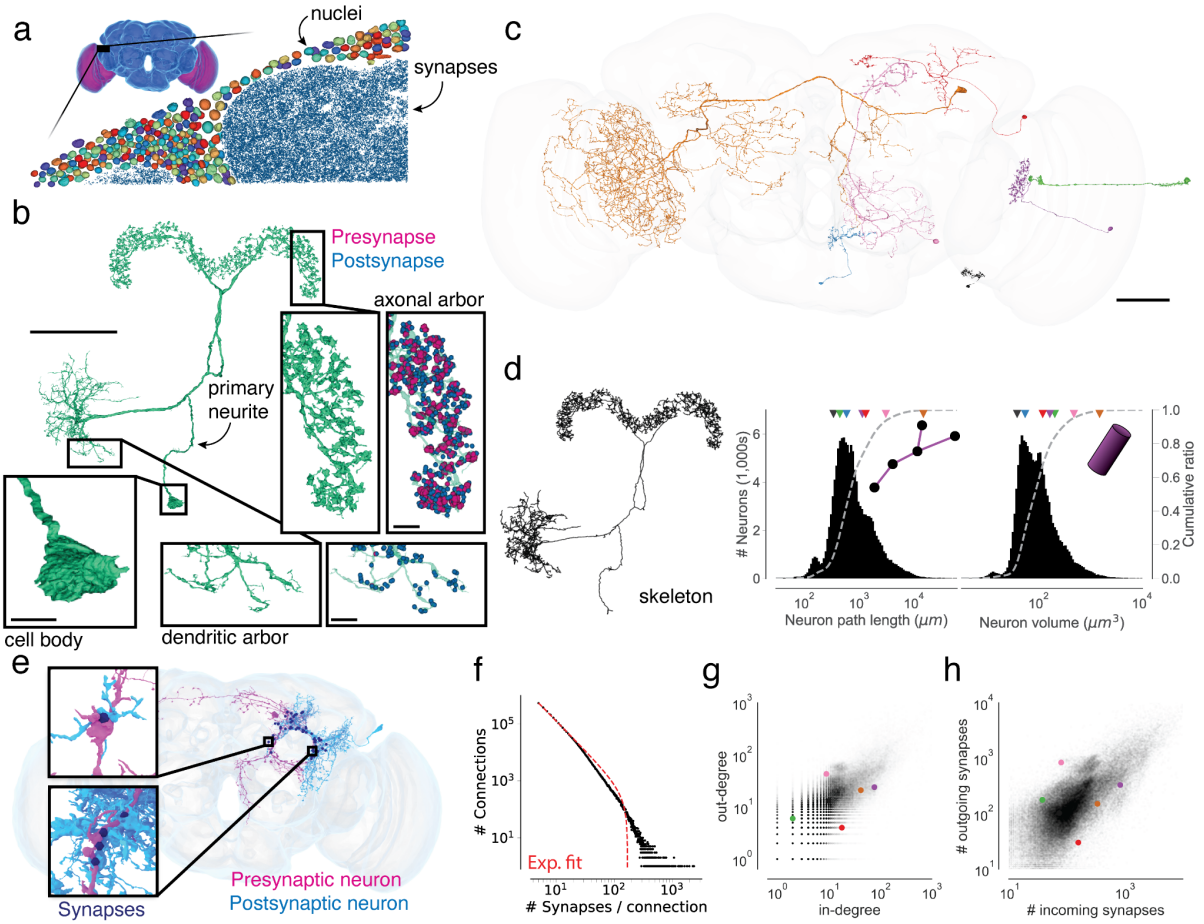

Figure 3. Neuron and connection sizes. (a) The synapse-rich (synapses in blue) neuropil is surrounded by a layer of nuclei (random colors) located at the outside of the brain as well as between the optic lobes (purple) and the central brain (blue). (b) An LPsP neuron can be divided into morphologically distinct regions. Synapses (purple and blue) are found on the neuronal twigs and only rarely on the backbone. (c) We selected seven diverse neurons as a reference for the following panels. (d) The morphology of a neuron can be reduced to a skeleton from which the path length can be measured. The histograms show the distribution of path length and volume (the sum of all internal voxels) for all neurons. The triangles on top of the distributions indicate the measurements of the neurons in (b). (e) Connections in the fly brain are usually multisynaptic as in this example of neurons connecting with 71 synapses. (f) The number of connections with a given number of synapses and a fitted truncated power law distribution. (g) In degree and out degree of intrinsic neurons in the fly brain are linearly correlated (R=0.76). (h) The number of synapses per neuron varies between neurons by over a magnitude and the number of incoming and outgoing synapses is linearly correlated (R=0.80). Only intrinsic neurons were included in this plot. Scale bars: 50 µm (b, c), 10 µm (b-insets)

Neurons and glia

A basic property of the fly brain is that cell bodies are spatially segregated from neurites. Cell bodies reside near the surface (“rind”) of the brain (Fig. 3a), surrounding a synapse-rich interior that mainly consists of entangled neurons and glia, fiber bundles or tracts, as well as tubules of the tracheal system (Fig. 1f, Ext. Data Figure 1-4a, Colodner et al*, in prep*).

A typical non-sensory *Drosophila* neuron is unipolar and consists of a primary neurite that leaves the cell body (soma), enters the neuropil, and branches into secondary and higher-order neurites (Fig. 3b). Secondary neurites can sometimes be classified as axons if

presynapses clearly dominate, or dendrites if postsynapses clearly dominate (Eckstein et al. 2023; Winding et al. 2023; Schneider-Mizell et al. 2016). Such an axon-dendrite distinction was made, for example, when defining visual projection and centrifugal neurons above.

But some mixture of presynapses and postsynapses is generally found on all non-primary neurites (Fig. 3b). In addition, the soma of insect neurons is separated from the main processes via a typically thin neural filament (primary neurite, Fig. 3b). Given this structure, the concept that signals pass from dendrites to soma to axon, which is often a good approximation for mammalian neurons, does not apply for non-sensory neurons in the fly.

Neurons vary greatly in size and shape (Fig. 3c). We computed skeletons for all reconstructed neurons (Fig. 3d) to measure neuronal path lengths. The median path length of a neuronal arbor was 656 μm (Fig. 3d). It has been argued that branched arbors are optimal for achieving a high degree of connectivity with other neurons (Chklovskii 2004). Neurons with short path lengths are exceptions, and can be found in both the optic lobes and central brain. Path length and volume both varied over two orders of magnitude (Fig. 3d, path length percentiles: 0.1%: 0.059 mm, 99.9%: 19.211 mm, volume percentiles: 0.1%: 80 μm^3, 99.9%: 459 μm^3). In total, the brain contains ~146 m of neuronal path length.

Sizes vary significantly between different cell superclasses (Ext. Data Fig. 3-1a-f). Optic lobe neurons are on average much shorter than central brain neurons (0.70 mm vs 2.15 mm on average) and take up a smaller volume (0.0066 mm^3 vs 0.0086 mm^3 total neuronal volume), which is why the optic lobes dominate the brain by neuron number but not by volume or synapse count. Visual centrifugal neurons are among the largest in the brain, and larger on average than visual projection neurons (5.05 mm vs 1.56 mm on average). While we measured much shorter path lengths and volumes for afferent neurons because only part of their axonal arbors is contained within the brain (Ext. Data Fig. 3-1b,e), arbors of efferents, motor and descending neurons which also have some of their arbor outside the brain, were among the largest we measured (Ext. Data Fig. 3-1c,f).

A small fraction of brain volume is glial cells, which are categorized in six types (Kremer et al. 2017; Yildirim et al. 2019). We estimated that 13% of the cell bodies in the EM dataset are non-neuronal or glial (Mu et al. 2021). Only a few astrocyte-like glia have been proofread (Ext. Data Fig. 1-4b). Sheet-like fragments of ensheathing glia are readily found near fiber bundles in the automated reconstruction. Further proofreading of glia could be prioritized in the future if there is community demand.

Synapses and connections

Our connectome includes only chemical synapses; the identification of electrical synapses awaits a future EM dataset with higher resolution (see Discussion). We use the term “synapse” to mean chemical synapse. A *Drosophila* synapse is generally polyadic, meaning that a single presynapse communicates with multiple target postsynapses (Fig. 1e). FlyWire represents a polyadic synapse as multiple synapses, each of which is a pair of presynaptic and postsynaptic locations (Buhmann et al. 2021). Polyadic synapses are common in other invertebrate species, such as *C. elegans*, and exist in some mammalian brain structures (e.g. retina).

We define a connection from neuron A to neuron B as the set of synapses from A to B. A connection typically contains multiple synapses, and the number can be large (Fig. 3 e,f). Connections with less than 10 synapses are typical, but a single connection can comprise >100 synapses (N=14,969) or even >1,000 synapses (N=27). The strongest connection was from a visual centrifugal neuron (LT39) onto a wide field lobula neuron (mALC2), and contained over 2300 synapses.

These numbers are much larger than the report of a maximum of 41 synapses connecting a pair of *C. elegans* neurons (Cook et al. 2019). To model such a distribution with a long tail, (Scheffer et al. 2020) used a power law with exponential cutoff (Fig. 3g). Our fit found comparable parameters, but the fit to our whole-brain distribution of connection strengths was not as good as their fit to the hemibrain distribution. A similar power law is also a reasonable fit to the distribution of connection strengths in *C. elegans*.

Setting a threshold of ≥5 synapses for determining a (strong) connection is likely to be adequate for avoiding false positives in the dataset, but not missing connections (see Methods). There are 2,613,129 such connections between the 124,891 identified neurons. There are several reasons to focus on strong connections. First, a connection with many synapses is expected to be strong in a physiological sense, other things being equal. Second, strong connections are likely to be more reproducible across individuals (Hall and Russell 1991; Witvliet et al. 2021; Philipp Schlegel et al. 2023)(Philipp Schlegel et al. 2023)(Hall and Russell 1991; Witvliet et al. 2021; Philipp Schlegel et al. 2023). Third, higher accuracy (both precision and recall) of automatic detection is expected for strong connections, assuming that errors are statistically independent (Schneider-Mizell et al. 2016; Scheffer et al. 2020).

One of the most basic properties of a node in any network is its degree, the number of nodes to which it is linked. To characterize the degree distribution in the *Drosophila* connectome, we focused on intrinsic neurons (N=114,423) because, unlike afferent and efferent neurons, they do not suffer from undercounting of connections due to truncation.

For any neuron, in-degree is defined as its number of presynaptic partners (input neurons), and out-degree is defined as its number of postsynaptic partners (output neurons). The median in-degree and out-degree of intrinsic neurons are 11 and 13 (Fig. 3g), respectively, with the restriction mentioned above to connections involving five or more synapses. These median values do not seem dramatically different from the median in-degree and out-degree of 10 and 19 for neurons in the *C. elegans* hermaphrodite, considering that the latter contains several hundred times fewer neurons than *Drosophila*.

The neuron in the *Drosophila* brain with maximum degree is a visual GABAergic interneuron (CT1), with 6329 postsynaptic partners and 4999 presynaptic partners. CT1 arborizes exclusively in the medulla neuropil of the optic lobe - indeed, most neuropils of the *Drosophila* brain contain one or a few large GABAergic neurons private to that neuropil, with high in-degree and out-degree (see Lin et al., *in prep*, for more analysis on connectivity motifs in FlyWire); these neurons are considered to be important for local feedback gain control (Prisco et al. 2021; Hong and Wilson 2015). In a *C. elegans* hermaphrodite (Cook et al. 2019), the neuron with maximum degree is a command interneuron for backward locomotion (AVAL), with 110 postsynaptic partners and 64 presynaptic partners. The

existence of neurons with much higher degree is a marked way in which the *Drosophila* connectome differs from that of *C. elegans*. That being said, the degree of AVAL is large in a relative sense because it is a large fraction of the total *C. elegans* neuron number (302).

The number of synapses established by a neuron is correlated with its total neurite path length (R=0.80 (pre), R=0.89 (post), Ext. Data Fig. 3-1g). Presynapse and postsynapse counts are similarly correlated per neuron (R=0.80, Fig. 3h). We asked whether large neurons tend to use their many synapses to create stronger connections with individual neurons versus more connections with many different neurons. The total number of synapses established by a neuron was much better correlated with its in and out degrees (R=0.93, R=0.93 respectively) than its average connection strength (R=0.26, R=0.31 respectively, Ext. Data Fig. 3-1h,i). It remains to be tested whether the additional partners are from the same or different cell types.

Connections and neurons are not necessarily the functional units of neural computation. For certain large fly neurons, the arbors are composed of multiple compartments that function somewhat independently (Meier and Borst 2019; Amin et al. 2020). Perhaps these subcellular compartments, rather than whole cells, should be regarded as nodes of the connectome. Then CT1 would be replaced by many nodes with lower degrees. And the connection from LT39 to mALC2 would be replaced by many connections with fewer synapses between compartments of these neurons. A connectome of neuronal compartments can in principle be studied using our resource, which includes the location of every synapse.

Neurotransmitter identity

A statistical prediction of the small molecule neurotransmitter (GABA, glutamate, acetylcholine, serotonin, dopamine, and octopamine) secreted by each neuron is available. A number of validations suggest that the predictions are highly accurate in aggregate (Eckstein et al. 2023), though for any given synapse the prediction could be wrong. We assume that every neuron secretes a single small molecule neurotransmitter and combine the predictions for all outgoing synapses to an estimate which we assign to all outgoing synapses of a neuron, i.e. we assume neurons obey Dale's law, although it is known that co-transmission does occur in the fly brain (Sherer et al. 2020; Mao and Davis 2009; Waddell et al. 2000; Croset, Treiber, and Waddell 2018).

GABAergic and glutamatergic neurons had much higher degrees than cholinergic neurons (Ext. Data Fig. 3-1j). Across all neuron categories, we found that GABAergic neurons were on average longer than glutamatergic and cholinergic neurons (Ext. Data Fig. 3-1k).

As a rule, we will assume that cholinergic neurons are excitatory and GABAergic and glutamatergic neurons are inhibitory(Molina-Obando et al. 2019; McCarthy et al. 2011; Lu et al. 2022; Liu and Wilson 2013). A companion paper identifies all GABAergic and glutamatergic neurons that are bidirectionally coupled with large numbers of cholinergic neurons (Lin et al., *in prep*). This reciprocal inhibitory-excitatory motif is widespread throughout the fly brain (Lin et al. 2014; Scheffer et al. 2020).

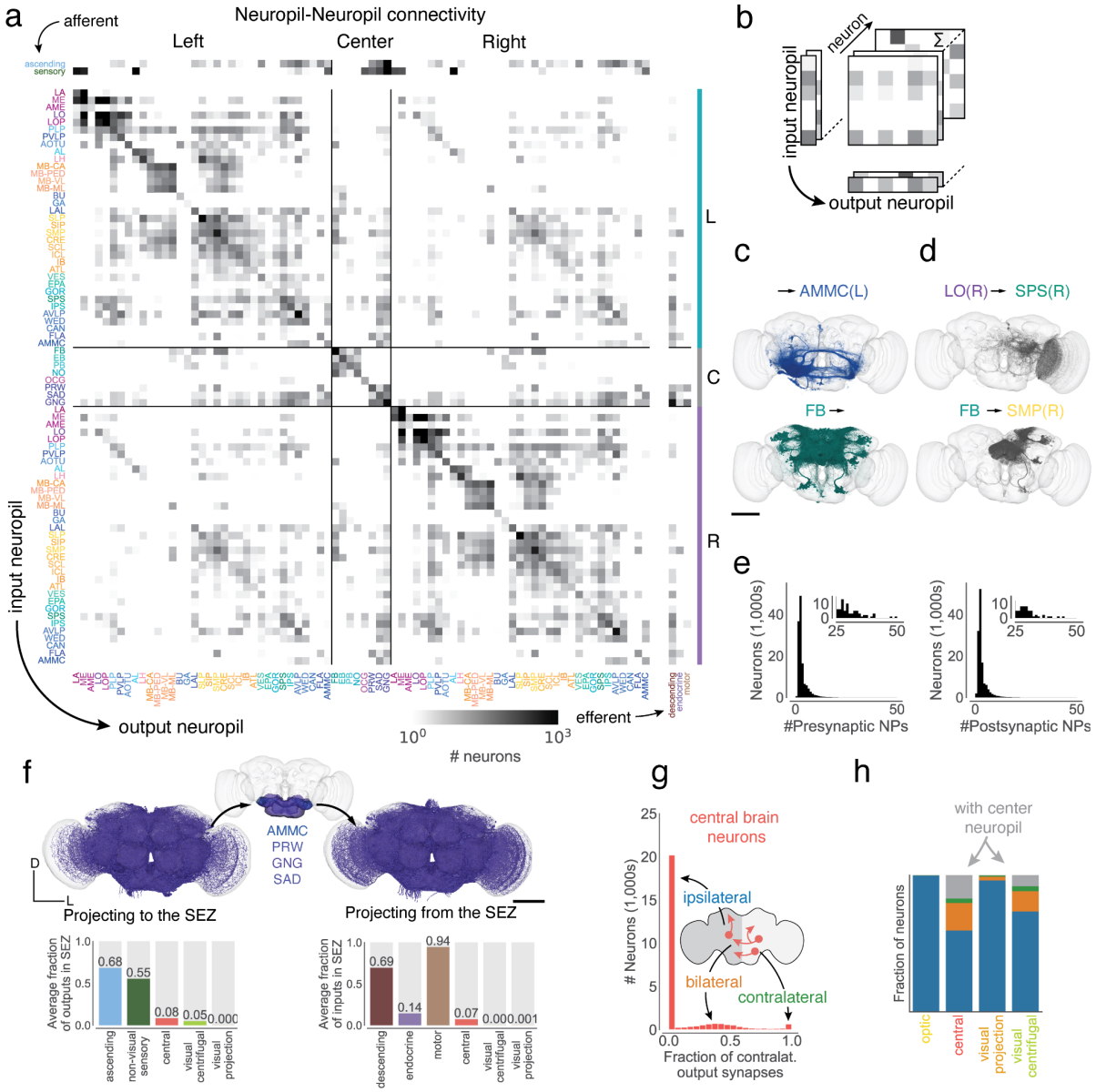

Figure 4. Neuropil projections and analysis of crossing neurons. (a) Whole brain neuropil-neuropil connectivity matrix. The main matrix was generated from intrinsic neurons, and afferent and efferent neuron classes are shown on the side. Incoming synapses onto afferent neurons and outgoing synapses from efferent neurons were not considered for this matrix. See Ext. Data Fig. 4-1 for neurotransmitter specific matrices. (b) Cartoon describing the generation of the matrix in (a). Each neuron's connectivity is mapped onto synaptic projections between different neuropils. (c) shows examples from the matrix with each render corresponding to one row or column in the matrix and (d) shows examples from the matrix with each render corresponding to one square in the matrix. (e) Most neurons have pre- and postsynaptic locations in less than four neuropils. (f) Renderings (subset of 3,000 each) and input and output fractions of neurons projecting to (N=11916) and from (N=7528) the SEZ. The SEZ is roughly composed of five neuropils (the AMMC has a left and right homologue). Average input and output fractions were computed by summing the row and column values of the SEZ neuropils in the super class specific projection matrices. (g) Fraction of contralateral synapses for each central brain neuron. (h) Fraction of ipsilateral, bilateral, contralateral, neurons projecting to and from the center neuropils per super class. (i) Morphology of ipsilateral, bilateral, and contralateral neurons from one hemisphere of all intrinsic super classes (up to 3,000 neurons per plot). Scale bars: 100 µm

From connectome to projectome

For mammals, tracer injection studies have mapped the axonal projections between brain regions of mouse (Zingg et al. 2014; Oh et al. 2014; Harris et al. 2019) and macaque (Felleman and Van Essen 1991; Markov et al. 2014). In fly, large numbers of light microscopic reconstructions of single neurons have been aggregated to map projections between brain regions (Meissner et al. 2023; Chiang et al. 2011; Shih et al. 2015). Such maps have been called projectomes (Kasthuri and Lichtman 2007) or mesoscale connectomes (Sporns, Tononi, and Kötter 2005). In such techniques, the sampling of axons is difficult to control, which means that accurate quantification of projection strength is challenging.

Here we compute a projectome from a synapse-level connectome (Fig. 4a, Ext. Data Fig. 4-1). The interior of the fly brain has been subdivided into hierarchical neuropil regions (Ito et al. 2014) (Ext. Fig. 1-1, Fig. 1d). Our fly projectome is defined as a map of projections between these neuropil regions. Because cell bodies are spatially separated from neuropils, a fly neuron cannot typically be assigned to a single brain region. This is unlike the situation for a mammalian neuron, which is conventionally assigned to the region containing its cell body. A typical fly neuron belongs to multiple neuropils.

The projectome is a neuropil-neuropil matrix computed as follows. Each intrinsic neuron contributes to the projections between neuropils where it has pre- and postsynaptic sites. We weighted neuron projections by the product of the respective number of synapses and normalized the result for every neuron such that the matrix sums to the total number of intrinsic neurons. Each column corresponds to all the neurons projecting to a neuropil and each row to all neurons projecting out of it (Fig. 4b). Each square then represents the summed fractional weight of all neurons projecting between two neuropils (Fig. 4c,d). We added afferent and efferent neurons to the matrix by calculating the sum of the weighted neuron projections per super class to and from all neuropils respectively.

While each neuropil is connected to many others, most neurons have synaptic sites in only a few neuropils (Fig. 4e). We repeated this process for each fast neurotransmitter type (Ext. Fig. 4-1). Some neuropil-neuropil connections exist strongly for one neurotransmitter but not others. For example, the neuropils making up the central complex (FP, EB, PB, NO) and the mushroom body (MB-CA, MB-PED, MB-VL, MB-ML) are largely tied together by excitatory connections.

We observed a strong symmetry between projections in the left and right hemisphere as well as with the central neuropils located on the midline (Ext. Data Fig. 4-2a,b); this highlights the strong similarity between the two sides of the brain. We observed that contralateral projections (projections from one side of the brain to the other) were generally weaker than projections to the same or ipsilateral neuropil (Ext. Data Fig. 4-2c).

The SEZ (Fig. 4f) is the ventral portion of the central brain, and has been shown to contribute to a variety of behaviors (Sterne et al. 2021). It is almost wholly unrepresented in the hemibrain reconstruction (Scheffer et al. 2020), and is also unreconstructed in the larval brain (Winding et al. 2023). The five neuropils in the SEZ (left and right AMMC, GNG, SAD, and PRW; Fig. 4f) amount to 17.8% of central brain neuropil volume (0.0018 mm^3 of 0.0103

mm^3); they contain afferents mostly from non-visual sensory neurons (mechanosensory and taste) and ascending neurons, as well as a large number of efferents (motor, endocrine, and descending neurons - in fact, descending neurons receive on average 69% of their inputs in one of the five SEZ neuropils). The SEZ is thus important for information flow to and from the brain. Judging from the projectome (Fig. 4a), the SEZ neuropils interact with almost all parts of the brain. Notable exceptions are the central complex (EB, FB, PB, and NO) and the mushroom body (MB), suggesting less crosstalk between those circuits and neurons in the SEZ (explored in more detail in Fig. 6).

Hemispheric organization

Our reconstruction includes both left and right brain hemispheres. This is important for tracing sensorimotor pathways that cross from one side to the other, and more generally for understanding interactions between the two hemispheres. The projectome (Fig. 4a) already reveals that most projections (88%) are ipsilateral or between neuropils on the same side of the brain.

The low fraction of non-ipsilateral neurons is primarily due to their scarceness in the optic lobes. Only 157 neurons (0.2%) in the optic lobes cross hemispheres, and cross the central brain without making synapses there (Supplemental Information 2) - these neurons are considered to be “fully contained” in the optic lobes because our definition depends only on synapse locations. These neurons mediate direct interactions between the two optic lobes, and their rarity suggests that these interactions represent a smaller fraction of the computations that occur within the optic lobes. Integration of information from both eyes may rely more on the abundant crossing connections between the central brain targets (AOTU, PLP, PVLP) of VPNs.

A higher proportion (40%) of central brain neurons are non-ipsilateral, largely owing to central neuropils, like those of the central complex and SEZ. To classify non-ipsilateral neurons, we started by examining the spatial distributions of their postsynapses (inputs). We divided the neuropils into three categories. Left and Right included the neuropils that come in mirror-symmetric pairs. Center included the seven remaining neuropils that are located on the midline. For each neuron, we computed the proportions of its postsynapses in Left, Right, and Center neuropils (Ext. Fig. 4-3). Each neuron was assigned to the dominant category, and near-ties were rare. The exceptions are symmetric neurons with cell bodies at the midline of the brain (Ext. Data Fig. 4-4, N=106).

Next, we asked how many neurons of Left and Right categories have presynapses (outputs) in the other hemisphere. Similar to the analysis of the 1st instar larval connectome (Winding et al. 2023), we found that neurons projecting to the other hemisphere can be grouped into bilateral neurons, those with outputs in both hemispheres, and contralateral neurons which almost exclusively had presynapses in the other hemisphere (Fig. 4g-i). Notably, many more visual centrifugal neurons projected to the contralateral hemisphere than visual projection neurons, and both visual centrifugal neurons and neurons of the central brain contain a large fraction of bilateral neurons (Fig. 4h) - as stated earlier, this analysis again revealed the dominance of ipsilateral connections in the brain. While mixing between the hemispheres is more rare, mixing between sensory modalities within a hemisphere is common (see Fig. 6 below).

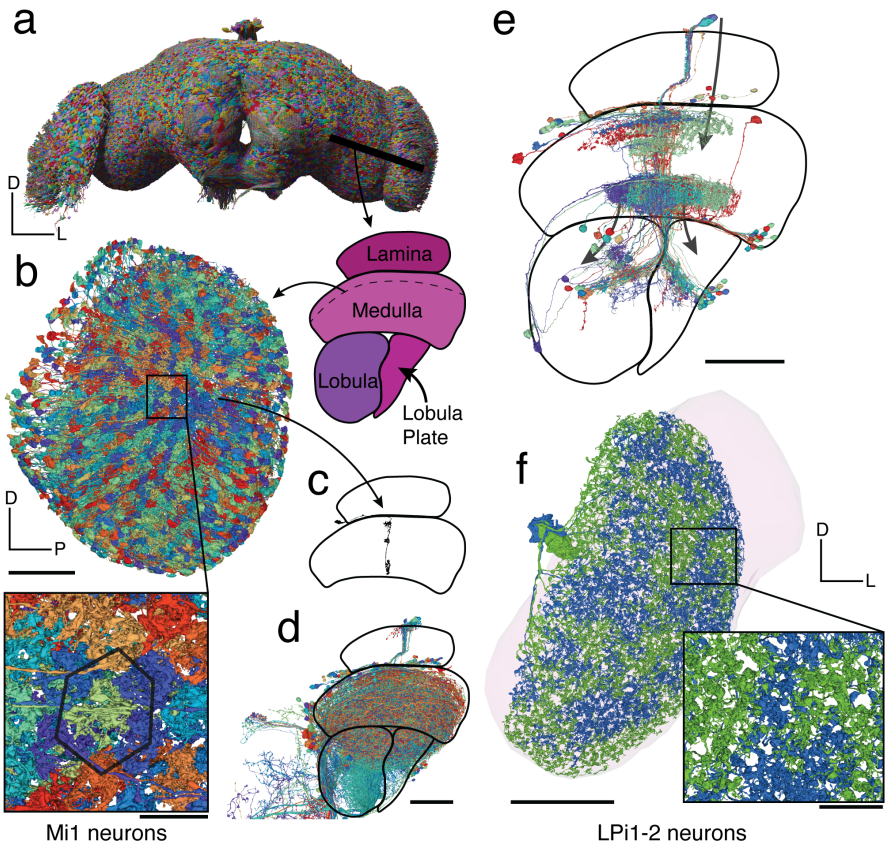

Figure 5: Optic lobes. (a) Rendering of a subset of the neurons in the fly brain. A cut through the optic lobe is highlighted. (b) All 779 Mi1 neurons in the right optic lobe. (c) A single Mi1 neuron, (d) all neurons crossing through the column in c as defined by a cylinder in the medulla with 1 µm radius through it, and (e) all neurons sharing a connection with the single Mi1 neuron shown in (c) (≥ 5 synapses) - 3 large neurons (CT1, OA-AL2b2, Dm17) were excluded for the visualization. (f) The two LPi1-2 neurons in the right lobula plate (neuropil shown in background). Scale bars: 50 µm (b,c,d,e,f), 10 µm (b-inset)

Many types of fly neurons are known to exhibit striking stereotypy across individuals, and also across both hemispheres of the same individual. A companion paper shows quantitatively using FlyWire and hemibrain data that these two kinds of stereotypy are similar in degree (Philipp Schlegel et al. 2023).

Optic lobes: columns and beyond

So far we have mentioned neurons that connect the optic lobes with each other, or with the central brain. The intricate circuitry within each optic lobe is also included in FlyWire's connectome. Photoreceptor axons terminate in the lamina and medulla, neuropils of the optic lobes (Fig. 5a,b). Each eye contains approximately 800 ommatidia that map to columns in the lamina arranged in a hexagonal lattice (Fig. 5b). This structure repeats in subsequent neuropils from lamina to medulla to lobula to lobula plate. The neuropils have been finely subdivided into layers that are perpendicular to the columns (Fischbach and Dittrich 1989). The 2D visual field is mapped onto each layer. Any given cell type prefers to synapse in some subset of the layers. Cell types vary greatly in size. Uni-columnar cell types are the smallest (Fig. 5b,c). At the other extreme are large cells that span almost all columns (Fig.

5d). In between there are many multi-columnar cell types that are still being classified (Fig. 5e).

Mi1 is a true “tiling” type, i.e., its arbors cover the visual field with little or no overlap, and have similar size and shape (Fig. 5b). Dm12 arbors overlap with each other, but the spatial arrangement is still regular. These and other distal medullary cell types were previously characterized by multicolor light microscopy (Nern, Pfeiffer, and Rubin 2015). Our EM reconstructions reveal even more detailed information about the spatial patterning of these types (e.g., co-fasciculation of neurites of neighboring Dm12 cells). More importantly, FlyWire’s reconstruction encompasses all multi-columnar cell types, including those outside the medulla. Judging from the many examples we have studied throughout the optic lobe, it seems that regular coverage of the visual field without gaps is a defining criterion for most cell types, similar to mammalian retina (Bae et al. 2018). There are, however, exceptional cell types that cover the visual field in an irregular manner. For example, there are exactly two LPi1-2 cells per optic lobe (Shinomiya et al. 2022). The shapes of each pair are complementary, as if they were created by cutting the visual field into two pieces with a jigsaw (Fig. 5f); this tiling was not evident when reconstructing only a portion of an optic lobe (Shinomiya et al. 2022).

Much of the existing research on widefield visual motion processing has relied on the simplifying idea that the computations are mostly in columnar circuits, and the columnar outputs are finally integrated by large tangential cells in the lobula plate. This research has been aided by wiring diagrams containing connections between cells in the same column or neighboring columns (S.-Y. Takemura et al. 2013; S. Takemura et al. 2017; Shinomiya et al. 2019). An absence of information across columns, has necessitated treating each column as identical in simulations of the optic lobe (Lappalainen et al. 2023). FlyWire’s connectome contains not only the columnar neurons (Fig. 5b), but also all neurons that extend across columns (Fig. 5d,e). These neurons are both excitatory and inhibitory, and can support interactions between even distant columns. This opens up the possibility of a much richer understanding of optic lobe computations, and this is explored in a companion paper on hue selectivity (Christenson et al. *in prep*).

Some columnar cell types are known to exhibit spatial gradients in connectivity (Dombrovski et al. 2023), and our reconstruction makes it possible to investigate such gradients for any columnar cell type in the optic lobe. Similar gradients have also been studied in mammalian retina (Yu et al. 2018), and such continuous variation is an interesting complement to the conventional notion that cell types are discrete.

Analysis of information flow

While afferent and efferent neurons make up a numerically small proportion of the brain (estimated 14.7% and 1.1% respectively), they are important because they connect the brain to the outside world. Examining connections to these neurons is useful when attempting to predict the functions of intrinsic neurons from the connectome. For example, one might try to identify the shortest path in the connectome from an afferent (input) neuron that leads to a given intrinsic neuron. The sensory modality of the afferent neuron could provide a clue as to the function of the intrinsic neuron. This approach, while intuitive, ignores connection strengths and multiplicities of parallel pathways. We therefore use a probabilistic model (P.

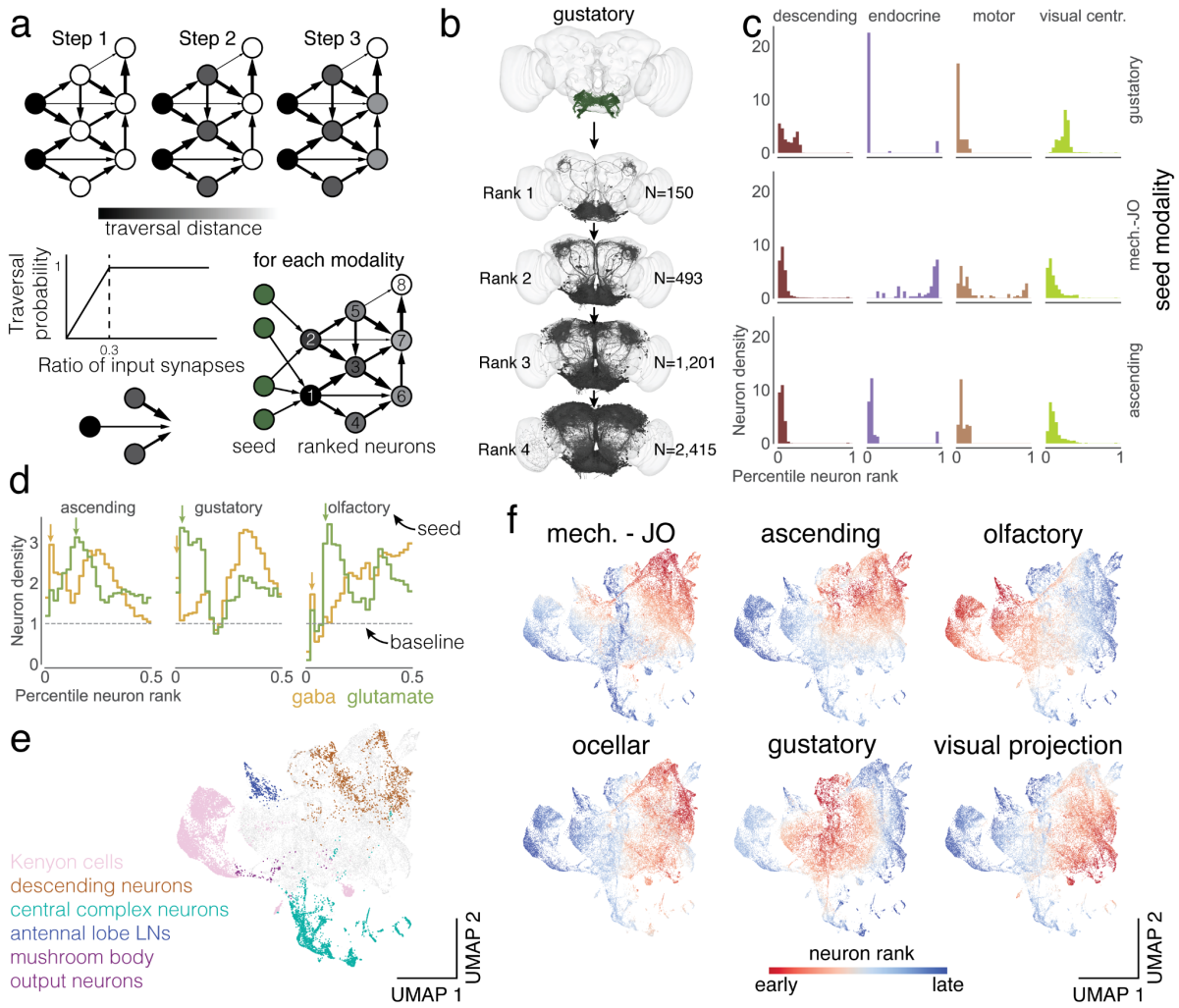

Figure 6. Information flow through the *Drosophila* central brain (a) We applied the information flow model for connectomes by Schlegel et al. (P. Schlegel et al. 2021) to the connectome of the central brain neurons. Neurons are traversed probabilistically according to the ratio of incoming synapses from neurons that are in the traversed. The information flow calculations were seeded with the afferent classes of neurons (including the sensory categories). (b) We rounded the traversal distances to assign neurons to layers. For gustatory neurons, we show a subset of the neurons (up to 1,000) that are reached in each layer. (c) For each sensory modality we used the traversal distances to establish a neuron ranking. Each panel shows the distributions of neurons of each super class within the sensory modality specific rankings (see Ext. Data Fig. 6-1a for the complete set). (d) We assign neurons to neurotransmitter types and show their distribution within the traversal rankings similar to (c). The arrows highlight the sequence of GABA - glutamate peaks found for almost all sensory modalities (see Ext. Data Fig. 6-1b for the complete set). (e) We UMAP projected the matrix of traversal distances to obtain a 2d representation of each neuron in the central brain. Neurons from the same class co-locate (see also Ext. Data Fig. 6-2) (f) Neurons in the UMAP plot are colored by the rank order in which they are reached from a given seed neuron set. Red neurons are reached earlier than blue neurons (see Ext. Data Fig. 6-1c for the complete set).

Schlegel et al. 2021) to estimate information flow in the connectome, starting from a set of seed neurons (Fig. 6a; see Methods).

The likelihood of a neuron being traversed increases with the fraction of inputs from already traversed neurons and caps out at an input fraction of 30%. We ran the traversal model for

every subset of afferent neurons as seeds (N=12 input modalities to the central brain, Fig. 6b, Fig. 2e, Supplemental Information 3, see Methods for full list). We then measured information flow from these starting neurons to all intrinsic and efferent neurons of the central brain (for this analysis, we ignore circuitry within the optic lobes, and consider VCNs (visual centrifugal neurons) as efferents of the central brain). We then ranked all neurons by their traversal distance from each set of starting neurons and normalized the order to percentiles. For instance, a neuron at the 20th percentile had a lower rank than 80% of neurons. This allowed us to determine how early information from each afferent modality reached various targets, including the descending neurons, endocrine neurons, motor neurons and visual centrifugal neurons (Fig. 6c, Ext. Data Fig. 6-1a). As expected, endocrine neurons are closest to the gustatory sensory neurons while motor and descending neurons were reached early for mechanosensory and visual afferents (Ext. Data Fig. 6-1a).

Do the afferent cell classes target inhibitory neurons early or late? We found that putative inhibitory neurons (neurons predicted to express GABA and glutamate) were overrepresented in the set of early neurons (Fig. 6d). Surprisingly, we identified a sequence of GABAergic and glutamatergic peaks in the sequence of neurons targeted that was replicated for almost all afferent modalities (Ext. Data Fig. 6-1b).

To visualize information flow in a common space, we treated the traversal distances starting from each seed population as a neuron embedding and built a UMAP projection from all of these embeddings (Fig. 6e). Within the map, we found that neurons of the same cell class (e.g. two groups of Kenyon cells, all mushroom body output neurons, all antennal lobe local neurons, and all central complex neurons) are clustered. Next, we displayed traversal order on top of the UMAP plot to compare traversal orders starting from different modalities. We find that every neuron in the central brain can be reached by starting from any modality - this “small world” property of the network is covered in more detail in a companion paper (Lin et al., *in prep*). Comparing orders revealed that almost all neurons in the central brain are reached early starting from some modality, with the exception of neurons in the central complex (Fig. 6f, Ext. Data Fig. 6-2), highlighting that the central complex is dominated by internal computations (Hulse et al. 2020). Kenyon cells were contained in two clusters - one of which is targeted very early from olfactory receptor neurons and the other targeted early by visual projection neurons (Vogt et al. 2016).

Our information flow analysis provides a compressed representation of the connectome, but ignores signs of connections and the biophysics of neurons and synapses, and therefore terms like “early” and “late” should not be interpreted as true latencies to sensory stimulation. A companion paper (Shiu et al. 2023) builds a leaky integrate-and-fire model of *Drosophila* brain dynamics, using the connectome and including connection weights (number of synapses) and putative connection signs (excitatory or inhibitory).

Cell types and other annotations

Neurons in *Drosophila* are considered to be identifiable across hemispheres and individuals (Luan et al. 2006; Pfeiffer et al. 2010), enabling cell type classification of all neurons in FlyWire - such classification is useful for generating testable hypotheses about circuit function from the connectome. FlyWire community members, experts in diverse regions of the fly brain, have shared 91,649 annotations of 59,548 neurons (Supplemental Information

4), including the majority of sexually-dimorphic neurons (Deutsch et al., *in prep*), sensory neurons (Eichler et al. 2023), as well as a diversity of cell types in the optic lobes and SEZ (Fig. 2f), two brain regions not covered in the hemibrain connectome. Each neuron in FlyWire is given a unique name based on the neuropil it receives and sends most of its synapses. Curation of these annotations continues, and we invite further community efforts to identify cell types, and these can be contributed through Codex (codex.flywire.ai).

In addition, matching between cell types identified in the hemibrain (Scheffer et al. 2020) and both hemispheres of FlyWire provides additional annotations for neurons contained in both datasets. Our companion paper (Philipp Schlegel et al. 2023) provides cell type annotations for 26,150 neurons via such matching.

All cell annotations can be queried in Codex. Some of these have already been mentioned, such as the “flow” annotations of intrinsic vs. afferent vs. efferent, super-class annotations of Fig. 2, neurotransmitter predictions, left-right annotations for cell body location, in addition to lineages, or groups of neurons derived from a single neuroblast (Schlegel et al. 2023).

Ocellar circuit structure and function: linking sensory inputs to motor outputs

The completeness of the FlyWire connectome enables tracing complete pathways from sensory inputs to motor outputs - here we demonstrate this capability by examining circuits that emanate from the ocellar ganglion and leveraging cell type information. In addition to the large compound eyes, flying insects have smaller visual sensory organs (Hofbauer and Buchner 1989), including the three ocelli on the dorsal surface of the head cuticle (Fig. 7a). The ocelli are under-focused eyes, projecting a blurry image of light level changes in the UV and blue color spectrum (Hu, Reichert, and Stark 1978; Stark, Sapp, and Carlson 1989); these eyes are thought to be useful for flight control and orientation relative to the horizon (Stange et al. 2002). Importantly, while the role of the ocelli has been hypothesized (e.g., light level differences between the eyes when the fly is shifted off axis should quickly drive righting motions of the head, wings, and body to stabilize gaze and re-orient the body), little is known about the circuitry downstream of this sensory organ that would mediate this function.

Photoreceptor axons (N=270) from the three ocelli innervate three distinct regions of the ocellar ganglion separated by glial sheets (Fig. 7a, b). The ocellar ganglion additionally contains 62 neurons that we categorized into four broad groups (Fig. 7c, Ext. Data Fig. 7-1a): local neurons (N=15), two types of interneurons, divided based on their arborizations and caliber (OCG01 (N=12), OCG02 (N=8)), descending neurons (DNp28, N=2), and centrifugal or feedback neurons (N=25). Ocellar local neurons are small (116 outgoing synapses, 449 µm path length on average) and connect sparsely with photoreceptors from all ocelli.

Twelve OCG01 interneurons and two descending neurons (DNp28, one per lateral ocellus) represent the main pathway from the ocellar ganglion to the central brain. DNp28 projects to the intermediate, haltere, wing, and neck tectula of the ventral nerve cord (Cheong et al. 2023; S.-Y. Takemura et al. 2023). In each ocellus, half of the OCG01s were inferred to express glutamate (likely inhibitory), and the other half acetylcholine (excitatory). There are four OCG01s per ocellus (Fig. 7d). OCG01s tile the ocellar ganglion, indicating their

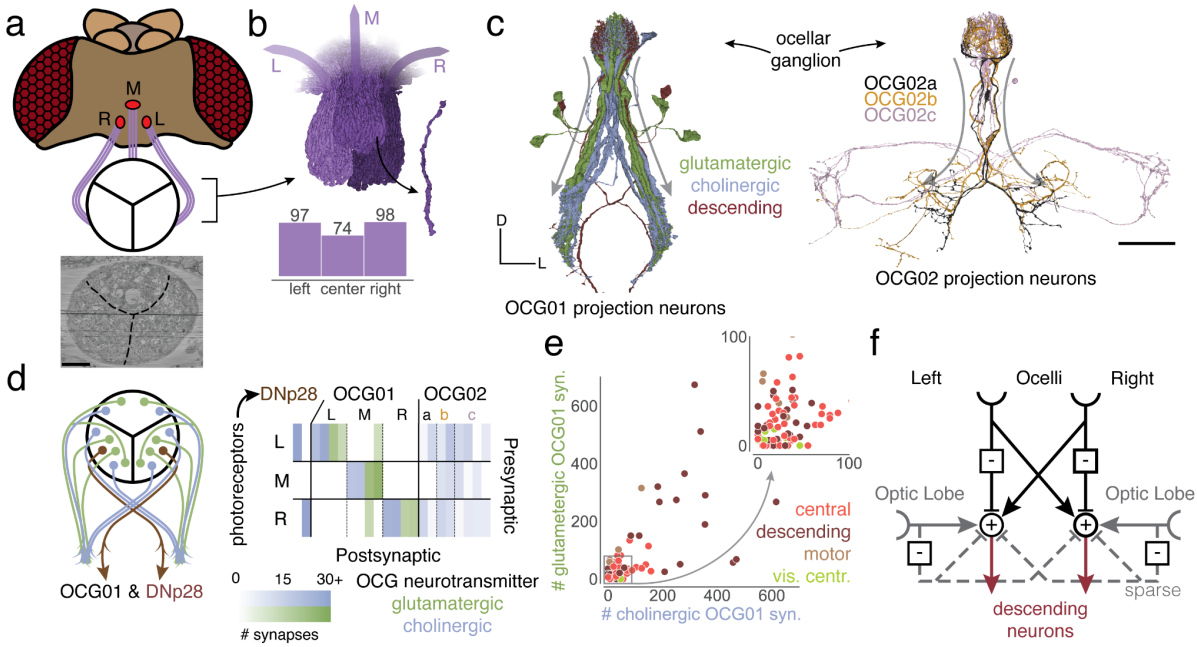

Figure 7. Ocellar circuits and their integration with visual projection neurons. (a) Overview of the three ocelli (left, medial, right) which are positioned on the top of the head. Photoreceptors from each ocellus project to a specific subregion of the ocellar ganglion which are separated by glia (marked with black lines on the EM). (b) Renderings of the axons of the photoreceptors and their counts, and (c) OCG01, OCG02 and DNp28 neurons with arbors. “Information flow” from pre- and postsynapses is indicated by arrows along the arbors. (d) Connectivity matrix of connections between photoreceptors and ocellar projection neurons, including two descending neurons (DNp28). (e) Comparison of number of glutamatergic and cholinergic synapses from ocellar projection neurons onto downstream neurons colored by super class (R=.65, p<1e-21). (f) Summary of the observed connectivity between ocellar projection neurons, visual projection neurons and descending neurons. Scale bar: 100 µm

receptive fields tile the visual fields of the ocelli (Ext. Data Fig. 7-1 b,c). OCG02 axons are much thinner than the OCG01s, and likely transmit signals slower. Two OCG02 subgroups (a, b) innervate similar neuropils to the OCG01s (IPS, SPS), and OCG02c neurons target the PLP, a brain region that also receives input from visual projection neurons from the compound eyes (Wu et al. 2016).

Neurons downstream from OCG01s in the IPS, SPS, and GNG receive inhibitory input from the ipsilateral ocellus and excitatory input from the contralateral ocellus (Fig. 7d, right), and the amount of synaptic input from each ocellus is tightly correlated (Fig. 7e, R=0.65, p<1e-21) - this balance is likely to be a key ingredient in how signals are integrated (the descending circuits are activated by a signal difference between the eyes). We found that 15 different descending neurons (DNs) each receive over 200 synapses from the OCG01 neurons. For example, two DNs in each hemisphere received over 30% of their synaptic inputs in the brain from ocellar projection neurons: DNp20/DNOVS1 (left: 57%, right: 44%), DNp22/DNOVS2 (left: 36%, right: 33%). DNOVS1 and other descending neurons with strong input from OCG01s generally receive strong input from ipsilateral visual projection neurons as well (Ext. Data Fig. 7-1d). For example, DNOVS1 is also activated by rotational optic flow fields across the compound eye, and projects to the neck motor system (Suver et al. 2016; Haag, Wertz, and Borst 2007). A handful of glutamatergic (putative inhibitory) visual

projection neurons sparsely innervate descending neurons in both hemispheres. As the ocelli transmit mainly information about light levels, the dense integration with motion direction signals from the compound eyes was not previously appreciated, but should aid in precision adjustments of head and body movements for gaze stabilization and flight control (A. J. Kim et al. 2017).

There is also extensive feedback from the brain directly to the ocellar ganglion via 25 ocellar centrifugal neurons (OCC). We found striking targeting specificity of two OCC subgroups (OCC01a, b) which synapse onto all OCG01 and DNp28 neurons with strong connections compared with their overall synaptic budget (Ext. Data Fig. 7-1e). The OCC01s receive input in a wide range of neuropils, notably the SEZ, as well as IPS and SPS, the same neuropils that receive inputs from the OCG projection neurons (Ext. Data Fig. 7-1f). It remains to be determined what role the OCCs play in gating visual information and potentially driving the OCGs in the absence of photoreceptor activity.

Based on the summary wiring diagram of Fig. 7f, we hypothesize how the pathways from the ocelli to descending neurons function. As in a Braitenberg vehicle for phototaxis (Braitenberg 1984), excitation and inhibition are organized so that the head and body of the fly should roll around the anteroposterior axis to orient the ocelli towards light. In this example, the whole-brain connectome, extending from brain inputs to outputs, uncovers new pathways and facilitates the generation of putative circuit mechanisms of sensorimotor behavior.

Discussion

By reconstructing a complete brain wiring diagram, FlyWire enables many kinds of studies that were not previously possible using wiring diagrams of portions of the fly brain. The optic lobes and the SEZ are two prominent regions mostly missing from the hemibrain, the previous state of the art. Both sides of the brain are included, enabling the tracing of pathways that cross the midline. Due to the presence of afferent and efferent neurons, one can trace pathways from sensory inputs to intrinsic neurons to brain outputs (motor, endocrine, and descending neurons). This was done in a global fashion using the information flow model, and more specifically to uncover the structure and hypothesize a circuit mechanism for behaviors supported by the ocelli. Our companion papers provide additional global analyses of the connectome (Lin et al., *in prep*) and studies of specific families of pathways.

Connectome annotation

Connectome annotation with structural and functional information is an important emerging field, analogous to genome annotation. Annotations are important because they make the connectome usable for hypothesis generation about circuit function. We carried out a hierarchical and systematic annotation of all neurons in the connectome as detailed in our companion paper (Philipp Schlegel et al. 2023), describing over 4000 robustly identifiable cell types. We also collected a large number of annotations from the community (57% of all neurons have an annotation label) leveraging a broad knowledge base - further curation of these labels will help to refine them.

Comparative connectomics

For the first time, one can now compare entire connectomes of different species, starting with *Drosophila melanogaster* and *C. elegans*, as touched on by the present manuscript, and explored in more depth by Lin et al (Lin et al., *in prep*). One can also compare connectomes of the same species at different developmental stages (Winding et al. 2023). While ours is still the only adult fly connectome, it can be compared with the hemibrain reconstruction where they overlap, to detect wiring differences between adults of the same species (Philipp Schlegel et al. 2023).

Connectomes, transcriptomes, and brain development

Transcriptomics with single cell resolution is being applied to mammalian brains (BRAIN Initiative Cell Census Network (BICCN) 2021), and to the *Drosophila* brain as well. Transcriptomic atlases of the central adult brain (Croset, Treiber, and Waddell 2018; Davie et al. 2018) and optic lobes (Kurmangaliyev et al. 2020; Özel et al. 2021) are appearing. Comparing connectomes with transcriptomes is already proving useful for studying molecular mechanisms of development (Kovács, Barabási, and Barabási 2020; Yoo et al. 2023; Alexander Shakeel Bates et al. 2019). Clearly more fly connectomes at multiple developmental stages are needed.

Brain simulation

Connectome-based brain simulation was one of the original motivations for connectomics (Seung 2012). A neural network simulation of visual motion detection based on the wiring diagram of columnar circuits in the optic lobe has been created (Lappalainen et al. 2023). Such a connectome-based approach can at last be scaled up to an entire brain, as shown by Shiu et al. (Shiu et al. 2023).

Block face versus serial section EM

The hemibrain was reconstructed (Scheffer et al. 2020) from images acquired by FIB-SEM (Knott et al. 2008; Xu et al. 2017; Hayworth et al. 2020), a form of block face EM (Denk and Horstmann 2004). FlyWire is based on transmission EM images of serial sections (ssTEM) that were manually cut and collected (Zheng et al. 2018), an evolution of the approach that was used for the *C. elegans* connectome (White et al. 1986). In the end, both block face and serial section EM have turned out to be viable for fly connectomes. Both approaches yield similar accuracy (Ext. Fig. 1-2, Ext. Fig. 1-3). Hybrid methods that combine both imaging approaches are also being developed (Hayworth et al. 2020).

Artificial and human intelligence

Owing to the use of artificial intelligence (AI), the hemibrain and FlyWire have yielded connectomes that are orders of magnitude larger than those of *C. elegans* (Cook et al. 2019) or the larval fly (Winding et al. 2023). The hemibrain images were automatically segmented using flood-filling convolutional nets (Januszewski et al. 2018), whereas FlyWire used the older approach of boundary-detecting convolutional nets (Jain et al. 2007; Turaga et al. 2010). FlyWire also required another kind of AI, alignment of serial section images using convolutional nets (Popovych et al. 2022). The improved alignment was crucial for making ssTEM as amenable as block face to automated reconstruction (Lee et al. 2019). In spite of

enormous progress in AI, both the hemibrain (Scheffer et al. 2020) and FlyWire (Methods) required an estimated 50 and 30 person-years of human effort for proofreading the automated segmentation respectively (see Methods). This is because AI has reduced the amount of human labor required per unit brain volume, but EM image volumes have increased even faster. Further reduction in human proofreading is necessary for reconstructing many fly connectomes to study variation, or to scale up to whole mammalian brains.

Imaging smaller

The EM images used by FlyWire were acquired at a resolution of 4×4×40 nm^3. Sharpening this resolution would presumably enable accurate attachment of twigs to backbones, which is currently the main factor limiting the accuracy of reconstructing synaptic connectivity. Higher resolution might also enable the reconstruction of electrical synapses, which are included in the *C. elegans* connectome. Increasing resolution by 2× in all three dimensions would increase the data volume by 8×. Handling much larger data volumes should be possible as methods for acquiring and analyzing EM images are progressing rapidly.

Imaging larger

Imaging a larger volume would open up other interesting opportunities. Imaging a whole fly CNS would enable the mapping of all pathways linking the brain and VNC. The volume of the whole CNS is not much larger than that of the brain. In the meantime, it is possible to establish correspondences between FlyWire and FANC, a reconstruction of a separate VNC (Phelps et al. 2021; Azevedo et al. 2022). The first *C. elegans* connectome was obtained similarly as a mosaic drawn from multiple worms (White et al. 1986). Imaging an entire fly, both CNS and body, would enable the addition of sensory organs and muscles to the reconstruction. This also has precedent in the *C. elegans* connectome, which includes neuromuscular junctions, and the first instar *Drosophila* larva for which a whole-animal EM dataset was recently published (Schoofs et al. 2023).

FlyWire and other related technologies have already been applied to millimeter-scale chunks of mammalian brain (MICrONS Consortium et al. 2021; Shapson-Coe et al. 2021), which are >50× larger in volume than a fly brain. The U.S. National Institutes of Health is planning a ten year project to reconstruct a whole mouse brain from an exabyte of EM images and a report from the Wellcome trust recently examined the road to a whole mouse brain connectome (Jefferis et al. 2023).

Openness

The 1996 Bermuda Principles mandated daily release of Human Genome Project sequences into the public domain (Collins, Morgan, and Patrinos 2003). We believe that openness is also important for large-scale connectomics projects, particularly because these projects are expensive, require coordinated effort, and take several years to complete - sharing connectomes only after proofreading and annotation are completed prevents scientific discovery that can occur while the connectome is being completed. Shortly after its inception, FlyWire has been open to any *Drosophila* researcher. As a result, hundreds of scientists and proofreaders from over 50 labs joined FlyWire with over 200 of them contributing over 100 edits (Supplemental Table 1) and 86 contributing ten or more

annotations (Supplemental Table 2). As a result, there are multiple studies that used completed portions of FlyWire's connectome as proofreading proceeded (Zhao et al. 2022; Mabuchi et al. 2023a; Eichler et al. 2023; Shiu et al. 2022; Baker et al. 2022; Zheng et al. 2022; Deutsch et al. 2020; Task et al. 2022; Chou et al. 2022; Israel et al. 2022; Kind et al. 2021; Sterne et al. 2021; P. Schlegel et al. 2021; Mabuchi et al. 2023b). Openness has also enabled FlyWire to move faster by incorporating data sources from the community. The EM data on which FlyWire is built was shared in 2018 by Bock and colleagues (Zheng et al. 2018). FlyWire's synapse data was previously published by Buhmann et al. (Buhmann et al. 2021) who incorporated synapse segmentations from Heinrich et al. (Heinrich et al. 2018), neurotransmitter labels for every synapse were made available ahead of publication by Eckstein et al. (Eckstein et al. 2023), numerous annotations were contributed by Schlegel et al., and over 90K (and counting) cell annotations have been shared by the community.

FlyWire Consortium

Doug Bland[1], Krzysztof Kruk[3], Zairene Lenizo[16], Alexander Shakeel Bates[4,5,12,13], Nseraf[3], Austin T Burke[1], Katharina Eichler[5], Nashra Hadjerol[16], Kyle Patrick Willie[1], Ryan Willie[1], Yijie Yin[5], John Anthony Ocho[16], Sven Dorkenwald[1,2], Joshua Bañez[16], Arti Yadav[4], Shirleyjoy Serona[16], Rey Adrian Candilada[16], Dustin Garner[17], Philipp Schlegel[4,5], Jet Ivan Dolorosa[16], Ariel Dagohoy[16], Remer Tancontian[16], Mendell Lopez[16], Regine Salem[16], Griffin Badalamente[5], annkri (Anne Kristiansen)[3], Kendrick Joules Vinson[16], Nelsie Panes[16], Laia Serratosa Capdevila[4], Anjali Pandey[4], Darrel Jay Akiatan[16], Ben Silverman[1], Dharini Sapkal[4], Shaina Mae Monungolh[16], Jay Gager[1], Varun Sane[5], Miguel Albero[16], AzureJay (Jaime Skelton)[3], Márcia dos Santos[5], David Deutsch[1,9], Zeba Vohra[4], Kaiyu Wang[14], Emil Kind[18], Chitra Nair[4], Dhwani Patel[4], Imaan F. M. Tamimi[5], Michelle Darapan Pantujan[16], James Hebditch[1], Alexandre Javier[4], Rashmita Rana[4], Bhargavi Parmar[4], Merlin Moore[1], Mark Lloyd Pielago[16], Allien Mae Gogo[16], Markus William Pleijzier[4], Mark Larson[19], Joseph Hsu[4], Thomas Stocks[3], Jacquilyn Laude[16], Itisha Joshi[4], Chereb Martinez[16], Dhara Kakadiya[4], John David Asis[16], Amalia Braun[20], Clyde Angelo Lim[16], Alvin Josh Mandahay[16], Marchan Manaytay[16], Marina Gkantia[5], Kaushik Parmar[4], Quinn Vanderbeck[12], Claire E. McKellar[1], Philip Lenard Ampo[16], Daril Bautista[16], Irene Salgarella[4], Christopher Dunne[5], John Clyde Saguimpa[16], Eva Munnelly[5], Chan Hyuk Kang[21], Jansen Seguido[16], Jinmook Kim[21], Gizem Sancer[22], Lucia Kmecova[23], Christa Baker[1], Jenna Joroff[12], Steven Calle[23], Cathy Pilapil[16], Yashvi Patel[4], Olivia Sato[19], Siqi Fang[4], Paul Brooks[24], Mai Bui[25], JousterL (Matthew Lichtenberger)[3], edmark tamboboy[16], Katie Molloy[19], Alexis E Santana-Cruz[23], Janice Salocot[16], Celia David[1], Kfay[3], Seongbong Yu[21], Arzoo Diwan[4], Farzaan Salman[26], Szi-chieh Yu[1], Monika Patel[4], TR77[3], Sarah Morejohn[1], Sebastian Molina-Obando[27], Sanna Koskela[14], Tansy Yang[14], bl4ckscor3 (Daniel Lehmann)[3], Sangeeta Sisodiya[4], Selden Koolman[1], Philip K. Shiu[28], Sky Cho[25], Brian Reicher[19], Marlon Blanquart[4], Marissa Sorek[1,3], Lucy Houghton[17], Hyungjun Choi[21], Matt Collie[19], Joanna Eckhardt[1], Benjamin Gorko[17], Li Guo[17], Zhihao Zheng[1], Alisa Poh[29], Marina Lin[25], István Taisz[4], Wes Murfin[52], Peter Gibb[12], Nils Reinhard[30], Nidhi Patel[4], Sandeep Kumar[1], Minsik Yun[31], Megan Wang[1], Devon Jones[1], Lucas Encarnacion-Rivera[32], Annalena Oswald[27], Akanksha Jadia[4], Leonie Walter[18], Nik Drummond[4], Ibrahim Tastekin[33], Yuta Mabuchi[34], Xin Zhong[18], Fernando J Figueroa Santiago[23], Urja Verma[4], Nick Byrne[19], Edda Kunze[18], Thomas Crahan[17], Hewhoamareismyself (Ryan Margossian)[3], Haein Kim[34], Iliyan Georgiev[3], Fabianna Szorenyi[23], Benjamin Bargeron[35], Tomke Stuerner[4], Damian Demarest[36], Atsuko Adachi[37], Burak Gür[27], Andrearwen[3], a5hm0r[3], Robert Turnbull[4], Andrea Sandoval[28], Diego A. Pacheco[12], Haley Croke[38], Alexander Thomson[14], Jonas Chojetzki[27], Connor Laughland[14], Suchetana B. Dutta[18], Paula Guiomar Alarcón de Antón[18], Binglin Huang[17], Patricia Pujols[23], Isabel Haber[19], Amanda González-Segarra[28], Albert Lin[1,6], Daniel T. Choe[39], Veronika Lukyanova[40], Marta Costa[5], Maria

Ioannidou[27], Zequan Liu[41], Tatsuo Okubo[12], Miriam A. Flynn[14], Gianna Vitelli[35], Meghan Laturney[28], Carolina Manyari-Diaz[35], Shuo Cao[42], Hyunsoo Yim[21], Anh Duc Le[38], Kate Maier[35], Seungyun Yu[21], Yeonju Nam[21], Mavil[3], Eleni Samara[20], Nino Mancini[35], Amanda Abusaif[28], Audrey Francis[43], Jesse Gayk[4], Sommer S. Huntress[44], Raquel Barajas[33], Mindy Kim[19], Xinyue Cui[34], Amy R Sterling[1,3], Anna Li[12], Gabriella R. Sterne[28], Lena Lörsch[27], Keehyun Park[21], Alan Mathew[4], Taewan Kim[21], Guan-ting Wu[45], Serene Dhawan[46], Margarida Brotas[33], Cheng-hao Zhang[45], Shanice Bailey[4], Alexander Del Toro[28], Arie Matsliah[1], Kisuk Lee[1,10], Thomas Macrina[1,2], Casey Schneider-Mizell[7], Mert Erginkaya[33], Sergiy Popovych[1,2], Oluwaseun Ogedengbe[1], Runzhe Yang[1,2], Akhilesh Halageri[1], Will Silversmith[1], Ryan Morey[1], Eric Mitchell[1], Andrew Champion[4], Dodam Ih[1], Nico Kemnitz[1], Manuel Castro[1], Zhen Jia[1], Jingpeng Wu[1], Stephan Gerhard[47], Shang Mu[1], Barak Nehoran[1,2], Eric Perlman[8], J. Alexander Bae[1,11], Chris S. Jordan[1], Ran Lu[1], Derrick Brittain[7], Kai Kuehner[1], Nils Eckstein[14], David J. Anderson[42], Rudy Behnia[37], Salil S. Bidaye[35], Davi D. Bock[15], Alexander Borst[20], Eugenia Chiappe[33], Forrest Collman[7], Kenneth J. Colodner[44], Andrew Dacks[26], Barry Dickson[14], Álvaro Sanz Díez[37], Jan Funke[14], Denise Garcia[38], Stefanie Hampel[23], Volker Hartenstein[48], Bassem Hassan[18], Charlotte Helfrich-Forster[30], Wolf Huetteroth[49], Gregory S.X.E. Jefferis[4,5], Jinseop Kim[21], Sung Soo Kim[17], Young-Joon Kim[31], Wei-Chung Lee[12], Feng Li[14], Gerit A. Linneweber[18], Gaby Maimon[43], Richard Mann[37], Mala Murthy[1], Michael Pankratz[36], Lucia Prieto-Godino[46], Jenny Read[40], Michael Reiser[14], Katie von Reyn[38], Carlos Ribeiro[33], Kristin Scott[28], Andrew M. Seeds[23], Mareike Selcho[49], H. Sebastian Seung[1,2], Marion Silies[27], Julie Simpson[17], Mathias F. Wernet[18], Rachel I. Wilson[12], Fred W Wolf[50], Zepeng Yao[51], Nilay Yapici[34], Meet Zandawala[30]

[1]Princeton Neuroscience Institute, Princeton University, Princeton, USA
[2]Computer Science Department, Princeton University, Princeton, USA
[3]Eyewire, Boston, USA
[4]Neurobiology Division, MRC Laboratory of Molecular Biology, Cambridge, UK
[5]Drosophila Connectomics Group, Department of Zoology, University of Cambridge, Cambridge, UK
[6]Center for the Physics of Biological Function, Princeton University, Princeton, USA
[7]Allen Institute for Brain Science, Seattle, USA
[8]Yikes LLC, Baltimore, USA
[9]Department of Neurobiology, University of Haifa, Haifa, Israel
[10]Brain & Cognitive Sciences Department, Massachusetts Institute of Technology, Cambridge, USA
[11]Electrical and Computer Engineering Department, Princeton University, Princeton, USA
[12]Harvard Medical School, Boston, USA
[13]Centre for Neural Circuits and Behaviour, The University of Oxford, Oxford, UK
[14]Janelia Research Campus, Howard Hughes Medical Institute, Ashburn, USA
[15]Department of Neurological Sciences, University of Vermont, Burlington, USA
[16]SixEleven, Davao City, Philippines
[17]University of California, Santa Barbara, USA
[18]Freie Universität Berlin, Berlin, Germany
[19]Harvard, Boston, USA
[20]Department Circuits-Computation-Models, Max Planck Institute for Biological Intelligence, Planegg, Germany
[21]Sungkyunkwan University, Seoul, South Korea
[22]Department of Neuroscience, Yale University, New Haven, USA
[23]Institute of Neurobiology, University of Puerto Rico Medical Sciences Campus, San Juan, Puerto Rico
[24]Department of Zoology, University of Cambridge, UK
[25]Program in Neuroscience and Behavior, Mount Holyoke College, South Hadley, USA
[26]Department of Biology, West Virginia University, Morgantown, USA
[27]Johannes-Gutenberg University Mainz, Mainz, Germany
[28]University of California, Berkeley, USA
[29]University of Queensland, Brisbane, Australia
[30]Julius-Maximilians-Universität Würzburg, Würzburg, Germany
[31]Gwangju Institute of Science and Technology, Gwangju, South Korea
[32]Stanford University School of Medicine, Stanford, USA
[33]Champalimaud Foundation, Lisbon, Portugal

[34]Cornell University, Ithaca, USA
[35]Max Planck Florida Institute for Neuroscience, Jupiter, USA
[36]University of Bonn, Bonn, Germany
[37]Zuckerman Institute, Columbia University, New York, USA
[38]Drexel, Philadelphia, USA
[39]Seoul National University, Seoul, South Korea
[40]Newcastle University, Newcastle, UK
[41]RWTH Aachen University, Aachen, Germany
[42]Caltech, Pasadena, USA
[43]Rockefeller University, New York, USA
[44]Mount Holyoke College, South Hadley, USA
[45]National Hualien Senior High School, Hualien, Taiwan
[46]The Francis Crick Institute, London, UK
[47]Aware LLC, Zurich, Switzerland
[48]University of California, Los Angeles, USA
[49]Institute of Biology, Leipzig University, Leipzig, Germany
[50]University of California, Merced, USA
[51]University of Florida, Gainesville, USA
[52]Retired MD-PhD, Fort Collins, USA

Acknowledgements

We thank John Wiggins, G. McGrath, and Dave Barlieb for computer system administration and M. Husseini for project administration. We are grateful to J. Maitin-Shepard for Neuroglancer. Mala Murthy and Sebastian Seung acknowledge support from the National Institutes of Health (NIH) BRAIN Initiative RF1 MH117815, RF1 MH129268 and U24 NS126935, from the Princeton Neuroscience Institute, as well as assistance from Google. Davi Bock was supported by NIH NIMH BRAIN Initiative grant 1RF1MH120679-01 and a Neuronex2 award (NSF 2014862). Gregory S.X.E. Jefferis and Davi Bock were supported by Wellcome Trust Collaborative Award (203261/Z/16/Z). Gregory S.X.E. Jefferis was supported by Wellcome Trust Collaborative Award 220343/Z/20/Z, Neuronex2 award (MRC MC_EX_MR/T046279/1) and received core support from the MRC (MC-U105188491). Ibrahim Tastekin was supported with a Marie Skłodowska-Curie postdoctoral fellowship (H2020-WF-01-2018-867459 to Ibrahim Tastekin) and by the Portuguese Research Council (Grant PTDC/MED-NEU/4001/2021). Andrew Seeds and Stefanie Hampel were supported by National Institute Of Neurological Disorders And Stroke of the National Institutes of Health under Award Number RF1NS121911. Derrick Brittain, Casey Schneider-Mizell, and Forrest Collman thank the Allen Institute for Brain Science founder, P. G. Allen, for his vision, encouragement and support. This work was also supported by the Intelligence Advanced Research Projects Activity via Department of Interior/Interior Business Center contract no. D16PC0005 to H.S.S. The US Government is authorized to reproduce and distribute reprints for Governmental purposes notwithstanding any copyright annotation thereon. The views and conclusions contained herein are those of the authors and should not be interpreted as necessarily representing the official policies or endorsements, either expressed or implied, of Intelligence Advanced Research Projects Activity, Department of Interior/Interior Business Center or the US Government.

Contributions

Members of the FlyWire consortium contributed proofreading and annotations (see Supplemental Tables 1, 2). SGerhard provided braincircuits.io. TM and NK realigned the

dataset with methods developed by EM, BN and TM and infrastructure developed by SP, ZJ. JAB, SM wrote code for masking defects and misalignments. KL trained the convolutional net for boundary detection, using ground-truth data realigned by DI. JW used the convolutional net to generate an affinity map that was segmented by RL. NK, MAC, OO, AH, CSJ, KKuehner and ARS adapted and improved Neuroglancer for proofreading and annotations. JG, KKruk, AM, SD, FC and CSM created interactive analysis and annotation tools for the community. AM created Codex with help from ARS, SD, KKuehner and RM. ARS and AM created the website. ARS, CEM and MS onboarded community members and tested new proofreaders. ARS, MS, CSJ and CEM designed tutorials. CEM, ARS and MS provided community support. SD, FC, CSM, CSJ, AH, DBrittain and WMS built and maintained CAVE for FlyWire and managed user access. SD, PS, AM and EP curated the data and made it available for download. EP and DDB provided a coordinate mapping service. ASB, NE, GSXEJ and JF provided neurotransmitter information. SCY, CEM, MC, KE, YY and PS trained and managed proofreaders. SD, SCY, PS and GSXEJ led the targeted proofreading effort. SD, PS, AM, AChampion and KKuehner maintained the proofreading management platforms. SD evaluated the proofreading accuracy. SD, AL, HSS, DD and RY analyzed the data. SD, DBland and SCY annotated and analyzed the ocellar circuit. SD, HSS, MM, AL, PS and ARS wrote the manuscript with feedback from ASB, WHuetteroth, GSXEJ and contributions from all authors. HSS, MM, GSXEJ, DDB sponsored large-scale proofreading. GSXEJ, DDB led the Cambridge effort. MM, HSS led the overall effort.

Competing interests

T. Macrina, K. Lee, S. Popovych, D. Ih, N. Kemnitz, and H. S. Seung declare financial interests in Zetta AI.

Methods

Neuropils

Meshes for individual neuropils were based on work by Ito et al. (Ito et al. 2014). More specifically, we took meshes previously generated from a full brain segmentation of the JFRC2 template brain which are also used by the Virtual Fly Brain project (see also https://natverse.org/nat.flybrains/reference/JFRC2NP.surf.html). These meshes were moved from JFRC2 into FlyWire (FAFB14.1) space through a series of non-rigid transforms. In addition, we also generated two neuropil meshes for the laminae and for the ocellar ganglion. For these, the FlyWire synapse cloud was voxelized with 2 µm isotropic resolution, meshed using the marching cube algorithm using Python and manually post-processed in Blender 3d.

We calculated a volume for each neuropil using its mesh. In the aggregated volumes presented in the paper we assigned the lamina, medulla, accessory medulla, lobula, lobula plate to the optic lobe. The remaining neuropils but the ocellar ganglion were assigned to the central brain.

Neuropil synapse assignments

We assigned synapses to neuropils based on their presynaptic location. We used ncollpyde (https://pypi.org/project/ncollpyde/) to calculate if the location was within a neuropil mesh and assigned the synapse accordingly. Some synapses remained unassigned after this step because the neuropils only resemble rough outlines of the underlying data. We then assigned all remaining synapses to the closest neuropil if the synapse was within 10 µm from it. The remaining synapses were left unassigned.

Correction of left-right inversion

Our reconstruction used the FAFB EM dataset (Zheng et al. 2018). A number of consortium members (A. Bates, P. Kandimalla, S. Noselli) alerted us that the FAFB imagery seemed left-right inverted based on cell types innervating the asymmetric body (Lapraz et al. 2023). Eventually a left-right inversion during FAFB imaging was confirmed. All side annotations in figures, in Codex and elsewhere are based on the true biological side. For technical reasons we were unable to invert the underlying FAFB image data and therefore continue to show images and reconstructions in the same orientation as (Zheng et al. 2018) although we now know in such frontal views the fly's left is on the viewer's left. For full details of this issue including approaches to display FAFB and other brain data with the correct chirality, please see our companion paper (Schlegel et al., *in prep*).

Proofreading system

FlyWire uses the Connectome Annotation Versioning Engine (CAVE) for hosting the proofreadable segmentation and all of its annotations. CAVE's proofreading system is the PyChunkedGraph which has been described in detail elsewhere (Dorkenwald, Turner, et al. 2022; Dorkenwald, McKellar, et al. 2022).

Proofreading annotations

Any user in FlyWire was able to mark a cell as complete, indicating that a cell was good for analysis. However, such annotations did not prevent future proofreading of a cell as commonly smaller branches were added later on. We created an annotation table for these completion markings. Each completion marking was defined by a point in space and the cell segment that overlapped with this point at any given time during proofreading was associated with the annotation. We created a webservice allowing users to submit completion markings for any cell. For convenience, we added an interface to this surface directly into Neuroglancer such that users can submit completion information for cells right after proofreading (Supplemental Information 1). When users submitted completion annotations we also recorded the current state of the cell. We encouraged users to submit new completion markings for a cell that they edited to indicate that edits were intentional. Recording the status of a cell at submission allowed us to calculate volumetric changes to a cell through further proofreading and flag cells for review if they received substantial changes without new completion markings.

Onboarding proofreaders

Proofreaders came from several distinct labor pools: community members, citizen scientists from Eyewire (Flyers), and professional proofreading teams at Princeton and Cambridge. All proofreaders completed the built-in interactive tutorial and directed to Self-Guided Proofreading Training. For practice and learning purposes, the Sandbox, a complete replica of the FlyWire data, allowed new users to freely make edits and explore without affecting the actual “Production“ dataset. When ready, an Onboarding Coordinator tested the new proofreader before giving access to the Production dataset (Dorkenwald et al., 2022). Later onboarding called for users to send demonstration Sandbox edits that were reviewed by the Onboarding Coordinator. A new class of view-only users was introduced in early 2023, allowing researchers early data access for analysis purposes. All early access users attended a live onboarding session in Zoom prior to being granted edit or view access.

Training the professional proofreading team

The professional proofreading team received additional proofreading training. Correct proofreading relies on a diverse array of 2D and 3D visual cues. Proofreaders learned about 3D morphology, resulting from false merger or false split without the knowledge of knowing what types of cells they are. Proofreaders studied various types of ultrastructures as the ultrastructures provide valuable 2D cues and serve as reliable guides for accurate tracing. Before professional proofreaders were admitted into Production, each of them practiced on average >200 cells in a testing dataset where additional feedback was given. In this dataset, we determined the accuracy of test cells by comparing them to ground-truth reconstructions. To improve proofreading quality, peer learning was highly encouraged.

Recruitment of citizen scientists

The top 100 players from Eyewire, a gamified EM reconstruction platform that crowdsources reconstructions in mouse retina and zebrafish hindbrain (Kim et al. 2014), received an invitation to beta test proofreading in FlyWire. A new set of user onboarding and training materials were created for citizen scientists, including: a blog, forum, and public Google docs. We created bite-sized introduction videos, a comprehensive “FlyWire 101” resource,

as well as an Optic Lobe Cell Guide to aid users in understanding the unique morphology of flies. A virtual Citizen Science Symposium introduced players to the project, after which the self-dubbed “Flyers” began creating their own resources, such as a new comprehensive visual guide to cell types, conducting literature reviews, and even developing helpful FlyWire plugins. As of publication, FlyWire has 12 add-on apps ranging from a batch processor to cell naming helper (https://blog.flywire.ai/2022/08/11/flywire-addons/).

Proofreading strategy to complete the connectome

As previously described (Dorkenwald, McKellar, et al. 2022), proofreading of the connectome was focused on the microtubule-rich ‘backbones’ of neurons. Microtubule-free ‘twigs’ were only added if discovered incidentally or sought out specifically by members of the community. After proofreading, users marked neuronal segments as ‘complete’ indicating that neurons were ready for analysis but further changes remained possible. While *Drosophila* neuroscientist members of the FlyWire community generally contributed proofreading for their neurons of interest, the bulk of the segments was proofread by professional proofreaders in the following way: first we proofread all segments with an automatically detected nucleus in the central brain (Mu et al. 2021) by extending it as much as possible and removing all false mergers (pieces of other neurons or glia attached), and second, going through the remaining segments in descending order of their synapse count (pre+post) up to a predefined size threshold of 100 synapses.

Quality Assurance

To assess quality, a group of expert centralized proofreaders conducted a review of 3106 segments in the central brain. These specific neurons were chosen based on certain criteria such as significant change since being marked complete and small overall volume. An additional 826 random neurons were included in the review pool as well. Proofreaders were unaware which neurons were added for quality measurement and which ones because they were flagged by a metric. We compared the 826 neurons before and after the review and found that the initial reconstruction scored an average F1-Score of 99.2% by volume (Ext. Data Fig. 1-2a,b).

Quantification of proofreading effort

Any quantification of the total proofreading time that was required to create the FlyWire resource is a rough estimate because of the distributed nature of the community, the interlacing of analysis and proofreading and the variability in how proofreading was performed. The first public release, version 630, required 2,712,769 edits. We measured proofreading times during early proofreading rounds that included proofreading of whole cells in the central brain. We collected timings and number of edits for 29,135 independent proofreading tasks after removing outliers with more than 500 edits. From this data we were able to calculate an average time per edit. However, we observed that proofreading times per edit were much higher for proofreading tasks that required few edits (<5). That meant that our measurements were not representative for the second round of proofreading which went over segments with > 100 synapses. These usually required 1-5 edits. We adjusted for that by computing estimates for proofreading speeds of both rounds by limiting the calculations to a subset of the timed tasks: (round 1) The average time per edit in our proofreading time dataset, (round 2) the average time of tasks with 1-5 edits. We average

these times for an overall proofreading time because the number of tasks in each category were similar. The result was an average time of 79s per edit which adds up to an estimate of 29.8 person-years assuming a 2000h work year.

Completion rates

We adopted the completion rate calculations from the hemibrain (Scheffer et al. 2020). Every presynaptic and postsynaptic location was assigned to a segment. Using the neuropil assignments, we then calculated the fraction of presynapses that were assigned to segments marked as proofread for each neuropil and analogous for postsynaptic location.

Comparison with the hemibrain

We retrieved the latest completion rates and synapse numbers for the hemibrain from neuprint (v1.2.1). In some cases, neuropil comparisons were not directly possible because of redefined regions in the hemibrain dataset. We excluded these regions from the comparison.

Crowdsourced annotation

FlyWire's large community and diversity of expertise allowed us to crowdsource the identification of neurons. There is no limit to the number of annotations a neuron can receive. A standardized format is encouraged but not required. One user might first report that a neuron is a descending interneuron, while another might add that it is the Giant Fiber descending neuron, and another might add all its synonyms and citations from the literature. Contributors' names are visible so they can be consulted if there is disagreement. The disadvantage to this approach is that there isn't one precise name for every neuron, but the advantage is a richness of information and dialog. The annotations are not meant to be a finished, static list, but a continually growing, living data source. These annotations were solicited from the FlyWire community through Town Halls, email announcements, interest groups in the FlyWire Forum, online instructions, and by personal contact from the Community Manager. Citizen scientists also contributed annotations, after receiving training on particular cell types by experts.

Neuron categorizations

Neuron categorization, sensory modality annotations and nerve assignments are described in detail in Schlegel et al. In brief, neurons were assigned to one of three "flow" classes: afferent (to the brain), intrinsic (within the brain), and efferent (out of the brain). Intrinsic neurons had their entire arbor within the FlyWire dataset. This included cells that projected to and from the subesophageal zone (SEZ). Next, each flow class was divided into "super" classes in the following way. afferent: sensory, ascending. intrinsic: central, optic, visual projection (from the optic lobes to the central brain), visual centrifugal (from the central brain to the optic lobes). efferent: endocrine, descending, motor.

Skeletonization and path length calculation

We generated skeletons for all neurons marked as proofread using skeletor (https://github.com/navis-org/skeletor) which implements multiple skeletonization algorithms such as TEASAR (Sato et al. 2000). In brief, neuron meshes from the exported

segmentation (LOD 1) were downloaded and skeletonized using the “wavefront” method in skeletor. These raw skeletons were then further processed (e.g. to remove false twigs and heal breaks) and produce downsampled versions using navis (https://github.com/navis-org/navis). A modified version of this skeletonization pipeline is implemented in fafbseg (https://github.com/navis-org/fafbseg-py).

Synaptic connections

We imported the automatically predicted synapses from Buhmann et al. (Buhmann et al. 2021) which we combined with the predictions by Heinrich et al. to assign scores to all synapses (Heinrich et al. 2018) to improve precision. We removed synapses from the imported list if they fulfilled any of the following criteria: (1) either the pre- or postsynaptic location remained unassigned to a segment (proofread or unproofread), (2) It had a score ≤50.

Connection threshold

For all the analyses presented in this paper, save for synapse distributions, we employed a consistent threshold of >4. Our decision to use a synapse threshold on connections was due partly to the fact that synapses in the FlyWire dataset were not manually proofread. For these analyses, many of which demonstrate the high interconnectivity of the fly brain, we chose a conservative threshold to ensure that considered connections are real. Use of a threshold is also in keeping with previous work analyzing wiring diagrams in *Drosophila (Scheffer et al. 2020)*. Thus, we are likely undercounting the number of true connections. The distribution of synapse counts (FIgure 3f) does not display any bimodality that could be used to set the threshold. Therefore, the choice of 5 synapses per connection is a reasonable but arbitrary one. In the companion paper analyzing the network properties of the FlyWire connectome, it is found that statistical properties of the whole-brain network, such as reciprocity and clustering coefficient, are robust to our choice of threshold (Lin et al., *in prep*). The FlyWire data is available without an imposed threshold, so users can choose their own appropriate threshold for their specific use case.

Neuropil projectome construction

Under the simplifying assumptions that information flow through the neuron can be approximated by the fraction of synapses in a given region, and that inputs and outputs can be treated independently, we can construct a matrix representing the projections of a single neuron between neuropils. The fractional inputs of a given neuron are a 1 x N vector containing the fraction of incoming synapses the neuron has in each of the N neuropils, and the fractional outputs are a similar vector containing the fraction of outgoing synapses in each of the N neuropils. We multiply these vectors against each other to generate the N x N matrix of the neuron's fractional weights. Summing these matrices across all intrinsic neurons produces a matrix of neuropil-to-neuropil connectivity (Figure 4a). In this projectome, all neurons contribute an equal total weight of one.

Dominant input side

We assigned neuropils to the left and right hemispheres or the center if the neuropil has no homologue. We then counted how many postsynapses each neuron had in each of these three regions and assigned it to the one with the largest count.

Contralateral and bilateral neuron analysis

For each neuron, we calculated the fraction of presynapses in the left and right hemisphere. The hemisphere opposite its dominant input side was named the contralateral hemisphere. We excluded neurons that had either most of their presynapses or most of their postsynapses in the center region.

Rank analysis & Information Flow

We used the information flow algorithm implemented by Schlegel et al. (P. Schlegel et al. 2021) (https://github.com/navis-org/navis) to calculate a rank for each neuron starting with a set of seed neurons. The algorithm traverses the synapse graph of neurons probabilistically. The likelihood of a neuron being added to the traversed set increased linearly with the fraction of synapses it receives from already traversed neurons up to 30% and was guaranteed above this threshold. We repeated the rank calculation for all sets of afferent neurons as seed as well as the whole set of sensory neurons. The groups we used are:

olfactory receptor neurons, gustatory receptor neurons, mechanosensory Johnston's Organ neurons, head and neck bristle mechanosensory neurons, mechanosensory taste peg neurons, thermosensory neurons, hygrosensory neurons, visual projection neurons, visual photoreceptors, ocellar photoreceptors and ascending neurons.

Additionally, we created input seeds by combining all listed modalities, all sensory modalities, and all listed modalities with visual sensory groups excluded.

For each modality we then ordered the neurons according to their rank and assigned them a percentile based on their location in the order. To compute a reduced dimensionality, we treated the vector of all ranks (one for each modality) as neuron embedding and calculated two dimensional embeddings using UMAP (McInnes, Healy, and Melville 2018) with the following parameters: n_components=2, min_dist=0.35, metric="cosine", n_neighbors=50, learning_rate=.1, n_epochs=1000.

References

Aimon, Sophie, Karen Y. Cheng, Julijana Gjorgjieva, and Ilona C. Grunwald Kadow. 2022. "Combined Patterns of Activity of Major Neuronal Classes Underpin a Global Change in Brain State during Spontaneous and Forced Walk in*Drosophila*." *bioRxiv*. https://doi.org/10.1101/2022.01.17.476660.

Amin, Hoger, Anthi A. Apostolopoulou, Raquel Suárez-Grimalt, Eleftheria Vrontou, and Andrew C. Lin. 2020. "Localized Inhibition in the Drosophila Mushroom Body." *eLife* 9 (September). https://doi.org/10.7554/eLife.56954.

Arendt, Detlev, Maria Antonietta Tosches, and Heather Marlow. 2016. "From Nerve Net to Nerve Ring, Nerve Cord and Brain--Evolution of the Nervous System." *Nature Reviews. Neuroscience* 17 (1): 61–72.

Azevedo, Anthony, Ellen Lesser, Brandon Mark, Jasper Phelps, Leila Elabbady, Sumiya Kuroda, Anne Sustar, et al. 2022. "Tools for Comprehensive Reconstruction and Analysis of Drosophila Motor Circuits." *bioRxiv*. https://doi.org/10.1101/2022.12.15.520299.

Bae, J. Alexander, Shang Mu, Jinseop S. Kim, Nicholas L. Turner, Ignacio Tartavull, Nico Kemnitz, Chris S. Jordan, et al. 2018. "Digital Museum of Retinal Ganglion Cells with Dense Anatomy and Physiology." *Cell* 173 (5): 1293–1306.e19.

Baker, Christa A., Claire McKellar, Rich Pang, Aljoscha Nern, Sven Dorkenwald, Diego A. Pacheco, Nils Eckstein, Jan Funke, Barry J. Dickson, and Mala Murthy. 2022. "Neural Network Organization for Courtship-Song Feature Detection in Drosophila." *Current Biology: CB* 32 (15): 3317–33.e7.

Bates, Alexander Shakeel, Jasper Janssens, Gregory Sxe Jefferis, and Stein Aerts. 2019. "Neuronal Cell Types in the Fly: Single-Cell Anatomy Meets Single-Cell Genomics." *Current Opinion in Neurobiology* 56 (June): 125–34.

Bates, Alexander Shakeel, James D. Manton, Sridhar R. Jagannathan, Marta Costa, Philipp Schlegel, Torsten Rohlfing, and Gregory Sxe Jefferis. 2020. "The Natverse, a Versatile Toolbox for Combining and Analysing Neuroanatomical Data." *eLife*. https://doi.org/10.7554/elife.53350.

Bates, Alexander S., Philipp Schlegel, Ruairi J. V. Roberts, Nikolas Drummond, Imaan F. M. Tamimi, Robert Turnbull, Xincheng Zhao, et al. 2020. "Complete Connectomic Reconstruction of Olfactory Projection Neurons in the Fly Brain." *Current Biology: CB* 30 (16): 3183–99.e6.

Borst, Alexander, and Moritz Helmstaedter. 2015. "Common Circuit Design in Fly and Mammalian Motion Vision." *Nature Neuroscience* 18 (8): 1067–76.

BRAIN Initiative Cell Census Network (BICCN). 2021. "A Multimodal Cell Census and Atlas of the Mammalian Primary Motor Cortex." *Nature* 598 (7879): 86–102.

Braitenberg, Valentino. 1984. *Vehicles: Experiments in Synthetic Psychology*. Cambridge, MA: MIT Press.

Brezovec, Luke E., Andrew B. Berger, Shaul Druckmann, and Thomas R. Clandinin. 2022. "Mapping the Neural Dynamics of Locomotion across the Drosophila Brain." *bioRxiv*. https://doi.org/10.1101/2022.03.20.485047.

Brittin, Christopher A., Steven J. Cook, David H. Hall, Scott W. Emmons, and Netta Cohen. 2021. "A Multi-Scale Brain Map Derived from Whole-Brain Volumetric Reconstructions." *Nature* 591 (7848): 105–10.

Buhmann, Julia, Arlo Sheridan, Caroline Malin-Mayor, Philipp Schlegel, Stephan Gerhard, Tom Kazimiers, Renate Krause, et al. 2021. "Automatic Detection of Synaptic Partners in a Whole-Brain Drosophila Electron Microscopy Data Set." *Nature Methods* 18 (7): 771–74.

Cachero, S., A. D. Ostrovsky, Y. Y. Jai, and B. J. Dickson. 2010. "Sexual Dimorphism in the Fly Brain." *Current Biology: CB*. https://www.sciencedirect.com/science/article/pii/S0960982210009474.

Caron, Sophie J. C., Vanessa Ruta, L. F. Abbott, and Richard Axel. 2013. "Random

Convergence of Olfactory Inputs in the Drosophila Mushroom Body." *Nature* 497 (7447): 113–17.

Cheong, H. S. J., K. Eichler, T. Stuerner, S. K. Asinof, A. S. Champion, E. C. Marin, T. B. Oram, et al. 2023. "Transforming Descending Input into Behavior: The Organization of Premotor Circuits in the Drosophila Male Adult Nerve Cord Connectome." *bioRxiv*. https://doi.org/10.1101/2023.06.07.543976.

Chiang, Ann-Shyn, Chih-Yung Lin, Chao-Chun Chuang, Hsiu-Ming Chang, Chang-Huain Hsieh, Chang-Wei Yeh, Chi-Tin Shih, et al. 2011. "Three-Dimensional Reconstruction of Brain-Wide Wiring Networks in Drosophila at Single-Cell Resolution." *Current Biology: CB* 21 (1): 1–11.

Chklovskii, Dmitri B. 2004. "Synaptic Connectivity and Neuronal Morphology: Two Sides of the Same Coin." *Neuron* 43 (5): 609–17.

Chou, Ya-Hui, Chi-Jen Yang, Hao-Wei Huang, Nan-Fu Liou, Michael Raphael Panganiban, David Luginbuhl, Yijie Yin, et al. 2022. "Mating-Driven Variability in Olfactory Local Interneuron Wiring." *Science Advances* 8 (7): eabm7723.

Coen, Philip, Jan Clemens, Andrew J. Weinstein, Diego A. Pacheco, Yi Deng, and Mala Murthy. 2014. "Dynamic Sensory Cues Shape Song Structure in Drosophila." *Nature* 507 (7491): 233–37.

Cognigni, Paola, Johannes Felsenberg, and Scott Waddell. 2018. "Do the Right Thing: Neural Network Mechanisms of Memory Formation, Expression and Update in Drosophila." *Current Opinion in Neurobiology* 49 (April): 51–58.

Collins, Francis S., Michael Morgan, and Aristides Patrinos. 2003. "The Human Genome Project: Lessons from Large-Scale Biology." *Science* 300 (5617): 286–90.

Cook, Steven J., Travis A. Jarrell, Christopher A. Brittin, Yi Wang, Adam E. Bloniarz, Maksim A. Yakovlev, Ken C. Q. Nguyen, et al. 2019. "Whole-Animal Connectomes of Both Caenorhabditis Elegans Sexes." *Nature* 571 (7763): 63–71.

Costandi, Mo. 2012. "Anti-Connectome-Ism." *The Guardian*, September 21, 2012. https://www.theguardian.com/science/neurophilosophy/2012/sep/21/connectome-review.

Croset, Vincent, Christoph D. Treiber, and Scott Waddell. 2018. "Cellular Diversity in the Drosophila Midbrain Revealed by Single-Cell Transcriptomics." *eLife* 7 (April). https://doi.org/10.7554/eLife.34550.

Davie, Kristofer, Jasper Janssens, Duygu Koldere, Maxime De Waegeneer, Uli Pech, Łukasz Kreft, Sara Aibar, et al. 2018. "A Single-Cell Transcriptome Atlas of the Aging Drosophila Brain." *Cell* 174 (4): 982–98.e20.

Davis, Fred P., Aljoscha Nern, Serge Picard, Michael B. Reiser, Gerald M. Rubin, Sean R. Eddy, and Gilbert L. Henry. 2020. "A Genetic, Genomic, and Computational Resource for Exploring Neural Circuit Function." *eLife* 9 (January). https://doi.org/10.7554/eLife.50901.

Denk, Winfried, Kevin L. Briggman, and Moritz Helmstaedter. 2012. "Structural Neurobiology: Missing Link to a Mechanistic Understanding of Neural Computation." *Nature Reviews. Neuroscience* 13 (5): 351–58.

Denk, Winfried, and Heinz Horstmann. 2004. "Serial Block-Face Scanning Electron Microscopy to Reconstruct Three-Dimensional Tissue Nanostructure." *PLoS Biology* 2 (11): e329.

Deutsch, David, Diego Pacheco, Lucas Encarnacion-Rivera, Talmo Pereira, Ramie Fathy, Jan Clemens, Cyrille Girardin, et al. 2020. "The Neural Basis for a Persistent Internal State in Drosophila Females." *eLife* 9 (November). https://doi.org/10.7554/eLife.59502.

Dombrovski, Mark, Martin Y. Peek, Jin-Yong Park, Andrea Vaccari, Marissa Sumathipala, Carmen Morrow, Patrick Breads, et al. 2023. "Synaptic Gradients Transform Object Location to Action." *Nature* 613 (7944): 534–42.

Dorkenwald, Sven, Claire E. McKellar, Thomas Macrina, Nico Kemnitz, Kisuk Lee, Ran Lu, Jingpeng Wu, et al. 2022. "FlyWire: Online Community for Whole-Brain Connectomics." *Nature Methods* 19 (1): 119–28.

Dorkenwald, Sven, Philipp J. Schubert, Marius F. Killinger, Gregor Urban, Shawn Mikula,

Fabian Svara, and Joergen Kornfeld. 2017. “Automated Synaptic Connectivity Inference for Volume Electron Microscopy.” *Nature Methods* 14 (4): 435–42.

Dorkenwald, Sven, Nicholas L. Turner, Thomas Macrina, Kisuk Lee, Ran Lu, Jingpeng Wu, Agnes L. Bodor, et al. 2022. “Binary and Analog Variation of Synapses between Cortical Pyramidal Neurons.” *eLife* 11 (November). https://doi.org/10.7554/eLife.76120.

Eckstein, Nils, Alexander Shakeel Bates, Andrew Champion, Michelle Du, Yijie Yin, Philipp Schlegel, Alicia Kun-Yang Lu, et al. 2023. “Neurotransmitter Classification from Electron Microscopy Images at Synaptic Sites in Drosophila Melanogaster.” *bioRxiv*. https://doi.org/10.1101/2020.06.12.148775.

Eichler, Katharina, Stefanie Hampel, Adrián Alejandro-García, Steven A. Calle-Schuler, Alexis Santana-Cruz, Lucia Kmecova, Jonathan M. Blagburn, Eric D. Hoopfer, and Andrew M. Seeds. 2023. “Somatotopic Organization among Parallel Sensory Pathways That Promote a Grooming Sequence in Drosophila.” *bioRxiv*. https://doi.org/10.1101/2023.02.11.528119.

Felleman, D. J., and D. C. Van Essen. 1991. “Distributed Hierarchical Processing in the Primate Cerebral Cortex.” *Cerebral Cortex* 1 (1): 1–47.

Fischbach, K-F, and A. P. M. Dittrich. 1989. “The Optic Lobe of Drosophila Melanogaster. I. A Golgi Analysis of Wild-Type Structure.” *Cell and Tissue Research* 258 (3). https://doi.org/10.1007/bf00218858.

Fisher, Yvette E. 2022. “Flexible Navigational Computations in the Drosophila Central Complex.” *Current Opinion in Neurobiology* 73 (April): 102514.

Haag, Juergen, Adrian Wertz, and Alexander Borst. 2007. “Integration of Lobula Plate Output Signals by DNOVS1, an Identified Premotor Descending Neuron.” *The Journal of Neuroscience: The Official Journal of the Society for Neuroscience* 27 (8): 1992–2000.

Hall, D. H., and R. L. Russell. 1991. “The Posterior Nervous System of the Nematode Caenorhabditis Elegans: Serial Reconstruction of Identified Neurons and Complete Pattern of Synaptic Interactions.” *The Journal of Neuroscience: The Official Journal of the Society for Neuroscience* 11 (1): 1–22.

Harris, Julie A., Stefan Mihalas, Karla E. Hirokawa, Jennifer D. Whitesell, Hannah Choi, Amy Bernard, Phillip Bohn, et al. 2019. “Hierarchical Organization of Cortical and Thalamic Connectivity.” *Nature* 575 (7781): 195–202.

Hayworth, Kenneth J., David Peale, Michał Januszewski, Graham W. Knott, Zhiyuan Lu, C. Shan Xu, and Harald F. Hess. 2020. “Gas Cluster Ion Beam SEM for Imaging of Large Tissue Samples with 10 Nm Isotropic Resolution.” *Nature Methods* 17 (1): 68–71.

Heinrich, Larissa, Jan Funke, Constantin Pape, Juan Nunez-Iglesias, and Stephan Saalfeld. 2018. “Synaptic Cleft Segmentation in Non-Isotropic Volume Electron Microscopy of the Complete Drosophila Brain.” In *Medical Image Computing and Computer Assisted Intervention – MICCAI 2018*, 317–25. Springer International Publishing.

Hofbauer, A., and E. Buchner. 1989. “Does Drosophila Have Seven Eyes?” *Die Naturwissenschaften* 76 (7): 335–36.

Hong, Elizabeth J., and Rachel I. Wilson. 2015. “Simultaneous Encoding of Odors by Channels with Diverse Sensitivity to Inhibition.” *Neuron* 85 (3): 573–89.

Hu, Karin G., Heinrich Reichert, and William S. Stark. 1978. “Electrophysiological Characterization ofDrosophila Ocelli.” *Journal of Comparative Physiology* 126 (1): 15–24.

Hulse, Brad K., Hannah Haberkern, Romain Franconville, Daniel B. Turner-Evans, Shinya Takemura, Tanya Wolff, Marcella Noorman, et al. 2020. “A Connectome of the Drosophila Central Complex Reveals Network Motifs Suitable for Flexible Navigation and Context-Dependent Action Selection.” *bioRxiv*. https://www.biorxiv.org/content/10.1101/2020.12.08.413955v2.full-text.

Israel, Shai, Eyal Rozenfeld, Denise Weber, Wolf Huetteroth, and Moshe Parnas. 2022. “Olfactory Stimuli and Moonwalker SEZ Neurons Can Drive Backward Locomotion in Drosophila.” *Current Biology: CB* 32 (5): 1131–49.e7.

Ito, Kei, Kazunori Shinomiya, Masayoshi Ito, J. Douglas Armstrong, George Boyan, Volker

Hartenstein, Steffen Harzsch, et al. 2014. “A Systematic Nomenclature for the Insect Brain.” *Neuron* 81 (4): 755–65.

Jabr, F. 2012. “The Connectome Debate: Is Mapping the Mind of a Worm Worth It.” *Scientific American*, 2012.

Jain, V., J. F. Murray, F. Roth, S. Turaga, V. Zhigulin, K. L. Briggman, M. N. Helmstaedter, W. Denk, and H. S. Seung. 2007. “Supervised Learning of Image Restoration with Convolutional Networks.” In *2007 IEEE 11th International Conference on Computer Vision*, 1–8. ieeexplore.ieee.org.

Januszewski, Michał, Jörgen Kornfeld, Peter H. Li, Art Pope, Tim Blakely, Larry Lindsey, Jeremy Maitin-Shepard, Mike Tyka, Winfried Denk, and Viren Jain. 2018. “High-Precision Automated Reconstruction of Neurons with Flood-Filling Networks.” *Nature Methods* 15 (8): 605–10.

Jefferis, Gregory, Lucy Collins, Carles Bosch, Marta Costa, and Philipp Schlegel. 2023. “Scaling up Connectomics,” June. https://cms.wellcome.org/sites/default/files/2023-06/Connectomics-scaling-up-connectomics_0.pdf.

Jerison, H. J. 1955. “Brain to Body Ratios and the Evolution of Intelligence.” *Science* 121 (3144): 447–49.

Karuppudurai, Thangavel, Tzu-Yang Lin, Chun-Yuan Ting, Randall Pursley, Krishna V. Melnattur, Fengqiu Diao, Benjamin H. White, et al. 2014. “A Hard-Wired Glutamatergic Circuit Pools and Relays UV Signals to Mediate Spectral Preference in Drosophila.” *Neuron* 81 (3): 603–15.

Kasthuri, Narayanan, and Jeff W. Lichtman. 2007. “The Rise of the ‘Projectome.’” *Nature Methods*. Springer Science and Business Media LLC.

Kim, Anmo J., Lisa M. Fenk, Cheng Lyu, and Gaby Maimon. 2017. “Quantitative Predictions Orchestrate Visual Signaling in Drosophila.” *Cell* 168 (1-2): 280–94.e12.

Kim, Hyunsoo, Mihoko Horigome, Yuki Ishikawa, Feng Li, J. Scott Lauritzen, Gwyneth Card, Davi D. Bock, and Azusa Kamikouchi. 2020. “Wiring Patterns from Auditory Sensory Neurons to the Escape and Song-Relay Pathways in Fruit Flies.” *The Journal of Comparative Neurology* 528 (12): 2068–98.

Kim, J. S., Matthew J. Greene, Aleksandar Zlateski, Kisuk Lee, Mark Richardson, Srinivas C. Turaga, Michael Purcaro, et al. 2014. “Space-Time Wiring Specificity Supports Direction Selectivity in the Retina.” *Nature* 509 (7500): 331–36.

Kind, Emil, Kit D. Longden, Aljoscha Nern, Arthur Zhao, Gizem Sancer, Miriam A. Flynn, Connor W. Laughland, et al. 2021. “Synaptic Targets of Photoreceptors Specialized to Detect Color and Skylight Polarization in Drosophila.” *eLife* 10 (December). https://doi.org/10.7554/eLife.71858.

Klapoetke, Nathan C., Aljoscha Nern, Edward M. Rogers, Gerald M. Rubin, Michael B. Reiser, and Gwyneth M. Card. 2022. “A Functionally Ordered Visual Feature Map in the Drosophila Brain.” *Neuron* 110 (10): 1700–1711.e6.

Knott, Graham, Herschel Marchman, David Wall, and Ben Lich. 2008. “Serial Section Scanning Electron Microscopy of Adult Brain Tissue Using Focused Ion Beam Milling.” *The Journal of Neuroscience: The Official Journal of the Society for Neuroscience* 28 (12): 2959–64.

Kovács, István A., Dániel L. Barabási, and Albert-László Barabási. 2020. “Uncovering the Genetic Blueprint of the C. Elegans Nervous System.” *Proceedings of the National Academy of Sciences of the United States of America* 117 (52): 33570–77.

Kremer, Malte C., Christophe Jung, Sara Batelli, Gerald M. Rubin, and Ulrike Gaul. 2017. “The Glia of the Adult Drosophila Nervous System.” *Glia* 65 (4): 606–38.

Kurmangaliyev, Yerbol Z., Juyoun Yoo, Javier Valdes-Aleman, Piero Sanfilippo, and S. Lawrence Zipursky. 2020. “Transcriptional Programs of Circuit Assembly in the Drosophila Visual System.” *Neuron* 108 (6): 1045–57.e6.

Lappalainen, Janne K., Fabian D. Tschopp, Sridhama Prakhya, Mason McGill, Aljoscha Nern, Kazunori Shinomiya, Shin-Ya Takemura, Eyal Gruntman, Jakob H. Macke, and Srinivas C. Turaga. 2023. “Connectome-Constrained Deep Mechanistic Networks

Predict Neural Responses across the Fly Visual System at Single-Neuron Resolution." *bioRxiv*. https://doi.org/10.1101/2023.03.11.532232.

Lapraz, F., C. Boutres, C. Fixary-Schuster, B. R. De Queiroz, P. Y. Plaçais, D. Cerezo, F. Besse, T. Préat, and S. Noselli. 2023. "Asymmetric Activity of NetrinB Controls Laterality of the Drosophila Brain." *Nature Communications* 14 (1): 1052.

Lee, Kisuk, Nicholas Turner, Thomas Macrina, Jingpeng Wu, Ran Lu, and H. Sebastian Seung. 2019. "Convolutional Nets for Reconstructing Neural Circuits from Brain Images Acquired by Serial Section Electron Microscopy." *Current Opinion in Neurobiology*. https://doi.org/10.1016/j.conb.2019.04.001.

Li, Cai-Hong, and Jun-Li Yang. 2020. "Wolfberry Extracts Inhibit Aβ1-42 Aggregation and Rescue Memory Loss of AD Drosophila." *Food Science and Human Wellness* 9 (1): 64–70.

Lichtman, Jeff W., and Winfried Denk. 2011. "The Big and the Small: Challenges of Imaging the Brain's Circuits." *Science* 334 (6056): 618–23.

Lichtman, Jeff W., and Joshua R. Sanes. 2008. "Ome Sweet Ome: What Can the Genome Tell Us about the Connectome?" *Current Opinion in Neurobiology* 18 (3): 346–53.

Li, Feng, Jack W. Lindsey, Elizabeth C. Marin, Nils Otto, Marisa Dreher, Georgia Dempsey, Ildiko Stark, et al. 2020. "The Connectome of the Adult Drosophila Mushroom Body Provides Insights into Function." *eLife* 9 (December). https://doi.org/10.7554/eLife.62576.

Lin, Andrew C., Alexei M. Bygrave, Alix de Calignon, Tzumin Lee, and Gero Miesenböck. 2014. "Sparse, Decorrelated Odor Coding in the Mushroom Body Enhances Learned Odor Discrimination." *Nature Neuroscience* 17 (4): 559–68.

Liu, Wendy W., and Rachel I. Wilson. 2013. "Glutamate Is an Inhibitory Neurotransmitter in the Drosophila Olfactory System." *Proceedings of the National Academy of Sciences of the United States of America* 110 (25): 10294–99.

Loomba, Sahil, Jakob Straehle, Vijayan Gangadharan, Natalie Heike, Abdelrahman Khalifa, Alessandro Motta, Niansheng Ju, et al. 2022. "Connectomic Comparison of Mouse and Human Cortex." *Science* 377 (6602): eabo0924.

Luan, Haojiang, Nathan C. Peabody, Charles R. Vinson, and Benjamin H. White. 2006. "Refined Spatial Manipulation of Neuronal Function by Combinatorial Restriction of Transgene Expression." *Neuron* 52 (3): 425–36.

Lu, Jenny, Amir H. Behbahani, Lydia Hamburg, Elena A. Westeinde, Paul M. Dawson, Cheng Lyu, Gaby Maimon, Michael H. Dickinson, Shaul Druckmann, and Rachel I. Wilson. 2022. "Transforming Representations of Movement from Body- to World-Centric Space." *Nature* 601 (7891): 98–104.

Mabuchi, Yuta, Xinyue Cui, Lily Xie, Haein Kim, Tianxing Jiang, and Nilay Yapici. 2023a. "GABA-Mediated Inhibition in Visual Feedback Neurons Fine-Tunes Drosophila Male Courtship." *bioRxiv*. https://doi.org/10.1101/2023.01.25.525544.

Mabuchi, Yuta, Xinyue Cui, Lily Xie, Haein Kim, Tianxing Jiang, and Nilay Yapici. 2023b. "Visual Feedback Neurons Fine-Tune *Drosophila* Male Courtship via GABA-Mediated Inhibition." https://doi.org/10.2139/ssrn.4380792.

Macrina, T., K. Lee, R. Lu, N. L. Turner, J. Wu, and S. Popovych. 2021. "Petascale Neural Circuit Reconstruction: Automated Methods." *bioRxiv*. https://www.biorxiv.org/content/10.1101/2021.08.04.455162.abstract.

Mao, Zhengmei, and Ronald L. Davis. 2009. "Eight Different Types of Dopaminergic Neurons Innervate the Drosophila Mushroom Body Neuropil: Anatomical and Physiological Heterogeneity." *Frontiers in Neural Circuits* 3 (July): 5.

Marin, Elizabeth C., Billy J. Morris, Tomke Stuerner, Andrew S. Champion, Dominik Krzeminski, Griffin Badalamente, Marina Gkantia, et al. 2023. "Systematic Annotation of a Complete Adult Male Drosophila Nerve Cord Connectome Reveals Principles of Functional Organisation." *bioRxiv*. https://doi.org/10.1101/2023.06.05.543407.

Markov, Nikola T., Maria M. Ercsey-Ravasz, A. R. Ribeiro Gomes, Camille Lamy, Loic Magrou, Julien Vezoli, Pierre Misery, et al. 2014. "A Weighted and Directed Interareal Connectivity Matrix for Macaque Cerebral Cortex." *Cerebral Cortex* 24 (1): 17–36.

Ma, Xiaoya, Xianguang Hou, Gregory D. Edgecombe, and Nicholas J. Strausfeld. 2012. "Complex Brain and Optic Lobes in an Early Cambrian Arthropod." *Nature* 490 (7419): 258–61.

McCarthy, Ellena V., Ying Wu, Tagide Decarvalho, Christian Brandt, Guan Cao, and Michael N. Nitabach. 2011. "Synchronized Bilateral Synaptic Inputs to Drosophila Melanogaster Neuropeptidergic Rest/arousal Neurons." *The Journal of Neuroscience: The Official Journal of the Society for Neuroscience* 31 (22): 8181–93.

McInnes, Leland, John Healy, and James Melville. 2018. "UMAP: Uniform Manifold Approximation and Projection for Dimension Reduction." *arXiv [stat.ML]*. arXiv. http://arxiv.org/abs/1802.03426.

Meier, Matthias, and Alexander Borst. 2019. "Extreme Compartmentalization in a Drosophila Amacrine Cell." *Current Biology: CB* 29 (9): 1545–50.e2.

Meinertzhagen, Ian A. 2018. "Of What Use Is Connectomics? A Personal Perspective on the Drosophila Connectome." *The Journal of Experimental Biology* 221 (10). https://doi.org/10.1242/jeb.164954.

Meissner, Geoffrey W., Aljoscha Nern, Zachary Dorman, Gina M. DePasquale, Kaitlyn Forster, Theresa Gibney, Joanna H. Hausenfluck, et al. 2023. "A Searchable Image Resource of Drosophila GAL4 Driver Expression Patterns with Single Neuron Resolution." *eLife* 12 (February). https://doi.org/10.7554/eLife.80660.

Mesulam, M. M. 1998. "From Sensation to Cognition." *Brain: A Journal of Neurology* 121 (Pt 6) (June): 1013–52.

MICrONS Consortium, J. Alexander Bae, Mahaly Baptiste, Agnes L. Bodor, Derrick Brittain, Joann Buchanan, Daniel J. Bumbarger, et al. 2021. "Functional Connectomics Spanning Multiple Areas of Mouse Visual Cortex." *bioRxiv*. https://doi.org/10.1101/2021.07.28.454025.

Molina-Obando, Sebastian, Juan Felipe Vargas-Fique, Miriam Henning, Burak Gür, T. Moritz Schladt, Junaid Akhtar, Thomas K. Berger, and Marion Silies. 2019. "ON Selectivity in the Drosophila Visual System Is a Multisynaptic Process Involving Both Glutamatergic and GABAergic Inhibition." *eLife* 8 (September). https://doi.org/10.7554/eLife.49373.

Murthy, Mala, Ila Fiete, and Gilles Laurent. 2008. "Testing Odor Response Stereotypy in the Drosophila Mushroom Body." *Neuron* 59 (6): 1009–23.

Mu, Shang, Szi-Chieh Yu, Nicholas L. Turner, Claire E. McKellar, Sven Dorkenwald, Forrest Collman, Selden Koolman, et al. 2021. "3D Reconstruction of Cell Nuclei in a Full Drosophila Brain." *bioRxiv*. https://doi.org/10.1101/2021.11.04.467197.

Nern, A., B. D. Pfeiffer, and G. M. Rubin. 2015. "Optimized Tools for Multicolor Stochastic Labeling Reveal Diverse Stereotyped Cell Arrangements in the Fly Visual System." *Proceedings of the*. https://www.pnas.org/content/112/22/E2967.short.

Nguyen, Tri M., Logan A. Thomas, Jeff L. Rhoades, Ilaria Ricchi, Xintong Cindy Yuan, Arlo Sheridan, David G. C. Hildebrand, Jan Funke, Wade G. Regehr, and Wei-Chung Allen Lee. 2023. "Structured Cerebellar Connectivity Supports Resilient Pattern Separation." *Nature* 613 (7944): 543–49.

Oh, Seung Wook, Julie A. Harris, Lydia Ng, Brent Winslow, Nicholas Cain, Stefan Mihalas, Quanxin Wang, et al. 2014. "A Mesoscale Connectome of the Mouse Brain." *Nature* 508 (7495): 207–14.

Otsuna, Hideo, and Kei Ito. 2006. "Systematic Analysis of the Visual Projection Neurons of Drosophila Melanogaster. I. Lobula-Specific Pathways." *The Journal of Comparative Neurology* 497 (6): 928–58.

Özel, Mehmet Neset, Félix Simon, Shadi Jafari, Isabel Holguera, Yen-Chung Chen, Najate Benhra, Rana Naja El-Danaf, et al. 2021. "Neuronal Diversity and Convergence in a Visual System Developmental Atlas." *Nature* 589 (7840): 88–95.

Pacheco, Diego A., Stephan Y. Thiberge, Eftychios Pnevmatikakis, and Mala Murthy. 2021. "Auditory Activity Is Diverse and Widespread throughout the Central Brain of Drosophila." *Nature Neuroscience* 24 (1): 93–104.

Pfeiffer, Barret D., Teri-T B. Ngo, Karen L. Hibbard, Christine Murphy, Arnim Jenett, James W. Truman, and Gerald M. Rubin. 2010. "Refinement of Tools for Targeted Gene

Expression in Drosophila." *Genetics* 186 (2): 735–55.
Phelps, Jasper S., David Grant Colburn Hildebrand, Brett J. Graham, Aaron T. Kuan, Logan A. Thomas, Tri M. Nguyen, Julia Buhmann, et al. 2021. "Reconstruction of Motor Control Circuits in Adult Drosophila Using Automated Transmission Electron Microscopy." *Cell* 184 (3): 759–74.e18.
Popovych, Sergiy, Thomas Macrina, Nico Kemnitz, Manuel Castro, Barak Nehoran, Zhen Jia, J. Alexander Bae, et al. 2022. "Petascale Pipeline for Precise Alignment of Images from Serial Section Electron Microscopy." *bioRxiv*. https://doi.org/10.1101/2022.03.25.485816.
Prisco, Luigi, Stephan Hubertus Deimel, Hanna Yeliseyeva, André Fiala, and Gaia Tavosanis. 2021. "The Anterior Paired Lateral Neuron Normalizes Odour-Evoked Activity in the Drosophila Mushroom Body Calyx." *eLife* 10 (December). https://doi.org/10.7554/eLife.74172.
Repérant, J., R. Ward, D. Miceli, J. P. Rio, M. Médina, N. B. Kenigfest, and N. P. Vesselkin. 2006. "The Centrifugal Visual System of Vertebrates: A Comparative Analysis of Its Functional Anatomical Organization." *Brain Research Reviews* 52 (1): 1–57.
Sato, M., I. Bitter, M. A. Bender, A. E. Kaufman, and M. Nakajima. 2000. "TEASAR: Tree-Structure Extraction Algorithm for Accurate and Robust Skeletons." In . https://doi.org/10.1109/pccga.2000.883951.
Schaffer, Evan S., Neeli Mishra, Matthew R. Whiteway, Wenze Li, Michelle B. Vancura, Jason Freedman, Kripa B. Patel, et al. 2021. "Flygenvectors: The Spatial and Temporal Structure of Neural Activity across the Fly Brain." *bioRxiv*. https://doi.org/10.1101/2021.09.25.461804.
Scheffer, Louis K., C. Shan Xu, Michal Januszewski, Zhiyuan Lu, Shin-Ya Takemura, Kenneth J. Hayworth, Gary B. Huang, et al. 2020. "A Connectome and Analysis of the Adult Drosophila Central Brain." *eLife* 9 (September). https://doi.org/10.7554/eLife.57443.
Schlegel, P., A. S. Bates, T. Stürner, and S. R. Jagannathan. 2021. "Information Flow, Cell Types and Stereotypy in a Full Olfactory Connectome." *eLife*. https://elifesciences.org/articles/66018.
Schlegel, Philipp, Yijie Yin, Alexander S. Bates, Sven Dorkenwald, Katharina Eichler, Paul Brooks, Daniel S. Han, et al. 2023. "A Consensus Cell Type Atlas from Multiple Connectomes Reveals Principles of Circuit Stereotypy and Variation." *bioRxiv*.
Schneider-Mizell, Casey M., Stephan Gerhard, Mark Longair, Tom Kazimiers, Feng Li, Maarten F. Zwart, Andrew Champion, et al. 2016. "Quantitative Neuroanatomy for Connectomics in Drosophila." *eLife* 5 (March). https://doi.org/10.7554/eLife.12059.
Schoofs, Andreas, Anton Miroschnikow, Philipp Schlegel, Ingo Zinke, Casey M. Schneider-Mizell, Albert Cardona, and Michael J. Pankratz. 2023. "Serotonergic Reinforcement of a Complete Swallowing Circuit." *bioRxiv*. https://doi.org/10.1101/2023.05.26.542464.
Schretter, Catherine E., Yoshinori Aso, Alice A. Robie, Marisa Dreher, Michael-John Dolan, Nan Chen, Masayoshi Ito, et al. 2020. "Cell Types and Neuronal Circuitry Underlying Female Aggression in Drosophila." *eLife* 9 (November). https://doi.org/10.7554/eLife.58942.
Schüz, A., and G. Palm. 1989. "Density of Neurons and Synapses in the Cerebral Cortex of the Mouse." *The Journal of Comparative Neurology* 286 (4): 442–55.
Seung, Sebastian. 2012. *Connectome: How the Brain's Wiring Makes Us Who We Are*. HMH.
Shapson-Coe, A., M. Januszewski, D. R. Berger, and A. Pope. 2021. "A Connectomic Study of a Petascale Fragment of Human Cerebral Cortex." *bioRxiv*. https://www.biorxiv.org/content/10.1101/2021.05.29.446289v1.abstract.
Sherer, Lewis M., Elizabeth Catudio Garrett, Hannah R. Morgan, Edmond D. Brewer, Lucy A. Sirrs, Harold K. Shearin, Jessica L. Williams, Brian D. McCabe, R. Steven Stowers, and Sarah J. Certel. 2020. "Octopamine Neuron Dependent Aggression Requires dVGLUT from Dual-Transmitting Neurons." *PLoS Genetics* 16 (2): e1008609.

Shih, Chi-Tin, Olaf Sporns, Shou-Li Yuan, Ta-Shun Su, Yen-Jen Lin, Chao-Chun Chuang, Ting-Yuan Wang, Chung-Chuang Lo, Ralph J. Greenspan, and Ann-Shyn Chiang. 2015. "Connectomics-Based Analysis of Information Flow in the Drosophila Brain." *Current Biology: CB* 25 (10): 1249–58.

Shinomiya, Kazunori, Gary Huang, Zhiyuan Lu, Toufiq Parag, C. Shan Xu, Roxanne Aniceto, Namra Ansari, et al. 2019. "Comparisons between the ON- and OFF-Edge Motion Pathways in the Drosophila Brain." *eLife* 8 (January). https://doi.org/10.7554/eLife.40025.

Shinomiya, Kazunori, Aljoscha Nern, Ian A. Meinertzhagen, Stephen M. Plaza, and Michael B. Reiser. 2022. "Neuronal Circuits Integrating Visual Motion Information in Drosophila Melanogaster." *Current Biology: CB* 32 (16): 3529–44.e2.

Shiu, Philip K., Gabriella R. Sterne, Stefanie Engert, Barry J. Dickson, and Kristin Scott. 2022. "Taste Quality and Hunger Interactions in a Feeding Sensorimotor Circuit." *eLife* 11 (July). https://doi.org/10.7554/eLife.79887.

Shiu, Philip K., Gabriella R. Sterne, Nico Spiller, Romain Franconville, Andrea Sandoval, Joie Zhou, Neha Simha, et al. 2023. "A Leaky Integrate-and-Fire Computational Model Based on the Connectome of the Entire Adult Drosophila Brain Reveals Insights into Sensorimotor Processing." *bioRxiv*. https://doi.org/10.1101/2023.05.02.539144.

Sporns, Olaf, Giulio Tononi, and Rolf Kötter. 2005. "The Human Connectome: A Structural Description of the Human Brain." *PLoS Computational Biology* 1 (4): e42.

Stange, G., S. Stowe, J. S. Chahl, and A. Massaro. 2002. "Anisotropic Imaging in the Dragonfly Median Ocellus: A Matched Filter for Horizon Detection." *Journal of Comparative Physiology. A, Neuroethology, Sensory, Neural, and Behavioral Physiology* 188 (6): 455–67.

Stark, W. S., R. Sapp, and S. D. Carlson. 1989. "Ultrastructure of the Ocellar Visual System in Normal and Mutant Drosophila Melanogaster." *Journal of Neurogenetics* 5 (2): 127–53.

Sterne, Gabriella R., Hideo Otsuna, Barry J. Dickson, and Kristin Scott. 2021. "Classification and Genetic Targeting of Cell Types in the Primary Taste and Premotor Center of the Adult Drosophila Brain." *eLife* 10 (September). https://doi.org/10.7554/eLife.71679.

Suver, Marie P., Ainul Huda, Nicole Iwasaki, Steve Safarik, and Michael H. Dickinson. 2016. "An Array of Descending Visual Interneurons Encoding Self-Motion in Drosophila." *The Journal of Neuroscience: The Official Journal of the Society for Neuroscience* 36 (46): 11768–80.

Swanson, L. W. 1995. "Mapping the Human Brain: Past, Present, and Future." *Trends in Neurosciences* 18 (11): 471–74.

Takemura, Shin-Ya, Arjun Bharioke, Zhiyuan Lu, Aljoscha Nern, Shiv Vitaladevuni, Patricia K. Rivlin, William T. Katz, et al. 2013. "A Visual Motion Detection Circuit Suggested by Drosophila Connectomics." *Nature* 500 (7461): 175–81.

Takemura, Shin-Ya, Kenneth J. Hayworth, Gary B. Huang, Michal Januszewski, Zhiyuan Lu, Elizabeth C. Marin, Stephan Preibisch, et al. 2023. "A Connectome of the Male Drosophila Ventral Nerve Cord." *bioRxiv*. https://doi.org/10.1101/2023.06.05.543757.

Takemura, S., A. Nern, D. B. Chklovskii, and L. K. Scheffer. 2017. "The Comprehensive Connectome of a Neural Substrate for 'ON'motion Detection in Drosophila." *eLife*. https://cdn.elifesciences.org/articles/24394/elife-24394-v2.pdf.

Task, Darya, Chun-Chieh Lin, Alina Vulpe, Ali Afify, Sydney Ballou, Maria Brbic, Philipp Schlegel, et al. 2022. "Chemoreceptor Co-Expression in Drosophila Melanogaster Olfactory Neurons." *eLife* 11 (April). https://doi.org/10.7554/eLife.72599.

Turaga, Srinivas C., Joseph F. Murray, Viren Jain, Fabian Roth, Moritz Helmstaedter, Kevin Briggman, Winfried Denk, and H. Sebastian Seung. 2010. "Convolutional Networks Can Learn to Generate Affinity Graphs for Image Segmentation." *Neural Computation* 22 (2): 511–38.

Turner, Nicholas L., Thomas Macrina, J. Alexander Bae, Runzhe Yang, Alyssa M. Wilson, Casey Schneider-Mizell, Kisuk Lee, et al. 2022. "Reconstruction of Neocortex: Organelles, Compartments, Cells, Circuits, and Activity." *Cell*, February.

https://doi.org/10.1016/j.cell.2022.01.023.
Tuthill, John C., Aljoscha Nern, Gerald M. Rubin, and Michael B. Reiser. 2014. “Wide-Field Feedback Neurons Dynamically Tune Early Visual Processing.” *Neuron* 82 (4): 887–95.
Varshney, Lav R., Beth L. Chen, Eric Paniagua, David H. Hall, and Dmitri B. Chklovskii. 2011. “Structural Properties of the Caenorhabditis Elegans Neuronal Network.” *PLoS Computational Biology* 7 (2): e1001066.
Vogt, Katrin, Yoshinori Aso, Toshihide Hige, Stephan Knapek, Toshiharu Ichinose, Anja B. Friedrich, Glenn C. Turner, Gerald M. Rubin, and Hiromu Tanimoto. 2016. “Direct Neural Pathways Convey Distinct Visual Information to Drosophila Mushroom Bodies.” *eLife* 5 (April). https://doi.org/10.7554/eLife.14009.
Waddell, S., J. D. Armstrong, T. Kitamoto, K. Kaiser, and W. G. Quinn. 2000. “The Amnesiac Gene Product Is Expressed in Two Neurons in the Drosophila Brain That Are Critical for Memory.” *Cell* 103 (5): 805–13.
Wang, Kaiyu, Fei Wang, Nora Forknall, Tansy Yang, Christopher Patrick, Ruchi Parekh, and Barry J. Dickson. 2021. “Neural Circuit Mechanisms of Sexual Receptivity in Drosophila Females.” *Nature* 589 (7843): 577–81.
White, J. G., E. Southgate, J. N. Thomson, and S. Brenner. 1986. “The Structure of the Nervous System of the Nematode Caenorhabditis Elegans.” *Philosophical Transactions of the Royal Society of London. Series B, Biological Sciences* 314 (1165): 1–340.
Winding, Michael, Benjamin D. Pedigo, Christopher L. Barnes, Heather G. Patsolic, Youngser Park, Tom Kazimiers, Akira Fushiki, et al. 2023. “The Connectome of an Insect Brain.” *Science* 379 (6636): eadd9330.
Witvliet, Daniel, Ben Mulcahy, James K. Mitchell, Yaron Meirovitch, Daniel R. Berger, Yuelong Wu, Yufang Liu, et al. 2021. “Connectomes across Development Reveal Principles of Brain Maturation.” *Nature* 596 (7871): 257–61.
Wu, Ming, Aljoscha Nern, W. Ryan Williamson, Mai M. Morimoto, Michael B. Reiser, Gwyneth M. Card, and Gerald M. Rubin. 2016. “Visual Projection Neurons in the Drosophila Lobula Link Feature Detection to Distinct Behavioral Programs.” *eLife* 5 (December). https://doi.org/10.7554/eLife.21022.
Xu, C. Shan, Kenneth J. Hayworth, Zhiyuan Lu, Patricia Grob, Ahmed M. Hassan, José G. García-Cerdán, Krishna K. Niyogi, Eva Nogales, Richard J. Weinberg, and Harald F. Hess. 2017. “Enhanced FIB-SEM Systems for Large-Volume 3D Imaging.” *eLife* 6 (May). https://doi.org/10.7554/eLife.25916.
Yildirim, Kerem, Johanna Petri, Rita Kottmeier, and Christian Klämbt. 2019. “Drosophila Glia: Few Cell Types and Many Conserved Functions.” *Glia* 67 (1): 5–26.
Yoo, Juyoun, Mark Dombrovski, Parmis Mirshahidi, Aljoscha Nern, Samuel A. LoCascio, S. Lawrence Zipursky, and Yerbol Z. Kurmangaliyev. 2023. “Identifying Determinants of Synaptic Specificity by Integrating Connectomes and Transcriptomes.” *bioRxiv*. https://doi.org/10.1101/2023.04.03.534791.
Yu, Wan-Qing, Rana N. El-Danaf, Haruhisa Okawa, Justin M. Pacholec, Ulf Matti, Karin Schwarz, Benjamin Odermatt, et al. 2018. “Synaptic Convergence Patterns onto Retinal Ganglion Cells Are Preserved despite Topographic Variation in Pre- and Postsynaptic Territories.” *Cell Reports* 25 (8): 2017–26.e3.
Zhao, Arthur, Eyal Gruntman, Aljoscha Nern, Nirmala A. Iyer, Edward M. Rogers, Sanna Koskela, Igor Siwanowicz, et al. 2022. “Eye Structure Shapes Neuron Function in Drosophila Motion Vision.” *bioRxiv*. https://doi.org/10.1101/2022.12.14.520178.
Zheng, Zhihao, J. Scott Lauritzen, Eric Perlman, Camenzind G. Robinson, Matthew Nichols, Daniel Milkie, Omar Torrens, et al. 2018. “A Complete Electron Microscopy Volume of the Brain of Adult Drosophila Melanogaster.” *Cell* 174 (3): 730–43.e22.
Zheng, Zhihao, Feng Li, Corey Fisher, Iqbal J. Ali, Nadiya Sharifi, Steven Calle-Schuler, Joseph Hsu, et al. 2022. “Structured Sampling of Olfactory Input by the Fly Mushroom Body.” *Current Biology: CB* 32 (15): 3334–49.e6.
Zingg, Brian, Houri Hintiryan, Lin Gou, Monica Y. Song, Maxwell Bay, Michael S. Bienkowski, Nicholas N. Foster, et al. 2014. “Neural Networks of the Mouse Neocortex.” *Cell* 156 (5): 1096–1111.

Extended Data Figures

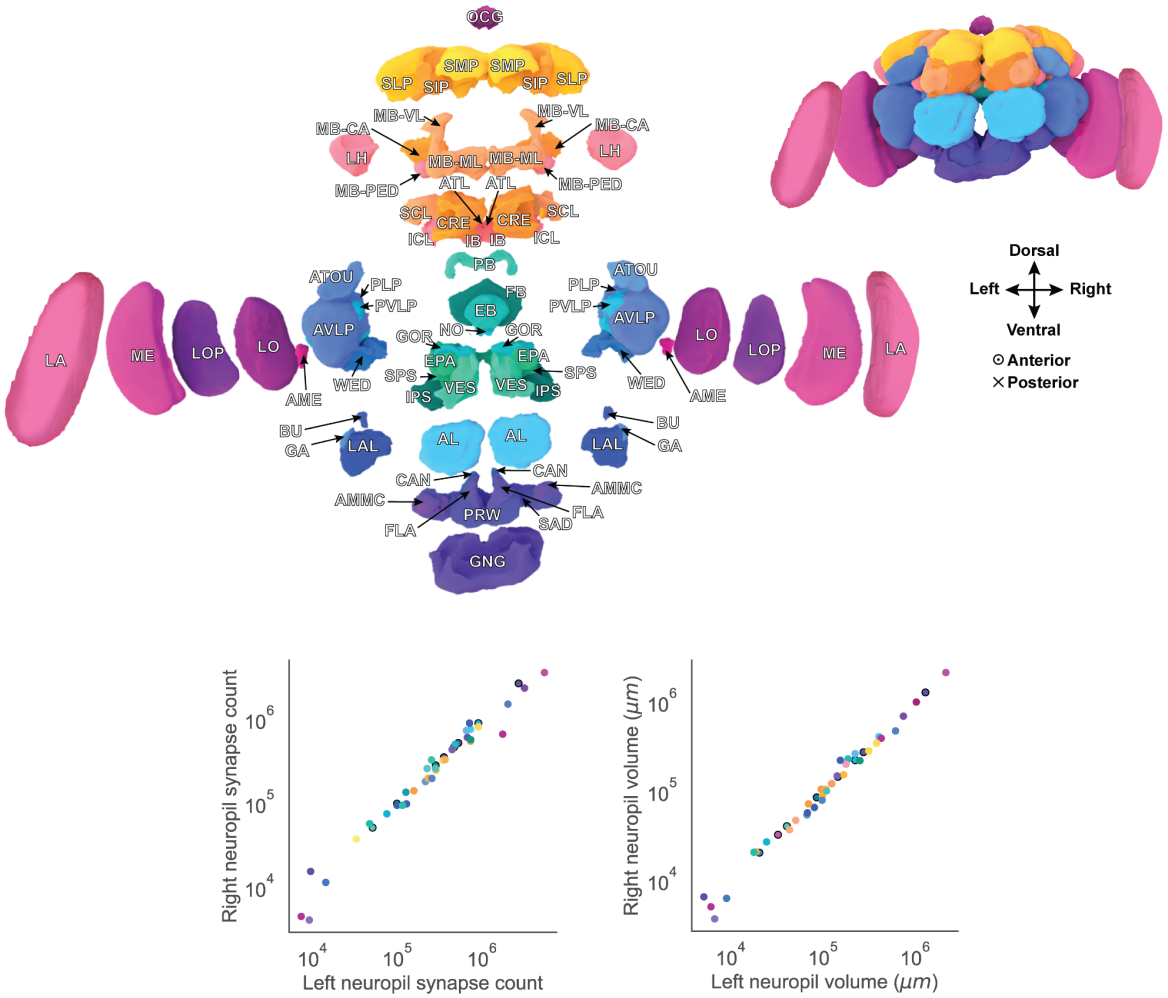

Ext.-Figure 1-1. Neuropils of the fly brain.

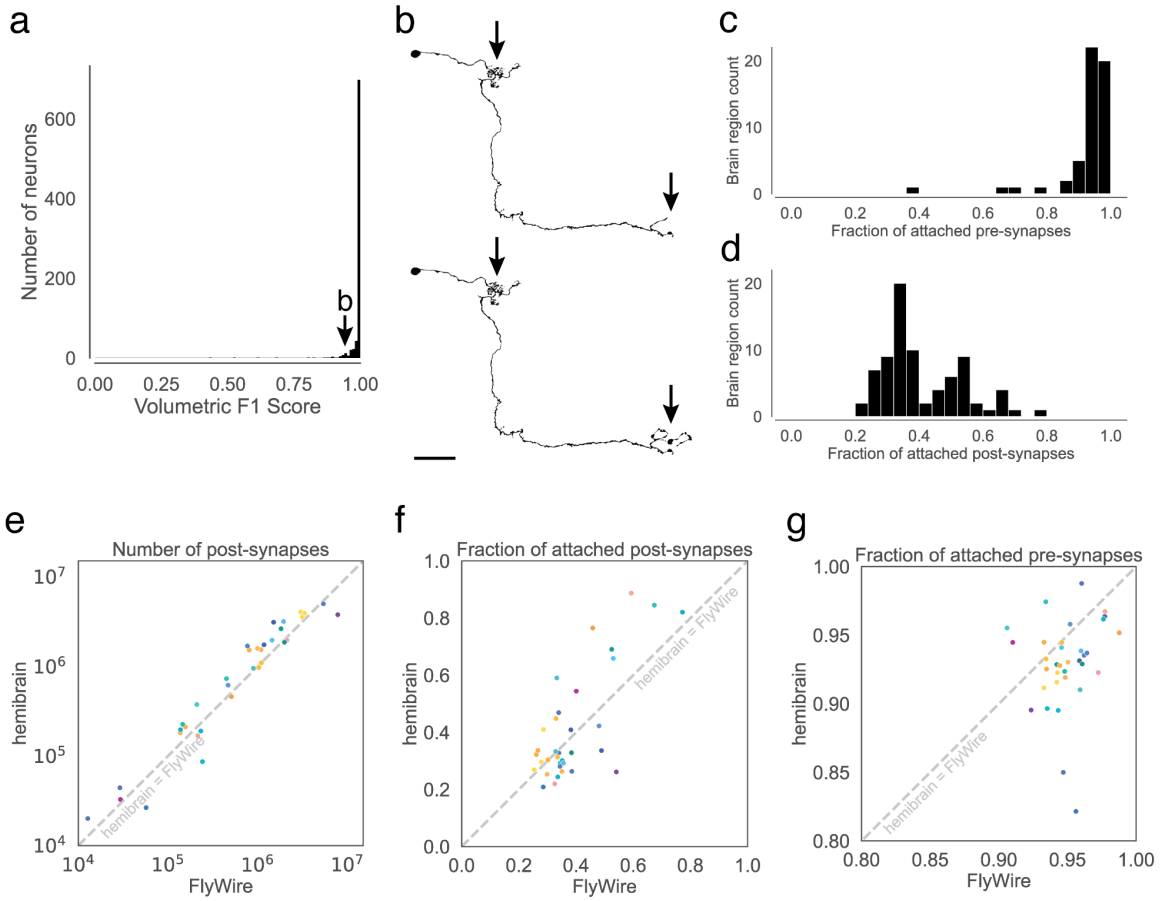

Ext. Figure 1-2. Completeness and accuracy of FlyWire's reconstruction. (a) shows the result of our evaluation of proofread segments in the central brain. Experts attempted further proofreading of 826 neurons. We computed volumetric overlaps between the original and the final segment to calculate precision, recall, and F1 Scores. (b) Examples (top: before, bottom: after) of the changes made during further proofreading for a neuron scoring an F1-Score of 0.936. Arrows highlight locations that changed. (c,d) For each neuropil, we quantified what fraction of the synapses within it are pre- and postsynaptically attached to a proofread segment. (c) displays the distribution for presynaptic attachment and (d) the distribution for postsynaptic attachment. (e, f, g) Comparisons between FlyWire's reconstruction and the hemibrain were made for overlapping neuropils. Dots represent neuropils and are colored according to Ext. Data Fig. 1-1. (e) Comparison of the number of automatically detected synapses. The axes are log-transformed. (f) Comparison of post-synaptic completion rates and (g) pre-synaptic completion rate. The axes are truncated.

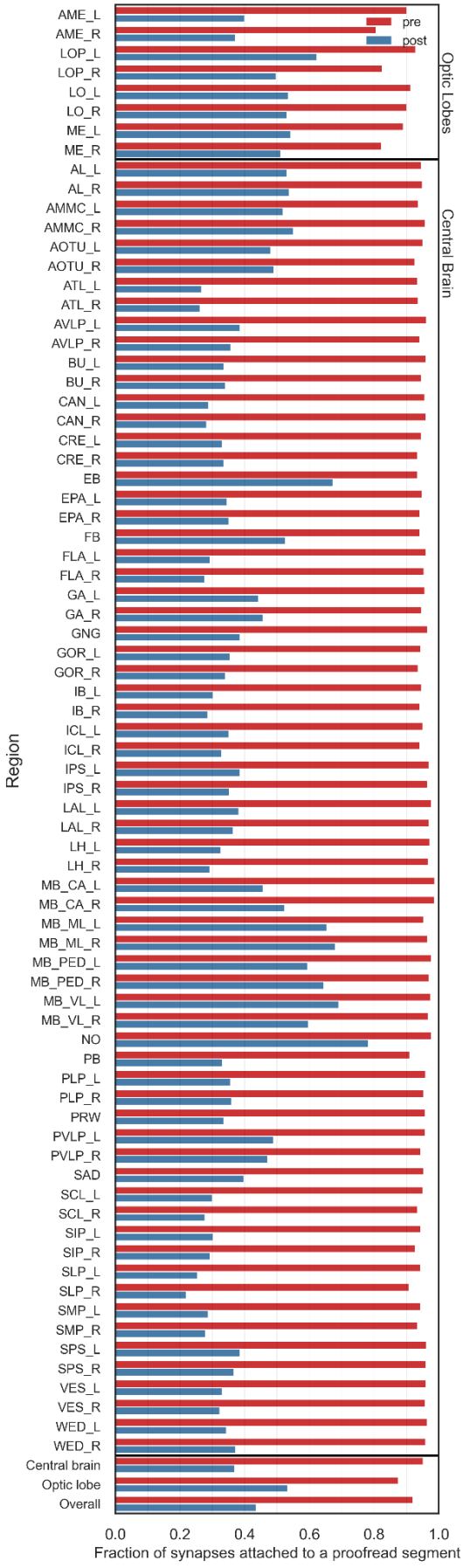

Ext. Figure 1-3. Completion rates by neuropil.

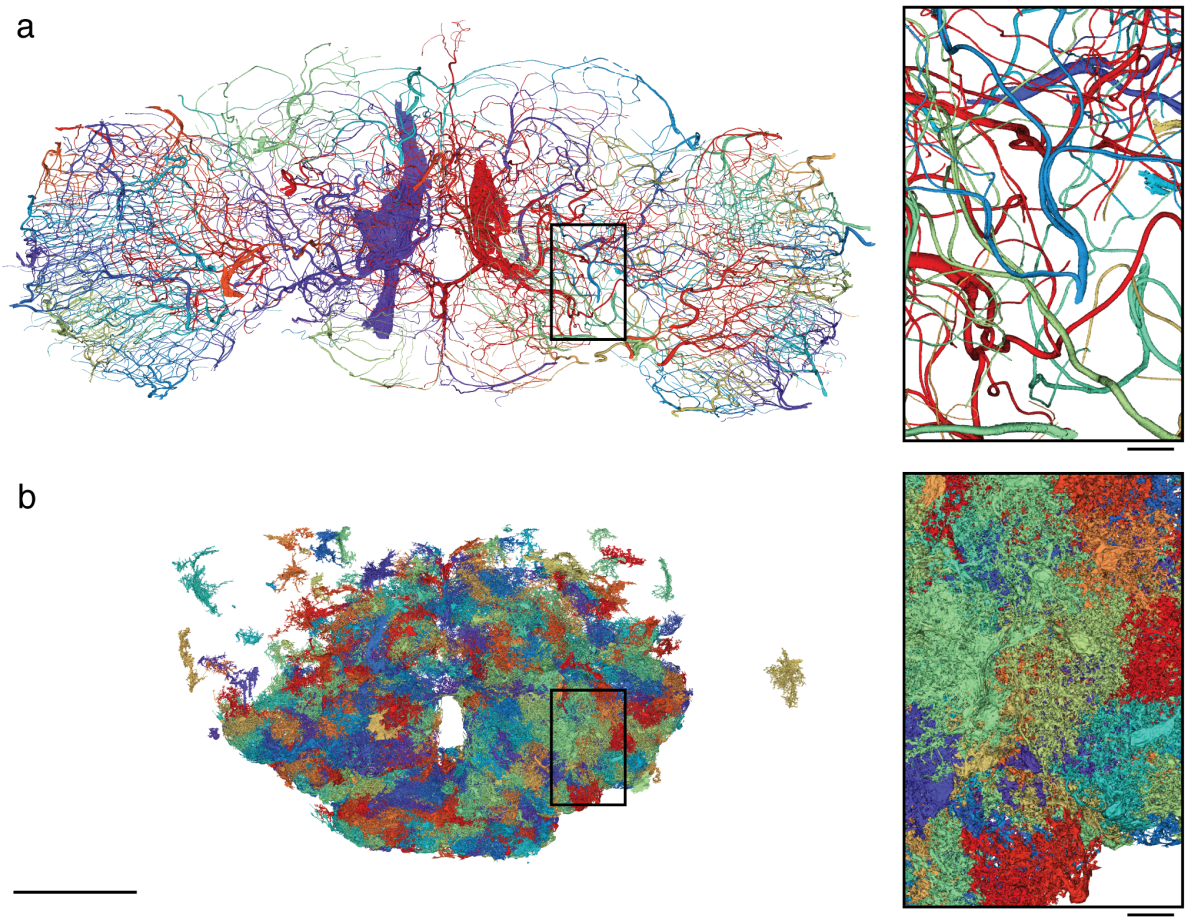

Ext. Figure 1-4. Trachea and glia cells. (a) Rendering of all trachea segments in the FlyWire dataset. (b) Rendering of some reconstructed glia cells in the FlyWire dataset. At the time of writing, only a subset of the glia cells, with bias towards the central brain, have been proofread and labeled. Scale bar: 100 µm; insets: 10 µm.

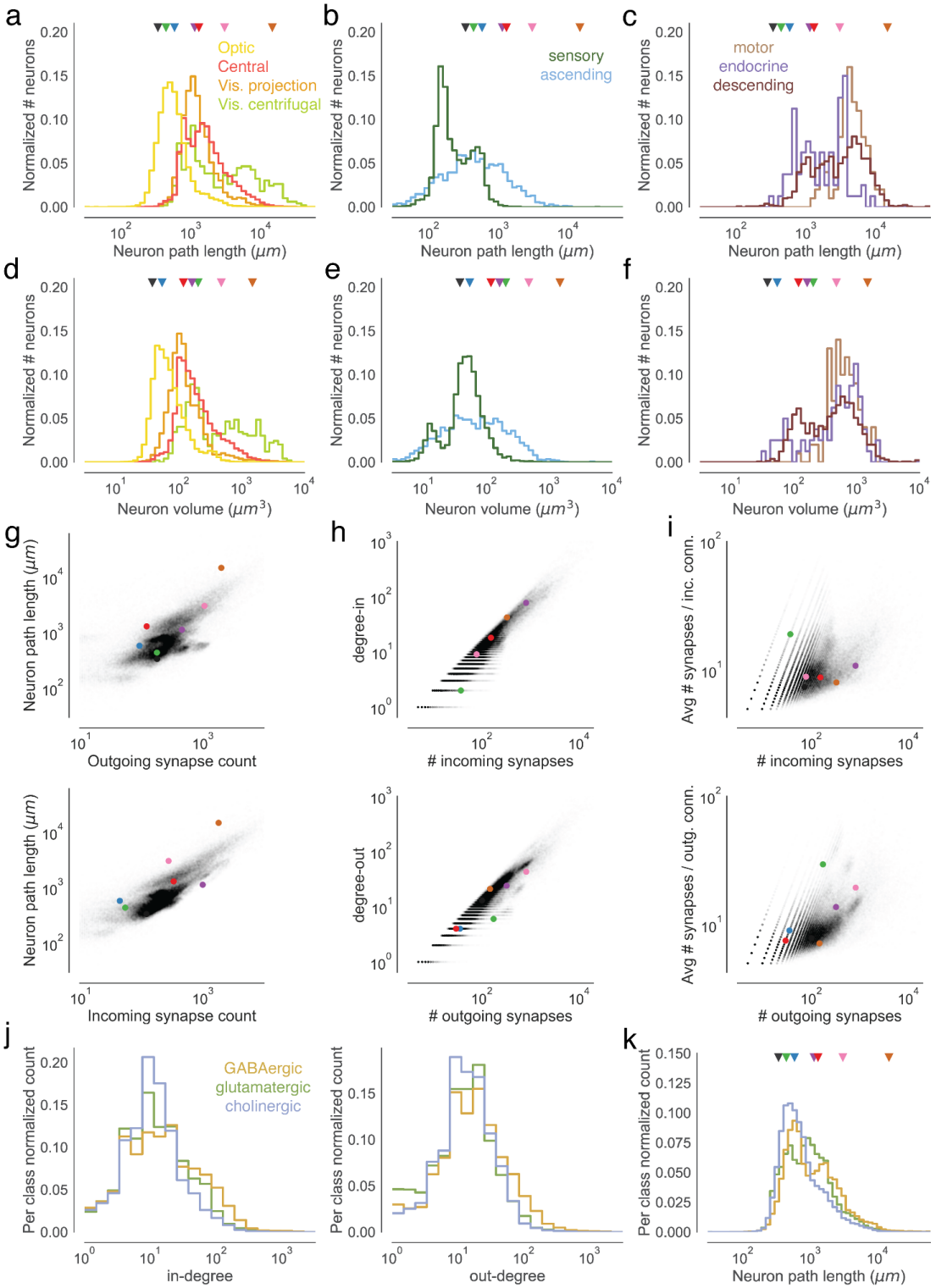

Extended Data Figure 3-1. Measurements of neuron size. Colored markers refer to neurons in Fig. 3b. (a) Neuron path lengths of intrinsic neurons, (b) afferent neurons, and (b) efferent neurons by super class. (d) Volumes of intrinsic neurons, (e) afferent neurons, and (f) efferent neurons by super class. (g) Comparisons of path lengths and number of incoming and outgoing synapses. (h) For intrinsic neurons, comparisons of the in- and out-degrees with the number of incoming and outgoing synapses. Every dot is a neuron. (i) Comparison of average connection strengths (synapses per connection) with the number of synapses. Every dot is a neuron. (j) In- and out-degree distributions by neurotransmitter type. (k) Neuron path lengths by neurotransmitter type.

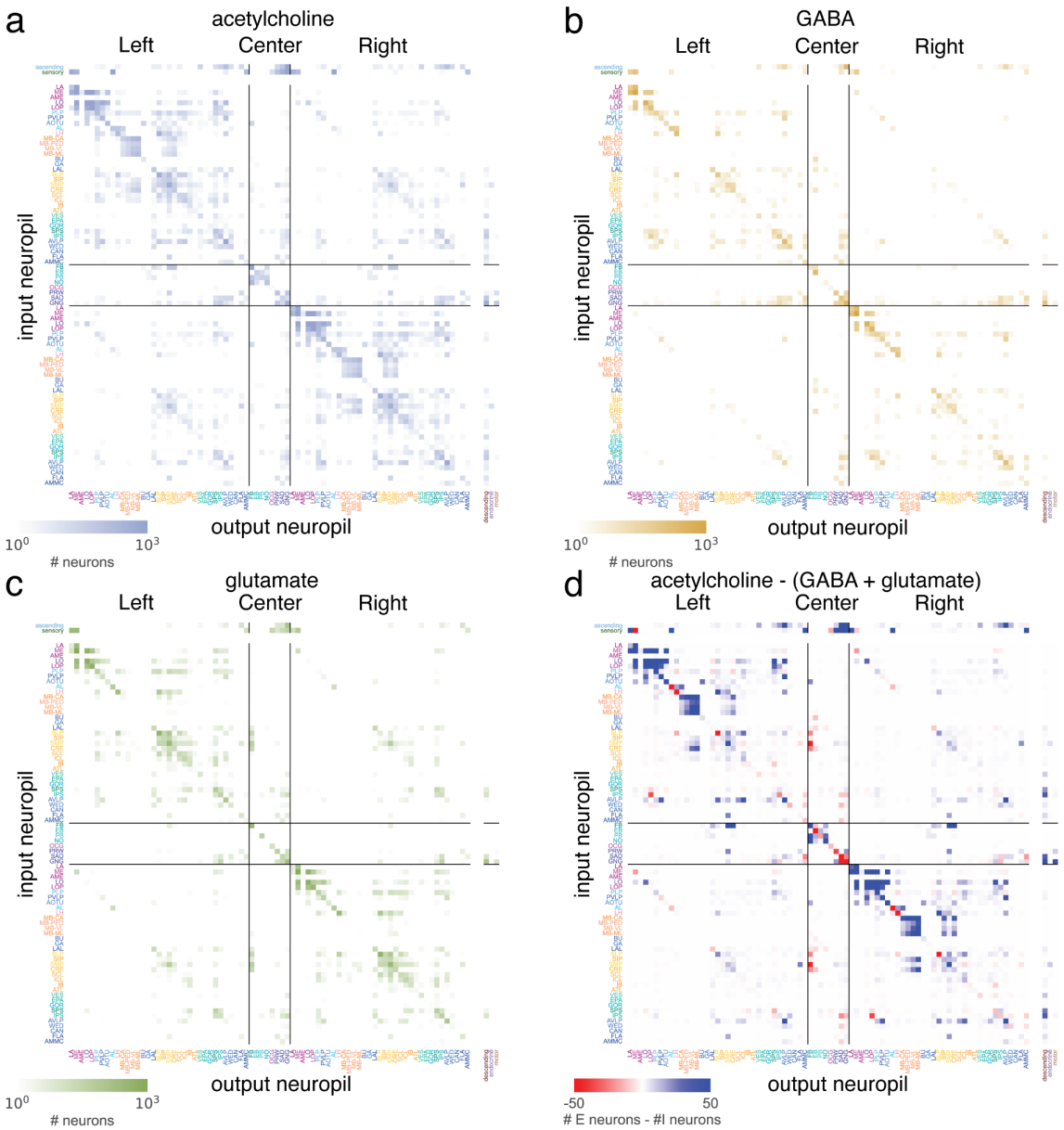

Ext. Figure 4-1. Neuropil-neuropil projection maps. (a) Projection maps produced as in Fig. 4a limited to connections from cholinergic, (b) GABAergic, and (c) glutamatergic neurons. (d) The difference between the putative excitatory (acetylcholine) and the putative inhibitory (GABA, glutamate) projection maps.

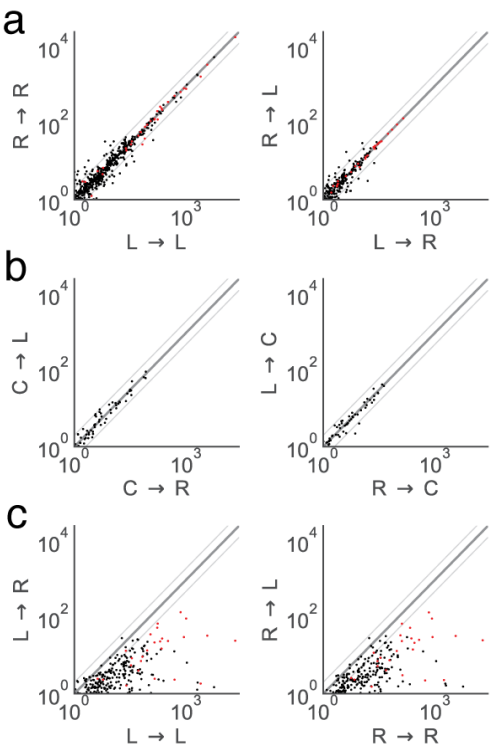

Ext. Figure 4-2. Neuropil-neuropil projections compared between hemispheres. Each dot is a neuropil-neuropil projection in one hemisphere and the axes show the fractional weights as calculated in Fig. 4a,b. Red dots are comparisons between the same neuropils in different hemispheres (e.g. AMMC(L) -> VLP(L) vs AMMC(R) -> VLP(R). (a) Comparison of projections between neuropils in both hemispheres and between hemispheres. (b) Comparisons of projections with the center neuropils. (c) Comparisons of projections between ipsilateral and contralateral neuropil projections.

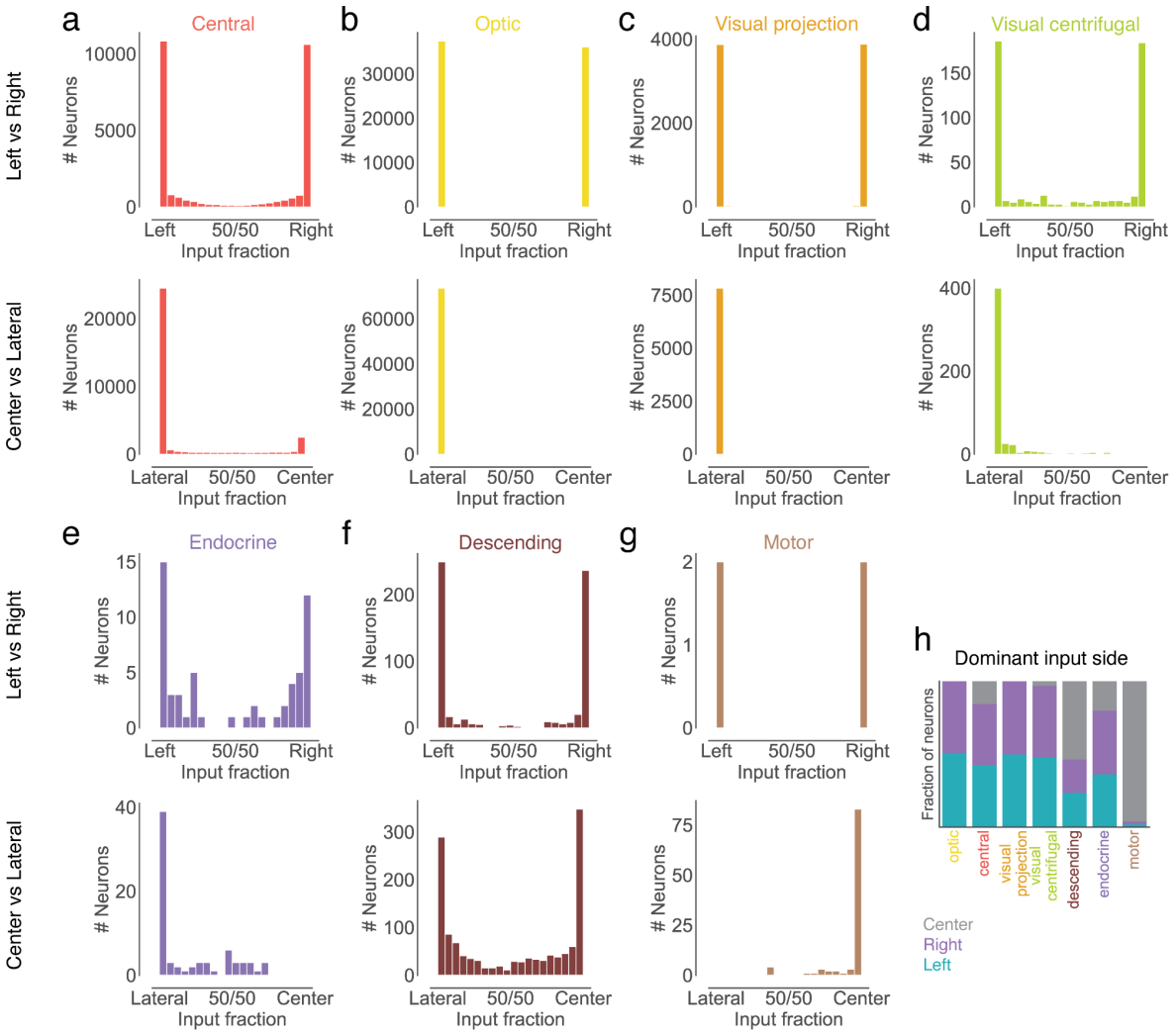

Ext. Figure 4-3. Input side analysis. We assigned postsynaptic locations to either the center region or the left or right hemisphere. (a-g) For each super class, the fraction of synapses in the left vs right hemisphere is shown for those neurons receiving most of their neurons laterally (top plot). The lower plot shows the fraction of synapses in the center vs the lateral regions for all neurons. (h) Each neuron was assigned to the side where it received most of its inputs.

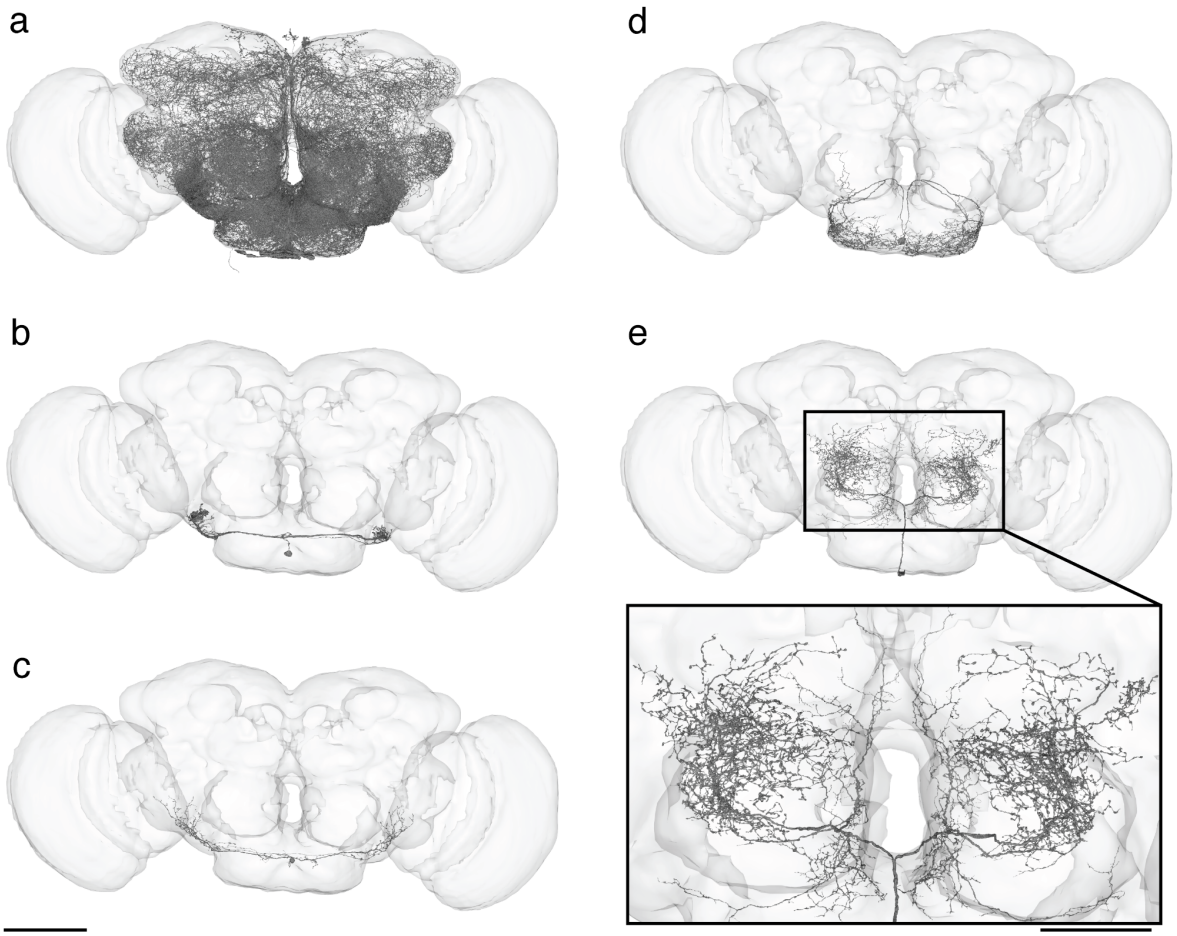

Ext. Figure 4-4. Neurons on the midline with dendrites in both hemispheres. (a) All symmetric neurons with a cell body on the midline (N=106). (b-e) examples of individual neurons. Scale bar: 100 µm, inset: 50 µm

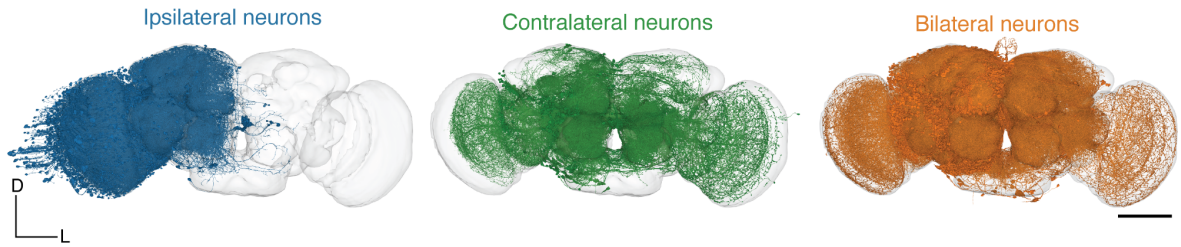

Ext. Figure 4-5. Renderings of neurons for each cross-hemisphere category (up to 3,000 neurons rendered per group). Scale bar: 100 µm

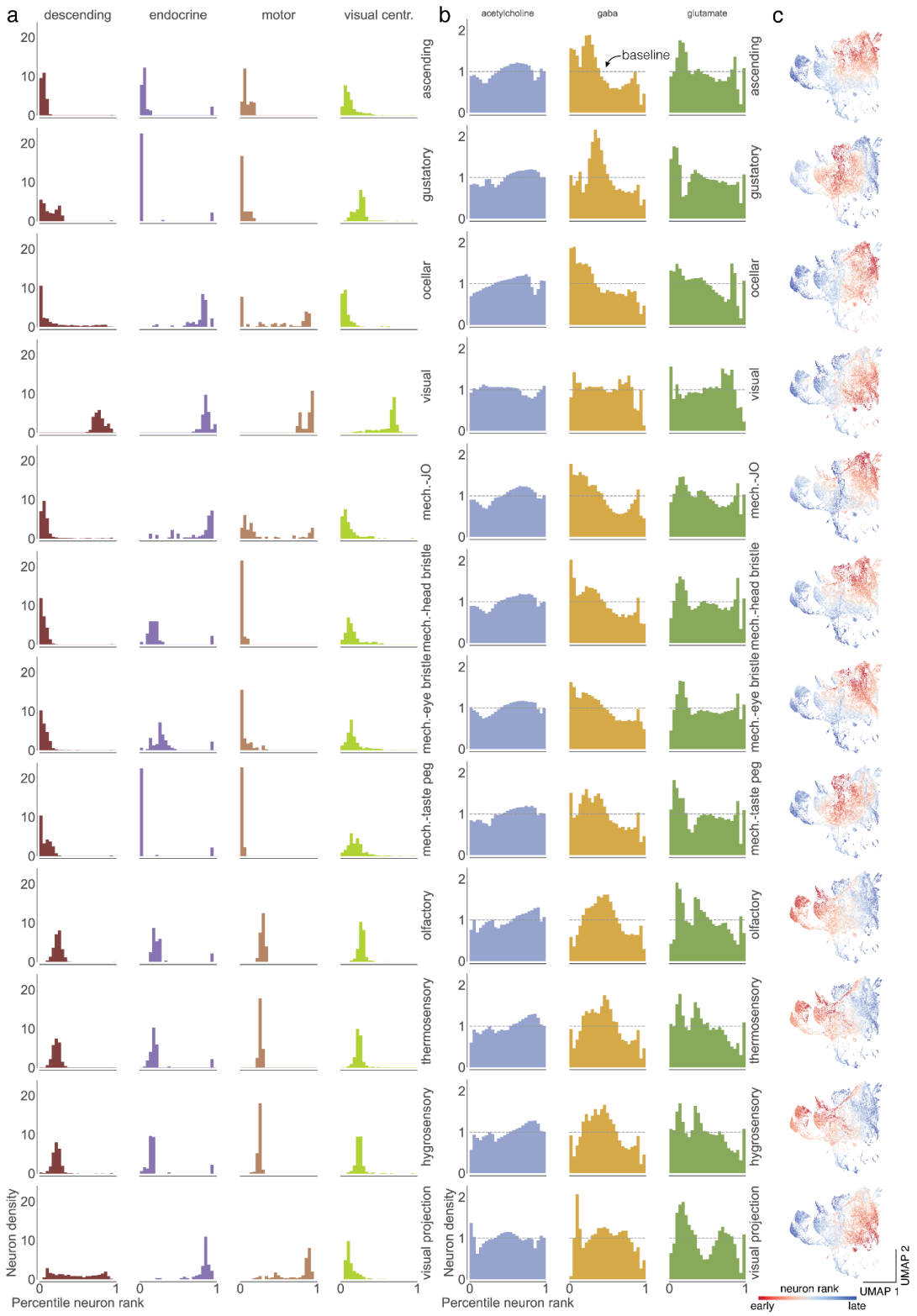

Extended Data Figure 6-1. Percentile ranks for every modality. (a) For each sensory modality we used the traversal distances to establish a neuron ranking. Each panel shows the distributions of neurons of each super class within the sensory modality specific rankings. (b) Same as in (a) for the fast neurotransmitters. (c) Neurons in the UMAP plot are colored by the rank order in which they are reached from a given seed neuron set. Red neurons are reached earlier than blue neurons.

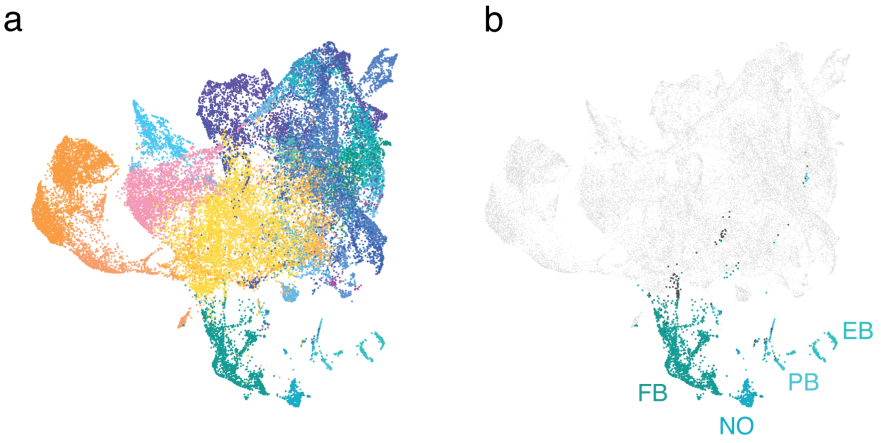

Extended Data Figure 6-2. Rank-based UMAP projection and neuropils. (a) Every neuron in the central brain was assigned to the neuropil where it received the most synapses. Every dot is then colored by the assigned neuropil (Ext. Data Fig. 1-1). (b) Same as in a but limited to the central complex neurons. Neurons in the central complex with an assigned neuropil other than the ones shown are shown are colored black.

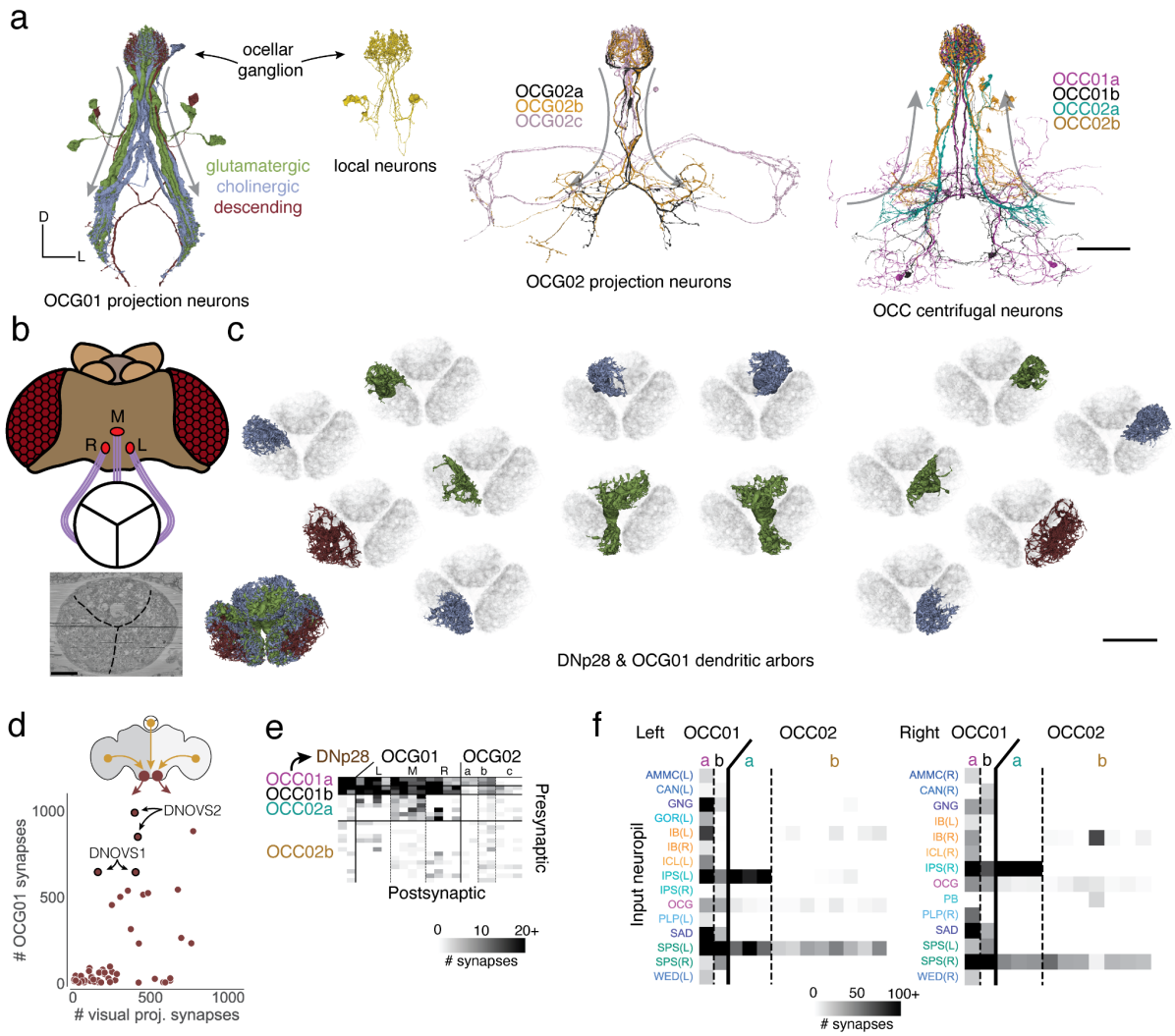

Extended Data Figure 7-1. Ocellar circuit. (a) Renderings of all neurons (excluding the photoreceptors) with arbors in the ocellar ganglion. “Information flow” from pre- and postsynapses is indicated by arrows along the arbors. (b) Overview of the three ocelli (left, medial, right) which are positioned on the top of the head. Photoreceptors from each ocellus project to a specific subregion of the ocellar ganglion which are separated by glia (marked with black lines on the EM). (c) Top view of the dendritic arbors within the ocellar ganglion of each DNp28 (brown) and OCG01 (blue: cholinergic, green: glutamatergic). The render on the lower shows all 12 OCG01s and 2 DNp28s. Each other render shows one neuron in color and all others in the background in gray for reference. (d) Comparison of number of synapses from OCG01 neurons and visual projection neurons onto descending neurons. (e) Connectivity matrix for connections between ocellar centrifugal neurons and ocellar projection neurons. (f) Inputs to ocellar centrifugal neurons by neuropil. Scale bars: 100 µm (a), 20 µm (c)

a

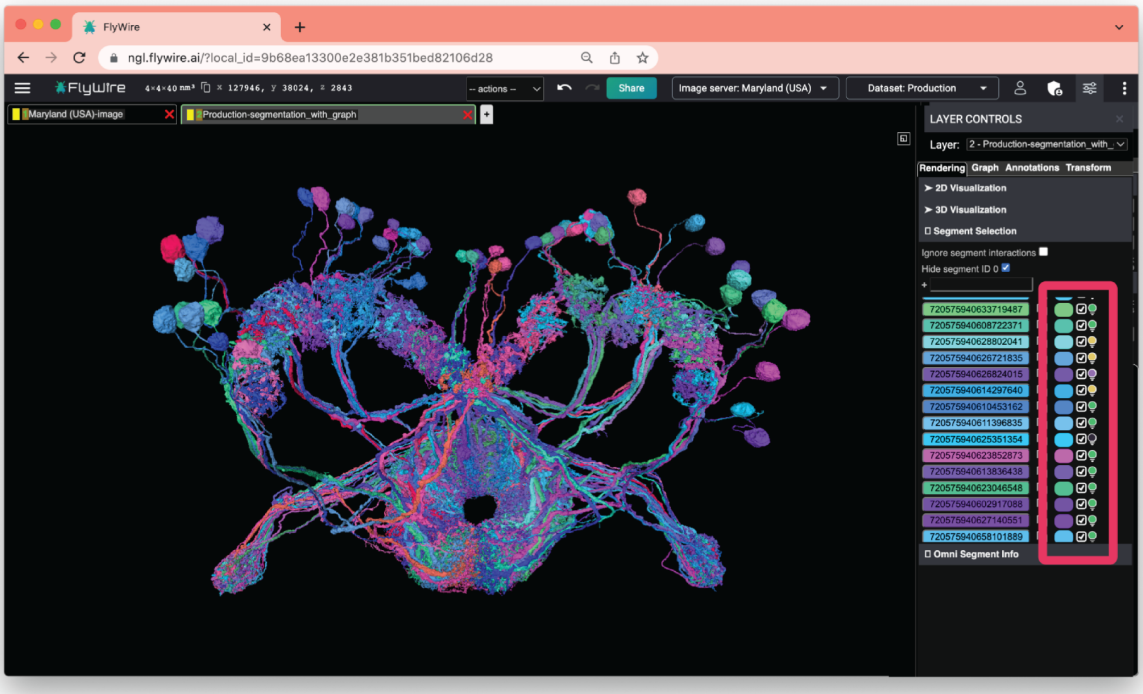

b

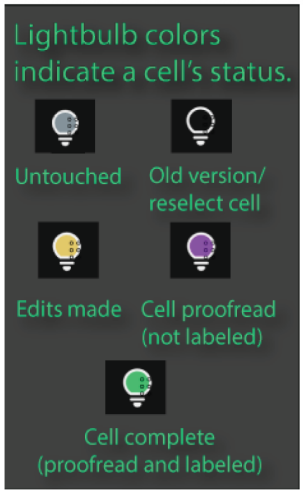

c

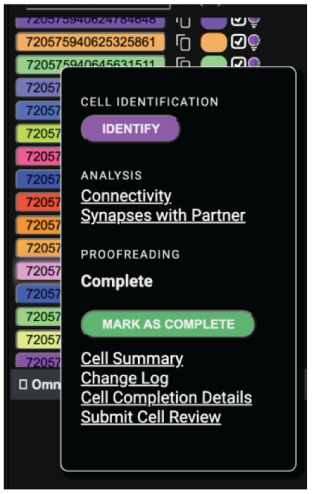

Supplemental Information 1: Neuroglancer Interface and Lightbulb. (a) FlyWire's lightbulb menu displays the proofreading and annotation status of every segment (red box). (b) It is color coded for easy reference (yellow: cell has not been declared complete; purple: complete but not labeled; green: proofread and labeled; black: out of date segmentation). (c) Users can load cell identification directly within the FlyWire editor, perform basic connectivity analysis, and view a cell's edit history.

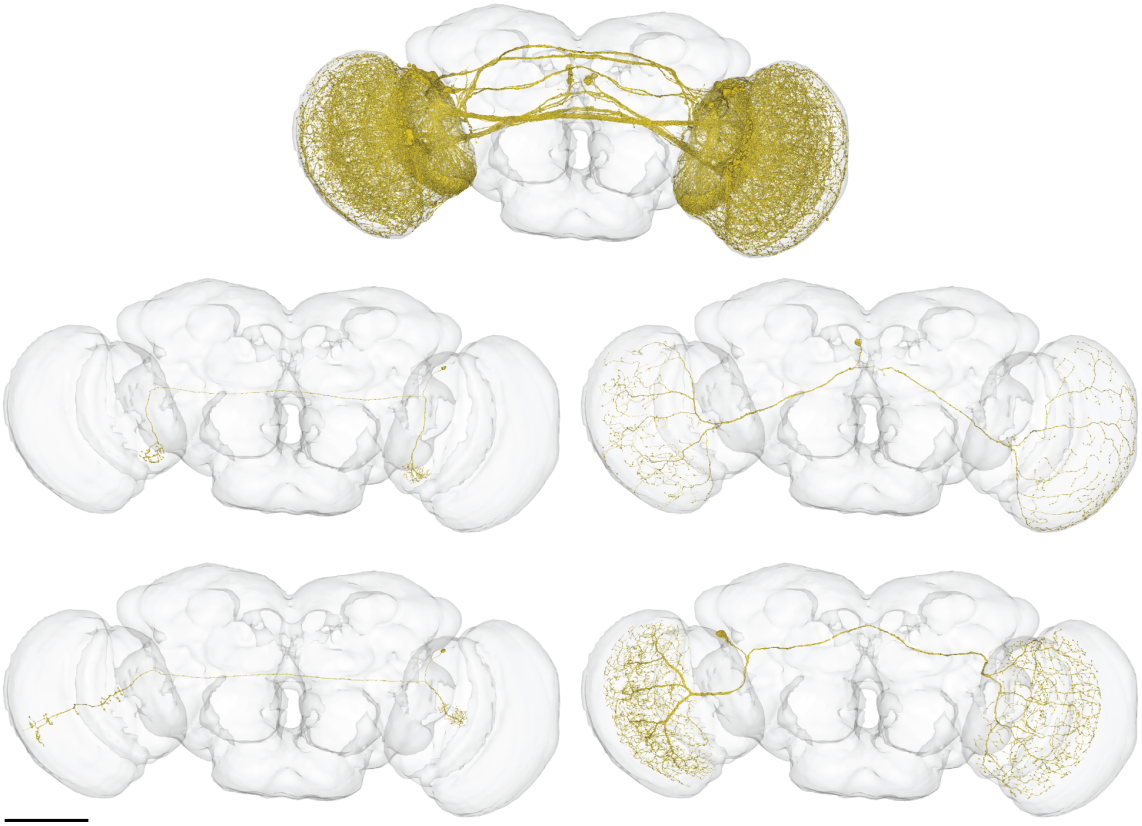

Supplemental Information 2: Bilateral optic lobe neurons. On the left: putative LC14 (top) and putative LC14b (bottom). Scale bar: 100 µm

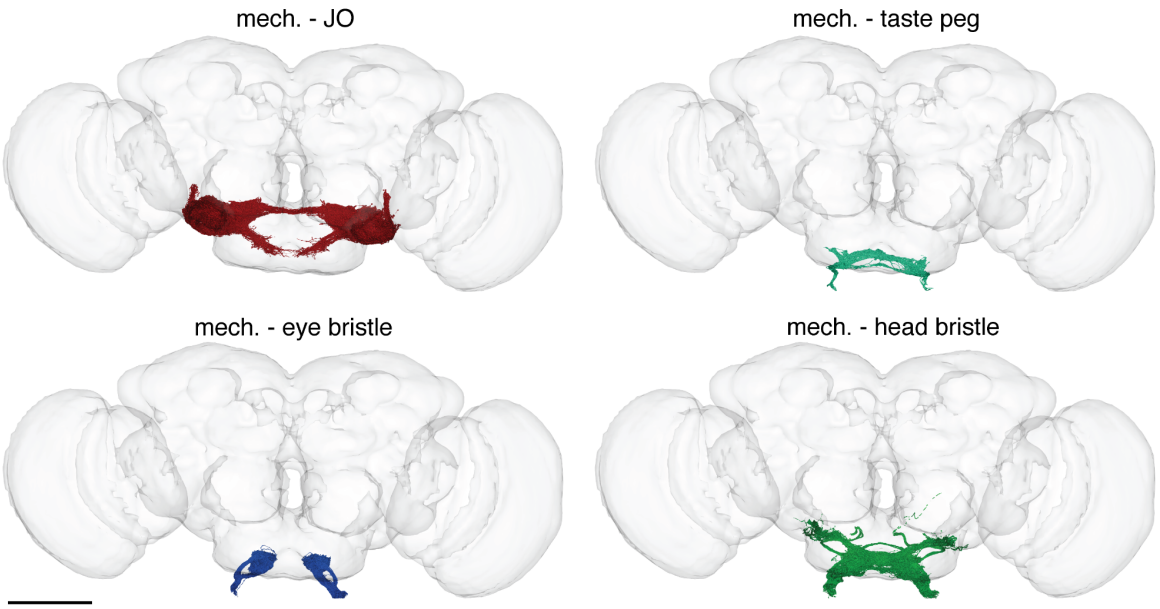

Supplemental Information 3: Mechanosensory neuron subtypes. Scale bar: 100 µm

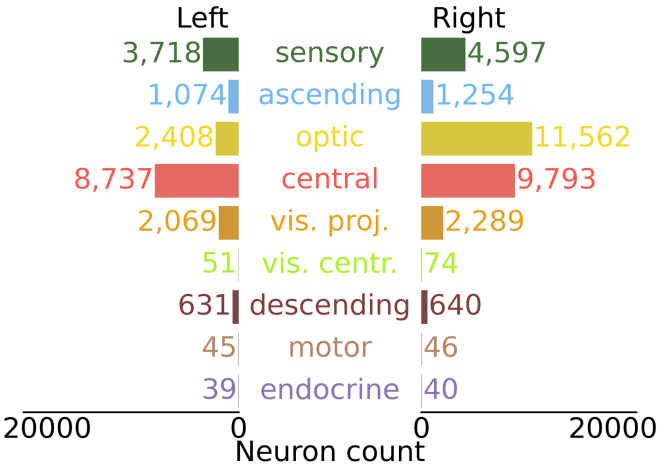

Supplemental Information 4: Distribution of community annotations by cell type

Name	Lab Affiliation	total edits
Doug Bland	Mala Murthy Lab, Sebastian Seung Lab	247,366
Zairene Lenizo	Mala Murthy Lab, Sebastian Seung Lab	122,932
Nseraf	Flyers (citizen scientist)	110,082
Kyle Patrick Willie	Mala Murthy Lab, Sebastian Seung Lab	83,635
Nashra Hadjerol	Mala Murthy Lab, Sebastian Seung Lab	81,700
Austin T Burke	Mala Murthy Lab, Sebastian Seung Lab	80,647
Ryan Willie	Mala Murthy Lab, Sebastian Seung Lab	74,951
John Anthony Ocho	Mala Murthy Lab, Sebastian Seung Lab	67,436
Arti Yadav	Greg Jefferis Lab	59,394
Joshua Bañez	Mala Murthy Lab, Sebastian Seung Lab	59,014
Shirleyjoy Serona	Mala Murthy Lab, Sebastian Seung Lab	55,859
Yijie Yin	Greg Jefferis Lab	50,805
Rey Adrian Candilada	Mala Murthy Lab, Sebastian Seung Lab	50,492
Jet Ivan Dolorosa	Mala Murthy Lab, Sebastian Seung Lab	46,454
Mendell Lopez	Mala Murthy Lab, Sebastian Seung Lab	43,885
Ariel Dagohoy	Mala Murthy Lab, Sebastian Seung Lab	43,124
Regine Salem	Mala Murthy Lab, Sebastian Seung Lab	42,181
Griffin Badalamente	Greg Jefferis Lab	41,195
Remer Tancontian	Mala Murthy Lab, Sebastian Seung Lab	41,130
Nelsie Panes	Mala Murthy Lab, Sebastian Seung Lab	39,801
Laia Serratosa Capdevila	Greg Jefferis Lab, Rachel Wilson Lab	39,798
Kendrick Joules Vinson	Mala Murthy Lab, Sebastian Seung Lab	38,646
Anjali Pandey	Greg Jefferis Lab	37,344
Darrel Jay Akiatan	Mala Murthy Lab, Sebastian Seung Lab	36,987
Dustin Garner	Sung Soo Kim Lab	36,209
Ben Silverman	Mala Murthy Lab, Sebastian Seung Lab	34,676
Dharini Sapkal	Greg Jefferis Lab	31,244
Shaina Mae Monungolh	Mala Murthy Lab, Sebastian Seung Lab	28,721
Jay Gager	Mala Murthy Lab, Sebastian Seung Lab	28,317
Krzysztof Kruk	Flyers (citizen scientist)	27,486
Miguel Albero	Mala Murthy Lab, Sebastian Seung Lab	26,831
Katharina Eichler	Greg Jefferis Lab, Seeds Hamepl Lab	24,481
Zeba Vohra	Greg Jefferis Lab	24,431
Emil Kind	Mathias Wernet Lab	24,052
Varun Sane	Greg Jefferis Lab	23,762
annkri (Anne Kristiansen)	Flyers (citizen scientist)	22,020
Chitra Nair	Greg Jefferis Lab	21,696
Márcia dos Santos	Greg Jefferis Lab	21,209
Dhwani Patel	Greg Jefferis Lab	20,389
Imaan F. M. Tamimi	Greg Jefferis Lab	19,937
Michelle Darapan Pantujan	Mala Murthy Lab, Sebastian Seung Lab	18,846
James Hebditch	Mala Murthy Lab, Sebastian Seung Lab	18,719

Alexandre Javier	Greg Jefferis Lab	17,813
Rashmita Rana	Greg Jefferis Lab	17,547
Bhargavi Parmar	Greg Jefferis Lab	17,133
Merlin Moore	Mala Murthy Lab, Sebastian Seung Lab	16,590
Mark Lloyd Pielago	Mala Murthy Lab, Sebastian Seung Lab	16,566
Allien Mae Gogo	Mala Murthy Lab, Sebastian Seung Lab	16,243
Mark Larson	Wei-Chung Lee Lab	15,692
Joseph Hsu	Greg Jefferis Lab, Scott Waddell Lab	15,496
Jacquilyn Laude	Mala Murthy Lab, Sebastian Seung Lab	14,764
Itisha Joshi	Greg Jefferis Lab	14,717
Chereb Martinez	Mala Murthy Lab, Sebastian Seung Lab	14,638
Dhara Kakadiya	Greg Jefferis Lab	14,544
John David Asis	Mala Murthy Lab, Sebastian Seung Lab	14,202
Clyde Angelo Lim	Mala Murthy Lab, Sebastian Seung Lab	14,139
Alvin Josh Mandahay	Mala Murthy Lab, Sebastian Seung Lab	14,112
Thomas Stocks	Flyers (citizen scientist)	13,683
AzureJay (Jaime Skelton)	Flyers (citizen scientist)	13,540
Marchan Manaytay	Mala Murthy Lab, Sebastian Seung Lab	13,244
Kaushik Parmar	Greg Jefferis Lab	13,136
Philipp Schlegel	Greg Jefferis Lab	12,750
Philip Lenard Ampo	Mala Murthy Lab, Sebastian Seung Lab	12,572
Daril Bautista	Mala Murthy Lab, Sebastian Seung Lab	12,539
Irene Salgarella	Greg Jefferis Lab	12,475
John Clyde Saguimpa	Mala Murthy Lab, Sebastian Seung Lab	11,391
Chan Hyuk Kang	Jinseop Kim Lab	11,129
Markus William Pleijzier	Greg Jefferis Lab	10,498
Marina Gkantia	Greg Jefferis Lab	10,140
Jansen Seguido	Mala Murthy Lab, Sebastian Seung Lab	9,979
Jinmook Kim	Jinseop Kim Lab	9,879
Quinn Vanderbeck	Rachel Wilson Lab	8,845
Cathy Pilapil	Mala Murthy Lab, Sebastian Seung Lab	8,738
Yashvi Patel	Greg Jefferis Lab	8,485
Eva Munnelly	Greg Jefferis Lab	8,102
Olivia Sato	Wei-Chung Lee Lab	8,055
Siqi Fang	Greg Jefferis Lab	7,981
Paul Brooks	Greg Jefferis Lab	6,838
Claire E. McKellar	Mala Murthy Lab, Sebastian Seung Lab	6,802
Christopher Dunne	Greg Jefferis Lab	6,307
Mai Bui	Ken Colodner Lab	6,228
JousterL (Matthew Lichtenberger)	Flyers (citizen scientist)	5,883
edmark tamboboy	Mala Murthy Lab, Sebastian Seung Lab	5,801
Mareike Selcho	Mareike Selcho Lab	5,565
Lucia Kmecova	Seeds Hampel Lab	5,539
Katie Molloy	Wei-Chung Lee Lab	5,492

Alexis E Santana-Cruz	Seeds Hampel Lab	5,274
Janice Salocot	Mala Murthy Lab, Sebastian Seung Lab	5,133
Steven Calle	Seeds Hampel Lab	4,922
Kfay	Flyers (citizen scientist)	4,886
Seongbong Yu	Jinseop Kim Lab	4,832
Arzoo Diwan	Greg Jefferis Lab	4,787
Monika Patel	Greg Jefferis Lab	4,482
Gregory S.X.E. Jefferis	Greg Jefferis Lab	4,472
Sarah Morejohn	Mala Murthy Lab, Sebastian Seung Lab	4,090
Sanna Koskela	Michael Reiser Lab	3,822
bl4ckscor3 (Daniel Lehmann)	Flyers (citizen scientist)	3,735
Celia David	Mala Murthy Lab, Sebastian Seung Lab	3,611
Sangeeta Sisodiya	Greg Jefferis Lab	3,493
Tansy Yang	Janelia Tracers	3,422
Selden Koolman	Mala Murthy Lab, Sebastian Seung Lab	3,384
Christa Baker	Mala Murthy Lab	3,381
Szi-chieh Yu	Mala Murthy Lab, Sebastian Seung Lab	3,376
Gerit A. Linneweber	Gerit Linneweber Lab	3,237
Amalia Braun	Alexander Borst Lab	3,125
Sky Cho	Ken Colodner Lab	2,972
Wolf Huetteroth	Wolf Huetteroth Lab	2,830
Brian Reicher	Wei-Chung Lee Lab	2,794
TR77	Flyers (citizen scientist)	2,775
Marlon Blanquart	Greg Jefferis Lab	2,662
Farzaan Salman	Andrew Dacks Lab	2,524
Hyungjun Choi	Jinseop Kim Lab	2,373
Li Guo	Julie Simpson Lab	2,095
Forrest Collman	Allen Institute Connectomics	2,016
Marissa Sorek	Mala Murthy Lab, Sebastian Seung Lab	2,007
Joanna Eckhardt	Mala Murthy Lab	1,995
Alisa Poh	Barry Dickson Lab	1,922
Marina Lin	Ken Colodner Lab	1,920
Stefanie Hampel	Seeds Hampel Lab	1,645
Wes Murfin	Citizen Scientist	1,578
Peter Gibb	Rachel Wilson Lab	1,448
Zhihao Zheng	Sebastian Seung Lab	1,421
Nidhi Patel	Greg Jefferis Lab	1,394
Lucy Houghton	Sung Soo Kim Lab	1,357
Devon Jones	Mala Murthy Lab, Sebastian Seung Lab	1,295
Annalena Oswald	Marion Silies Lab	1,187
Lucas Encarnacion-Rivera	Mala Murthy Lab	1,164
Akanksha Jadia	Greg Jefferis Lab	1,141
Leonie Walter	Mathias Wernet Lab	1,102
Nik Drummond	Alexander Borst Lab	1,099

Xin Zhong	Mathias Wernet Lab	1,083
Benjamin Gorko	Sung Soo Kim Lab	1,064
Fernando J Figueroa Santiago	Seeds Hampel Lab	1,049
István Taisz	Greg Jefferis Lab	1,043
Urja Verma	Greg Jefferis Lab	1,033
Ibrahim Tastekin	Carlos Ribeiro Lab	1,025
Sandeep Kumar	Mala Murthy Lab	987
Yuta Mabuchi	Nilay Yapici Lab	963
Nick Byrne	Wei-Chung Lee Lab	951
Edda Kunze	Gerit Linneweber Lab	907
Thomas Crahan	Sung Soo Kim Lab	901
Hewhoamareismyself (Ryan Margossian)	Flyers (citizen scientist)	874
Iliyan Georgiev	Flyers (citizen scientist)	825
Fabianna Szorenyi	Seeds Hampel Lab	817
Tomke Stuerner	Greg Jefferis Lab	736
Atsuko Adachi	Richard Mann Lab, Rudy Behnia Lab	695
Minsik Yun	Young-Joon Kim Lab	625
Andrearwen	Flyers (citizen scientist)	607
Robert Turnbull	Greg Jefferis Lab	586
Alexander Thomson	Janelia Tracers, Michael Reiser Lab	527
a5hm0r	Flyers (citizen scientist)	516
Sebastian Molina-Obando	Marion Silies Lab	470
Connor Laughland	Janelia Tracers, Michael Reiser Lab	469
Suchetana B. Dutta	Bassem Hassan Lab	458
Paula Guiomar Alarcón de Antón	Mathias Wernet Lab	426
Patricia Pujols	Seeds Hampel Lab	423
Binglin Huang	Sung Soo Kim Lab	423
Kenneth J. Colodner	Ken Colodner Lab	421
Isabel Haber	Rachel Wilson Lab	392
Albert Lin	Mala Murthy Lab	362
Alexander Shakeel Bates	Greg Jefferis Lab, Rachel Wilson Lab	340
Daniel T. Choe	Jinseop Kim Lab	340
Veronika Lukyanova	Jenny Read Lab	337
Marta Costa	Greg Jefferis Lab	334
Maria Ioannidou	Marion Silies	332
Jonas Chojetzki	Marion Silies	331
Zequan Liu	Xueying "Snow" Wang (Lichtman Lab)	317
Haley Croke	Katie von Reyn Lab	308
Gizem Sancer	Mathias Wernet Lab	308
Tatsuo Okubo	Rachel Wilson Lab	306
Miriam A. Flynn	Janelia Tracers, Michael Reiser Lab	297
Meghan Laturney	Kristin Scott Lab	274
Benjamin Bargeron	Salil Bidaye Lab	273
Davi D. Bock	Davi Bock Lab	255

Hyunsoo Yim	Jinseop Kim Lab	240
Anh Duc Le	Denise Garcia Lab	237
Seungyun Yu	Jinseop Kim Lab	224
Yeonju Nam	Jinseop Kim Lab	221
Mavil	Flyers (citizen scientist)	217
Eleni Samara		213
Audrey Francis	Gaby Maimon Lab	196
Jesse Gayk	Greg Jefferis Lab	195
Zepeng Yao	Kristin Scott Lab	194
Sommer S. Huntress	Ken Colodner Lab	192
Carolina Manyari-Diaz	Salil Bidaye Lab	191
Raquel Barajas	Carlos Ribeiro Lab	186
Mindy Kim	Wei-Chung Lee Lab	185
Burak Gür	Marion Silies Lab	182
Nils Reinhard	Charlotte Helfrich-Forster Lab	177
Amanda Abusaif	Kristin Scott Lab	176
Anna Li	Rachel Wilson Lab	173
Sven Dorkenwald	Sebastian Seung Lab	169
Fred W Wolf	Fred Wolf Lab	163
Lena Lörsch	Marion Silies Lab	159
Keehyun Park	Jinseop Kim Lab	155
Xinyue Cui	Nilay Yapici Lab	152
Haein Kim	Nilay Yapici Lab	145
Alan Mathew	Greg Jefferis Lab	141
Taewan Kim	Jinseop Kim Lab	135
Guan-ting Wu	National Hualien Senior High School	124
Margarida Brotas	Eugenia Chiappe Lab	112
Cheng-hao Zhang	National Hualien Senior High School	109
Philip K. Shiu	Kristin Scott Lab	108
Shanice Bailey	Greg Jefferis Lab	102

Supplementary Table 1: Number of proofreading edits by consortium members. Only members with ≥100 edits are shown.

Name	Lab Affiliation	total Labels
Volker Hartenstein	Volker Hartenstein Lab	13,762
Alexander Shakeel Bates	Greg Jefferis Lab, Rachel Wilson Lab	11,260
Krzysztof Kruk	Flyers (citizen scientist)	11,138
Sven Dorkenwald	Sebastian Seung Lab	6,375
Katharina Eichler	Greg Jefferis Lab, Seeds Hampel Lab	6,366
Philipp Schlegel	Greg Jefferis Lab	3,751
David Deutsch	Mala Murthy Lab	2,549
Kaiyu Wang	Barry Dickson Lab	2,443
Yijie Yin	Greg Jefferis Lab	2,354
Stefanie Hampel	Seeds Hampel Lab	2,129
annkri (Anne Kristiansen)	Flyers (citizen scientist)	1,871
Dustin Garner	Sung Soo Kim Lab	1,782
Wolf Huetteroth	Wolf Huetteroth Lab	1,409
AzureJay (Jaime Skelton)	Flyers (citizen scientist)	1,303
Amalia Braun	Alexander Borst Lab	1,104
Austin T Burke	Mala Murthy Lab, Sebastian Seung Lab	1,013
Gizem Sancer	Mathias Wernet Lab	942
Jenna Joroff	Wei-Chung Lee Lab	900
Gregory S.X.E. Jefferis	Greg Jefferis Lab	716
Christa Baker	Mala Murthy Lab	622
Claire E. McKellar	Mala Murthy Lab, Sebastian Seung Lab	612
Markus William Pleijzier	Greg Jefferis Lab	541
Christopher Dunne	Greg Jefferis Lab	517
Márcia dos Santos	Greg Jefferis Lab	448
Varun Sane	Greg Jefferis Lab	442
Quinn Vanderbeck	Rachel Wilson Lab	424
Lucia Kmecova	Seeds Hampel Lab	412
Steven Calle	Seeds Hampel Lab	408
Rey Adrian Candilada	Mala Murthy Lab, Sebastian Seung Lab	364
Sebastian Molina-Obando	Marion Silies Lab	347
Philip K. Shiu	Kristin Scott Lab	321
Eva Munnelly	Greg Jefferis Lab	311
Remer Tancontian	Mala Murthy Lab, Sebastian Seung Lab	308
Doug Bland	Mala Murthy Lab, Sebastian Seung Lab	306
Ariel Dagohoy	Mala Murthy Lab, Sebastian Seung Lab	306
Joshua Bañez	Mala Murthy Lab, Sebastian Seung Lab	301
Marina Gkantia	Greg Jefferis Lab	300
Jet Ivan Dolorosa	Mala Murthy Lab, Sebastian Seung Lab	280
Nashra Hadjerol	Mala Murthy Lab, Sebastian Seung Lab	264
Zairene Lenizo	Mala Murthy Lab, Sebastian Seung Lab	236

Matt Collie	Rachel Wilson Lab	223
Farzaan Salman	Andrew Dacks Lab	219
Marion Silies	Marion Silies	183
Kendrick Joules Vinson	Mala Murthy Lab, Sebastian Seung Lab	175
John Anthony Ocho	Mala Murthy Lab, Sebastian Seung Lab	166
Thomas Stocks	Flyers (citizen scientist)	161
Kenneth J. Colodner	Ken Colodner Lab	161
Gerit A. Linneweber	Gerit Linneweber Lab	156
Celia David	Mala Murthy Lab, Sebastian Seung Lab	151
TR77	Flyers (citizen scientist)	147
Megan Wang	Mala Murthy Lab	130
Szi-chieh Yu	Mala Murthy Lab, Sebastian Seung Lab	129
Lucy Houghton	Sung Soo Kim Lab	123
Nils Reinhard	Charlotte Helfrich-Forster Lab	123
Ben Silverman	Mala Murthy Lab, Sebastian Seung Lab	121
Regine Salem	Mala Murthy Lab, Sebastian Seung Lab	111
Benjamin Gorko	Sung Soo Kim Lab	107
Nseraf	Flyers (citizen scientist)	107
Mareike Selcho	Mareike Selcho Lab	102
Haein Kim	Nilay Yapici Lab	72
Minsik Yun	Young-Joon Kim Lab	71
Damian Demarest	Michael Pankratz Lab	70
István Taisz	Greg Jefferis Lab	66
Marissa Sorek	Mala Murthy Lab, Sebastian Seung Lab	62
Andrea Sandoval	Kristin Scott Lab	58
Diego A. Pacheco	Mala Murthy Lab	55
Kyle Patrick Willie	Mala Murthy Lab, Sebastian Seung Lab	53
Zhihao Zheng	Sebastian Seung Lab	51
Benjamin Bargeron	Salil Bidaye Lab	47
Burak Gür	Marion Silies Lab	44
Sandeep Kumar	Mala Murthy Lab	40
Tansy Yang	Janelia Tracers	37
Amanda González-Segarra	Kristin Scott Lab	36
Gianna Vitelli	Salil Bidaye Lab	29
Joanna Eckhardt	Mala Murthy Lab	26
Shuo Cao	David Anderson Lab	24
Haley Croke	Katie von Reyn Lab	22
Nino Mancini	Salil Bidaye Lab	21
Jonas Chojetzki	Marion Silies	18
Gabriella R. Sterne	Gabriella Sterne Lab	16
Kate Maier	Salil Bidaye Lab	16
Amy R Sterling	Sebastian Seung Lab	15

Yuta Mabuchi	Nilay Yapici Lab	12
Lucas Encarnacion-Rivera	Mala Murthy Lab	10
Alexander Del Toro	Kristin Scott Lab	10
Zepeng Yao	Kristin Scott Lab	10

Supplementary Table 2: Number of annotations by consortium members. Only members with ≥10 annotations are shown.